Optical and spectroscopic properties of Er^{3+}, Yb^{3+} doped and co-doped phosphate and tellurite glasses

Presented by
M.C. Haggeo Desirena Enrriquez

Thesis submitted in partial fulfillment of the requirements for the degree of

DOCTOR OF SCIENCES (Optics)
At Centro de Investigaciones en Óptica

Dr. Elder De la Rosa Cruz
Advisor

March 17, 2010
León Guanajuato, México 2010

For the LORD gives wisdom, and from his mouth come knowledge and understanding (Proverbs 2:6).

Dedication

To God and my father Hernan

Acknowledgements

First of all, I would like to express my deep gratitude to God, who gave me the life and encouragement to perform my PhD at Centro de Investigaciones en Optica.

I am particularly grateful to my advisor, Dr. Elder de la Rosa who gave me the opportunity to work at his research group at Centro de Investigaciones en Optica. His peerless experience and knowledge in optical material and fiber optics were very helpful in my PhD studies.

My special thanks to Prof. Nasser Peyghambarian who let me works at his research group for one year at College of Optical Science in Tucson Arizona.

My deepest thanks from the bottom of my heart must go to my father, Hernan for his love, support, encouragement and patience.

Many thanks, to my friends Luis Armando, Jose Luis, Mauricio, Claudio, Cornelio, Daniel and Lily

ABSTRACT

In this dissertation, the complete procedure for the fabrication of Er^{3+}, Yb^{3+} and Ce^{3+} doped and un-doped glasses with optical quality is described. Various properties were investigated in these glasses, such as spectroscopic, optical, physical and thermo-mechanical. For phosphate glass an improvement in the fluorescence emission was obtained by modifying the glass composition and co-doping with B_2O_3, Yb^{3+} and Ce^{3+} ions. These changes enhance greatly the NIR emission and reduce the up-conversion process. Fluorescence decay time as long as 9 ms, large emission cross section (8×10^{-21} cm^2) high quantum efficiency (90%) and low up-conversion can be obtained by choosing adequately both, glass composition and $Yb^{3+}/Er^{3+}/Ce^{3+}$ concentrations. The primary results indicate that this $Yb^{3+}/Er^{3+}/Ce^{3}$ co-doped material is a very promising candidate for laser and optical amplifiers.

On the other hand, a systematic study about the effect of alkalis (Li, Na, K, Rb and Cs) and network intermediates (Pb, Zn, Ba and Mg) on the physical, thermal and optical properties of tellurite glass were investigated. It was found that the Li_2O-ZnO-TeO_2 ternary glass composition presents good chemical durability, high refractive index, high density, low coefficient of thermal expansion and wide transmission region. The obtained glass composition was analyzed as a function of Er^{3+} and Yb^{3+} concentrations. Experimental results show that high Yb^{3+} and low Er^{3+} concentration enhance the fluorescence characteristics such as florescence lifetime, energy transfer efficiency, emission cross section and quantum efficiency. Such properties are also strongly influenced by introducing network modifiers (Li, Na and K) and the results indicate that K might be the best spectroscopic network modifier. In general, an enhancement of mechanical properties means a deleterious of spectroscopic properties and vice versa,

then, the right selection of glass composition depends on the application and there is often a compromise among many factors

RESUMEN

En este trabajo es descrito el procedimiento completo para fabricación de vidrios dopados y sin dopar con alta calidad óptica. Diferentes propiedades fueron investigadas, tales como espectroscópicas, ópticas, físicas y termomecánicas, con el objetivo de evaluar su correcto desempeño. En al caso particular del vidrio de fosfato la fluorescencia fue mejorada modificando la composición vítrea y dopando con iones de B_2O_3, Yb^{3+} y Ce^{3+}. Estos cambios mejoran la emisión en el infrarrojo (1.53 μm) y a su vez reduce los procesos de conversión hacia arriba. Escogiendo adecuadamente la composición vítrea y la concentración de B_2O_3, Yb^{3+} y Ce^{3+}, es posible obtener valores altos de tiempo de vida (9 ms), sección transversal de emisión (8×10^{-21} cm^2) y eficiencia quántica (90%). Los resultados preliminares indican que esta nueva composición es un excelente candidato para aplicaciones láser y amplificadores ópticos.

Por otra parte realizamos un estudio sistemático sobre el efecto de los metales alcalinos (Li, Na, K, Rb and Cs) y alcalinotérreos (Pb, Zn, Ba and Mg) en las propiedades físicas, térmicas y ópticas en vidrios de telurio. Los experimentos muestran que la composición vítrea dada por Li_2O-ZnO-TeO_2 presenta buena durabilidad química, alto índice de refracción, alta densidad, bajo coeficiente de expansión térmica y amplio rango de transmisión en el infrarrojo. La composición vítrea Li_2O-ZnO-TeO_2 dopado con el sistema Yb^{3+}/Er^{3+} fue analizado como función de la concentración de Er^{3+} y Yb^{3+} y los resultados indican que altas contracciones de Yb^{3+} y bajas de Er^{3+} mejoran las características de fluorescencia. Tales propiedades también son fuertemente influenciadas por la introducción de modificadores de red (Li, Na and K), y los resultados sugieren que K sea quizás el mejor modificador espectroscópico. Generalmente cuando las propiedades espectroscópicas mejoran los mecánicas son

deterioradas y viceversa. De esta manera la selección de la composición vítrea depende de la aplicación y a menudo es un compromiso entre muchos factores.

GENERAL OBJETIVES

- Design and fabrication of bulk glasses with optical quality for laser and optical amplifiers
- To develop novel tellurite and phosphate glasses that can be heavily doped with Er^{3+}, Yb^{3+} and Ce^{3+} ions.
- Spectroscopic and optical characterization of Er^{3+}, Yb^{3+} and Ce^{3+} doped phosphate glasses.
- To investigate the mechanical and physical properties of tellurite glass as a function of network intermediates.
- To enhance the spectroscopic properties of 1.53 μm signal emission by choosing adequately the ions concentration and glass composition.

PREFACE

Erbium doped glasses is one of the most important materials investigated to develop optical amplifiers and laser, because of the eye safe emission centered at 1.55 μm corresponding to the $^4I_{13/2} \rightarrow {}^4I_{15/2}$ transition. Among oxides, silica glass is one of the most studied hosts for these applications because of its good thermal-mechanical properties, chemical durability and glass stability. The main drawback of this glass is their narrow emission bandwidth and the low solubility of active ions that give rise to cluster formation. The narrow bandwidth limits the transmission capacity of information, reducing the performance of amplifiers. In addition due to their relative low phonon energy of 1000 cm^{-1}, they present the undesirable up-conversion that produces emission centered at 540 nm and hence this process also limits the gain of the amplifiers. Based in these requirements, new glass hosts such as phosphate and tellurite glasses have emerged to resolve this drawback. Both exhibits high gain, good chemical durability, ion exchangeability, good thermal-mechanical properties, good glass stability, broad bandwidth emission, high solubility of rare earth and low fluorescence quenching. The high solubility permits the introduction of large concentrations of active ions into relatively small volumes and promotes the design of compact device. Thus the goal with this kind of glass is to reduce the up-conversion emission by choosing a host with high phonon energy such as phosphate glass and increase the bandwidth using the tellurite glass. In the present dissertation the spectroscopic characterization as function of ions concentration of Er^{3+} doped, Yb^{3+}/Er^{3+} codoped and, for first time $Yb^{3+}/Er^{3+}/Ce^{3+}$ co-doped phosphate glasses will be described. Additionally a complete study of tellurite glasses concerning glass composition and ion concentration were investigated.

The general content of the thesis are presented as follow:

In chapter 1 the complete procedure to prepare phosphate and tellurite glasses including annealing process are described. The optimization of parameters such as time and temperature necessary for good annealing process that removes stress is also described.

In chapter 2 Er^{3+}doped and Er^{3+}/Yb^{3+} co-doped phosphate glasses were investigated. The Judd-Ofelt parameters, stimulated emission cross section and fluorescence lifetime were calculated and are discussed. The effect of the dopant concentration on the spectroscopic properties to obtain the highest quantum efficiency was analyzed.

In chapter 3 we present the first report of a comparative study of the fluorescence characteristics of Er^{3+}/Yb^{3+} co-doped borophosphate and $Er^{3+}/Yb^{3+}/Ce^{3+}$ co-doped phosphate glasses were analyzed. The effect of B_2O_3 and Ce^{3+} concentration on the emission intensity at the eye safe signal, decay time and emission cross section were measured. The best combination of $Yb^{3+}/Er^{3+}/Ce^{3+}$ and $Yb^{3+}/Er^{3+}/B_2O_3$ ions concentration in order to maximize the efficiency of the eye-safe laser emission were determined.

In chapter 4 twenty tellurite glasses were prepared and divided into four batches R_2O-PbO-TeO_2, R_2O-ZnO-TeO_2, R_2O-BaO-TeO_2, and R_2O-MgO-TeO_2 in order to explore and compare the effect of alkali metals and network intermediators on the thermo-mechanical, physical and optical properties. In addition to this, third order nonlinearities were measured in order to know the potential for non-lineal optical applications.

In chapter 5 Er^{3+}/Yb^{3+} co-doped tellurite glasses based on TeO_2-ZnO-Li_2O-La_2O_3 were prepared and the spectroscopic properties were studied in detail. Particularly, we focus this chapter to analyze the dependence of energy transfer between Er^{3+} and Yb^{3+} as a function of their concentration. The Judd-Ofelt intensity parameters and quantum efficiency were calculated, the emission intensity of both infrared and up-converted signal were investigated and the physical mechanisms were explained in the terms of the energy transfer and cross-relaxation processes.

In chapter 6 there is a comparative study of network modifiers R_2O (R = K, Na and Li) on the spectroscopic properties of Yb^{3+}/Er^{3+} co-doped tellurite glasses. The emission intensity and fluorescence lifetime at 1.53 μm were measured as well as visible up-conversion and energy transfer as a function of alkalis. The Judd-Ofelt parameter, quantum efficiency and emission cross section were calculated in order to know the best modifier for high performance of laser and amplifiers.

TABLE OF CONTENT

List of figures

List of tables

CHAPTER 1
GLASS COMPOSITION AND PREPARATION OF BULK GLASSES

In this chapter, it is reported a brief analysis on glass composition and preparation of different laser glass systems. The procedure for the fabrication of bulk glasses and the complete annealing process of samples has been studied and various parameters were considered in their fabrication composition, melting point, stirring, glass transition temperature and annealing process. All these will be described here.

1.1 Glass composition

A pure former does not have the ability to provide good laser, optical and physical properties by itself. Thus, to achieve those requirements the incorporation of network modifiers is necessary. Recently, a lot of work on the glass composition has been reported in tellurite and phosphate glasses [1-10]. There, it has been studied the effect of alkali metals and alkali earth in order to improve thermal-mechanical as well as laser properties. The typical composition of phosphate and tellurite glasses are P_2O_5-X_2O_3-R_2O-MO-La_2O_3 and TeO_2-MO-R_2O-La_2O_3 (R=Cs, Rb, K, Na and Li and M=Ba, Sr, Ca, Mg, Zn and Pb), where P_2O_5 and TeO_2 are the network former, La_2O_3 is the rare earth dopant and X_3O_2, R_2O and MO are network modifiers. Both, optical and mechanical properties depend on the content and combination of network former and modifiers. The most common composition of phosphate glasses contains from 55 to 70 mol % of P_2O_5. Below 50 mol% the glass formed has poor chemical durability and above 70 mol % is difficult to melt due to severe vaporization of phosphate during the glass melting process. The composition of tellurite glasses contains from 50 to 75 mol % of TeO_2, higher than 70 mol% produce glasses with a strong tendency to crystallize.

R_2O reduces the chemical durability but increase the negative thermo optic coefficient that in turn enhances thermal properties improving the laser beam quality [11, 12]. Furthermore, alkali metals improve the rare earth solubility and makes glasses suitable for the fabrication of optical waveguide devices by ion-exchange process [1, 13]. MO modifiers improve the physical properties but degraded slightly the laser properties. In particular MgO provides the smaller non-linear refractive index [4], which is beneficial for high power laser performance. X_3O_2 modifier is usually Al_2O_3 on the range from 5 to 15 mol%. If the concentration is higher than 15 mol % devitrification could occur, but if the content is lower than 5 mol% the chemical durability is poor. The Al^{3+} content improves the solubility of rare earth and thermal-mechanical properties such as chemical durability, thermal expansion and hardness. However, the Al^{3+} content has a deteriorative effect on the laser properties [14-16]. In general, the content of Al^{3+} should be as low as possible because high Al^{3+} content reduces the emission cross section [17].

Table 1.1 Several phosphate and tellurite glasses with different compositions

Tag	Glass composition (mol %)
LG-750 [16]	$(55\text{-}60)P_2O_5$-$(8\text{-}12)Al_2O_3$-$(13\text{-}17)K_2O$-$(10\text{-}15)BaO$-$(0\text{-}2)La_2O_3$
LHG-8 [16]	$(56\text{-}60)P_2O_5$-$(8\text{-}12)Al_2O_3$-$(13\text{-}17)K_2O$-$(10\text{-}15)BaO$-$(0\text{-}2)La_2O_3$
LG-770 [16]	$(58\text{-}62)P_2O_5$-$(6\text{-}10)Al_2O_3$-$(20\text{-}25)K_2O$-$(5\text{-}10)MgO$-$(0\text{-}2)La_2O_3$
QX/Er [29]	$67P_2O_5$-$14Al_2O_3$-$14Li_2O$-$1K_2O$-$4(Yb_2O_3 + Er_2O_3)$
TZN [12]	$75TeO_2$-$20ZnO$-$5Na_2O$

Table 1.1 shows different glass compositions most widely used in glasses for optical amplifiers and lasers applications. LG-750, LHG-8, LG-770 and QX/Er are commercial metha-phosphate laser glasses while TZN is the glass host base used for optical fiber amplifier. Some of the more important laser, optical, physical and thermal-mechanical properties of laser glasses are presented in Table 1.2. There, it can be seen

that there are many parameters to be considered. Unfortunately an improvement of laser properties is usually associated with degradation of thermal and physical properties and vice versa. Thus, the right selection of glass composition depends of the application and often is a compromise among many factors.

Table 1.2 Some optical, physical and thermal-mechanical properties of laser glasses

Laser and optical	Physical	Thermal
Cross section (σ_{abs} and σ_{emi})	*Chemical durability(DR)*	*Thermal expansion (α_e)*
Fluorescence lifetime (τ_{exp})	*Density(ρ)*	*Glass transition temperature (T_g)*
Fluorescence linewidth (FWHM)	*Hardness (H)*	*Thermal shock resistance*
Fluorescence peak (λ_L)	*Young's modulus (E)*	*Thermal conductivity (k)*
Refractive index (n)		
Non-linear refractive index (n_2)		

1.2 Fabrication of glasses

The samples glasses under study were prepared from the starting chemical constituents, sodium phosphate ($NaH_2PO_4H_2O$), tellurium oxide (TeO_2), aluminium oxide (Al_2O_3), barium oxide (BaO), magnesium oxide (MgO), zinc oxide (ZnO), lead oxide (PbO), litium oxide (Li_2O), sodium carbonate (Na_2CO_3), potassium carbonate (K_2CO_3), erbium oxide (Er_2O_3) and ytterbium oxide (Yb_2O_3) (all from Aldrich 99.99% pure) according to the following range composition: (55-70)P_2O_5-(6-12)Al_2O_3-(10-18)BaO-(10-15)K_2O-xLa_2O_3 and (60-75)TeO_2-(10-20)ZnO-(5-15)R_2O-(0-4.75)La_2O_3 .

The procedure for the fabrication of the glasses is described as follow. Calculated quantities of the compounds oxide were carefully weighted with an accuracy of 0.0001 g and mixed in a dish glass for a certain period of time until obtain a homogeneous mixture, see Figure 1.1. This procedure must be performed in a clean environment, in order to avoid contaminants from the outer surrounding.

Figure 1.1 Mix of chemical components.

The mixed components were introduced in an electric furnace preheated at 1100 and 850 ^{o}C for phosphate and tellurite glass respectively. Powders were melted for periods of 2 to 3 h using a platinum crucible. Every 40 min the mixture was stirred so that a homogeneously mixed melt was obtained. The stirring helps to the homogenization of the glass melting that in turn reduces striae and bubbles generated by reactions of raw materials. To remove the remaining bubbles the glass melt temperature is increased around 150 °C above the melting point. At this temperature, the solubility of the gas components decreases, bubbles will be formed and grow much more rapidly but the elevated temperature decreases the viscosity of the glass supporting the bubbles and thus they move up and vanish from the melt [18]. After 2 or 3 h, the furnace temperature was gradually reduced at cast temperature 950 and 700 ^{o}C for phosphate and tellurite glasses to increase the viscosity and reduce the micro bubbles into liquid glass. The melt was cast into a suitable aluminum mould preheated close to glass transition temperature (T_g), see Figure 1.2. If the mould preheated is far below T_g, the

glass can break it and mechanical stress are significantly increased, while if the mould temperature is too high (above T_g) the glass is adheres to the mould.

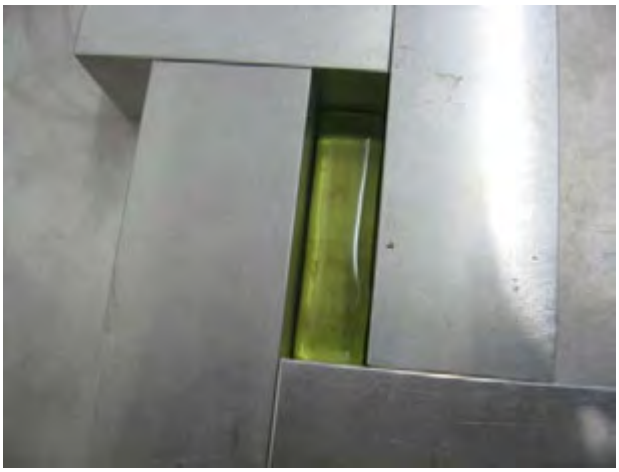

Figure 1.2 Aluminum mold for the fabrication of glasses.

The glass was immediately removed from the mould and quickly transferred to a PDI annealing furnace. The finished bulk phosphate and tellurite glasses are shown in Figure 1.3.

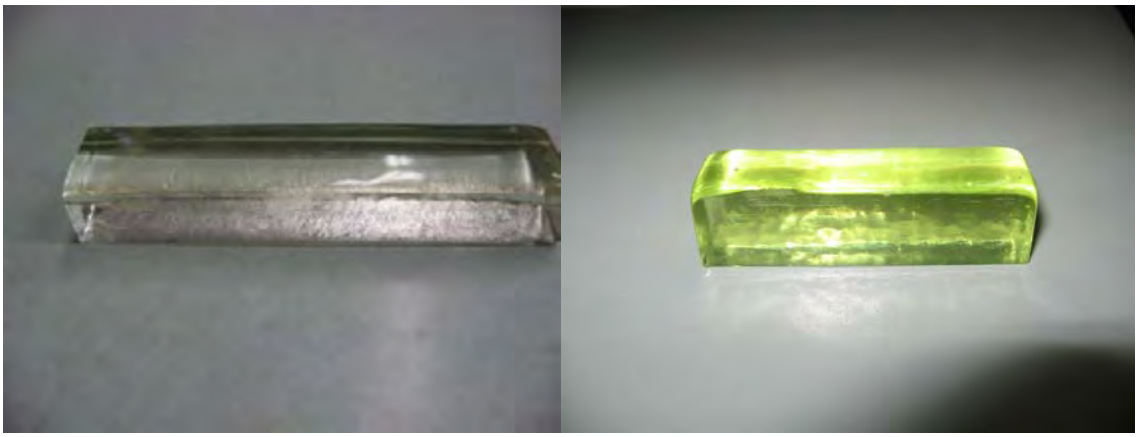

Figure 1.3 Bulk samples of a) phosphate and b) tellurite glass after annealing.

1.3 Annealing process for bulk glasses

The purpose of the annealing process is to reduce the mechanical stress as low as possible and hence to obtain a homogeneous refractive index inside the glass. It is recommended to anneal the glass close to the upper annealing point (maximum annealing temperature). At this point the mechanical stress inside the glass relaxes faster but is more difficult to support itself because the glass is soft and it tends to deform under its own weight. Therefore, the best option for stress relaxation is when the glass is normally heated up to temperatures slightly above the T_g [19]. In our sample the T_g for phosphate and tellurite glasses are around 420 and 300 °C respectively. The complete annealing process as a function of time took 21 h and the temperature curves are shown in Figure 1.4.

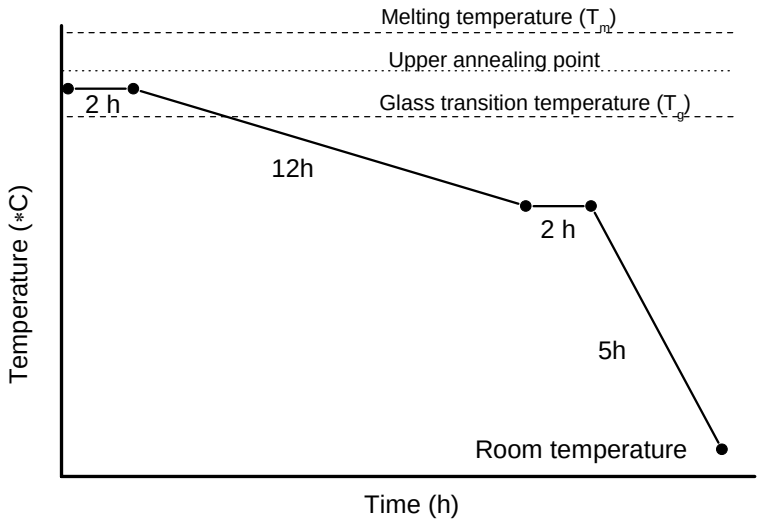

Figure 1.4 Schematic representation of temperature curves of an annealing process of phosphate glasses.

In this process the samples were annealed for 2 h at a temperature from 430 to 500 ºC for phosphate and 300 to 380 ºC for tellurite depending on glass composition. The long time at this step was selected to assure that all parts inside the glass have reached the T_g. Subsequently the temperature was gradually reduced to 70% of initial

temperature in a period of time of 12 h and kept there 2h. It is important to mention that this phase of cooling down is the critical part of the annealing process, thus the temperature rate should be as low as possible in order to avoid the formation and eliminate any mechanical stress. Finally the glasses were gradually cooled to room temperature in a period of time of 5 h. At temperatures far below T_g the cooling rate could be increased without any risk of mechanical stress.

Bibliography

[1]. J.S. Wang, E.M. Vogel, E. Snitzer, Opt. Mater., 3 (1994) 187.

[2]. L. L. Neindre, S. Jiang, B.C. Hwang, T. Luo, J. Watson, N. Peyghambarian, J. Non-Crystall. Solids 255 (1999) 97.

[3]. S. Shen, A. Jha, E. Zhang, S. J. Wilson, C. R. Chimie 5 (2002) 921.

[4]. J. S. Hayden, Y. T. Hayden, J. H. Campbell, SPIE 1277 (1990) 121.

[5]. J. H. Campbell, T. I. Suratwala, J. Non-Cryst. Solids 263-264 (2000) 318

[6]. K. Seneschal, F. Smektala, S. Jiang, T. Luo, B. Bureau, J. Lucas, N. Peyghambarian, J. Non-Cryst. Solids 324 (2003) 179.

[7] S. Jiang, T. Luo, Bor-Chyuan Hwang, G. Nunzi-Conti, M. Myers, D. Rhonehouse, S. Honkanen, N. Pheyghambarian, Opt. Eng. 37 (1998) 3282.

[8]. T. Minami, J. D. Makenzie, J. Am. Ceram. Soc. 60 (1977) 232

[9]. Jong-Oh Byun et al., Jpn. J. Appl. Phys. 33 (1994) 4907.

[10]. H. Takebe, Y. Nageno, and K. Morinaga, J. Am. Ceram Soc, 77 (1994) 2132.

[11]. S. Jiang, J. Myers, D. Rhonehouse, M. Myers, R. Beldford, S. Hamlin; SPIE 2138, (1994).

[12]. S. Jiang, J. Myers, R. Wu, G.M. Bishop, D. Rhonehouse, M. Myers, S. Hamlin; Procc. SPIE vol. 2379, 17(1995).

[13]. H. Lin, S. Jiang, J. Wu, F. Song, N. Peyghambarian and E.Y.B. Pun, J. Phys. D: Appl. Phys. 36 (2003) 812.

[14]. A. Martinez, L.A. Zenteno, J.C.K. Kuo; Appl. Phys. B, 67, 17(1998).

[15]. S. Bernesclu, M. Bettinelli, M. Brenci, G. Nunzi, S. Pelli, S. Sebastiani, C. Siligardi, A. Speghini, G.C. Righini; J. Non-Cryst. Solids 351, 1747(2005).

[16]. J. Y. Ding, S. W. Yung, P. Y. Shih, Phys. Chem. Glasses, 43 (2002) 300.

[17]. Z. Liu, C. Qi, S. Dai, Y. Jiang, L. Hu, Chin. Opt. Lett. 1 (2003) 37.

[18]. Schott glasses, Technical information TIE-28 : Bubbles and inclusion in optical glass, August 2004.

[19]. Schott glasses, Technical information TIE-27 : Stress in optical glass, July 2004.

CHAPTER 2
SPECTROSCOPIC ANALISIS OF Er^{3+} DOPED AND Er^{3+}/Yb^{3+} CO-DOPED PHOSPHATE GLASSES

This chapter is devoted to the spectroscopic properties of Er^{3+} and Er^{3+}/Yb^{3+} co-doped phosphate glass matrix analyzed by fitting the experimental data with the standard Judd-Ofelt theory. Various spectroscopic parameters were obtained such as Ω_t parameters, radiative transition probability, quantum efficiency, fluorescence lifetime and emission cross section. With the help of this parameters it was evaluated their dependence and the potential of the samples as a laser material in the eye–safe laser wavelength (1.53 μm) as a function of the Er^{3+} and Yb^{3+} concentration. The effect of Er^{3+} concentration on the quantum efficiency was discussed in terms of the cluster formation of the active ion and by the dynamics change induced by the presence of Yb^{3+}.

2.1 Name of glass samples and ions concentration

The glass samples were prepared from the starting chemical constituents, sodium phosphate ($NaH_2PO_4H_2O$), aluminium oxide (Al_2O_3), barium oxide (BaO), potassium carbonate (K_2CO_3), erbium oxide (Er_2O_3) and ytterbium oxide (Yb_2O_3) (all from Aldrich 99.99% pure) according to the following range composition: (55-70)P_2O_5-(6-12)Al_2O_3-(10-18)BaO-(10-15)K_2O-xLa_2O_3 where x = 0.5-3.5. The samples were prepared reducing the barium content with the Yb^{3+} and Er^{3+} addition; the change of the barium content ranges from 0.5 to 3.5 mol%. The rare earth doped samples were prepared as follows. Four samples were prepared for 0.5, 1.0, 2.0 and 3.0 mol% of Er_2O_3 denoted by PE05, PE1, PE2 and PE3, respectively. Four samples co-doped with 2.5 mol% of Yb_2O_3 and 0.25, 0.5, 0.75 and 1 mol% of Er_2O_3 were prepared and denoted

by PEY02525, PEY0525, PEY07525 and PEY125, respectively. Another three samples co-doped with 0.5 mol% of Er_2O_3 and 1.5, 2 and 3 mol% of Yb_2O_3 were prepared and denoted by PEY0515, PEY052 and PEY053, respectively. The name of glass samples and ion concentration in mol % and ions/cm^3 are presented in Table 2.1. The complete procedure to calculate the ions concentration can be found in [1] and the procedure to make phosphate glasses is well described in chapter 1.

Table 2.1 Name of glass samples and ions concentration

Name	Er^{3+}/Yb^{3+} (mol %)	Er^{3+}/Yb^{3+} (10^{20} ion/cm^3)
PE05	0.5/0	1.20/0
PE1	1.0/0	2.37/0
PE2	2.0/0	4.64/0
PE3	3.0/0	6.83/0
PEY02525	0.25/2.5	0.57/5.71
PEY0525	0.50/2.5	1.13/5.72
PEY07525	0.75/2.5	1.72/5.73
PEY125	1.0/2.5	2.29/5.73
PEY0515	0.5/1.5	1.16/3.48
PEY052	0.5/2.0	1.15/4.61
PEY053	0.5/3.0	1.13/6.79

2.2 Experimental measurements

The density of each sample was measured by Archimedes method using water distilled as immersion liquid. The samples were cut and then polished to 2 mm thick slabs for different measurements. The refractive index was measured by using an Abbe refractometer. The absorption spectra of Er^{3+} doped and Er^{3+}/Yb^{3+} co-doped phosphate glasses were measured from 300 to 1700 nm interval using a UV-VIS-NIR spectrophotometer (Perkin-Elmer Lambda 900) with a resolution of 1 nm. The fluorescence spectra in the wavelength range from 1400 to 1700 nm corresponding to $^4I_{13/2} \rightarrow {}^4I_{15/2}$ transition of Er^{3+} were acquired with a spectrograph (SP-500i, Acton Research) connected to a semiconductor photo detector (Oriel) and the signal was

processed on a PC. Samples were excited at low power with a CW AlGaAs semiconductor laser centered at 968 nm. The fluorescence decay time corresponding to 1.53 μm was measured using a SR540 chopper (Stanford) at 10 Hz and connecting the photo detector directly to an oscilloscope (LT344 LeCroy). All the optical measurements were performed at room temperature.

2.3 Judd-Ofelt (J-O) analysis

The room temperature absorption spectra of Er^{3+} doped and Er^{3+}/Yb^{3+} co-doped phosphate glasses are shown in Figure 2.1. All the absorption bands and their barycenters are found to be almost identical except with some differences in the band intensities. The absorption bands of Er^{3+} ion corresponds to transitions from the $^4I_{15/2}$ ground state to $^4I_{13/2}$, $^4I_{11/2}$, $^4I_{9/2}$, $^4F_{9/2}$, $^4S_{3/2}$, $^2H_{11/2}$, $^4F_{7/2}$, $^4F_{5/2}$, $^4F_{3/2}$, $^2G_{9/2}$, $^4G_{11/2}$, $^4G_{9/2}$ and $^2K_{15/2}$ excited levels. Because of the inhomogeneous broadening, the Stark structures are poorly resolved. The broadening of the absorption bands is a consequence of the absence of long-range order in the host producing changes in the micro symmetry around the Er^{3+} ion. The data from these absorption spectra can be used to predict several parameters such as, the Ω_t parameters, radiative transition probabilities, the branching ratio and the radiative lifetime of different transitions, in particular from $^4I_{13/2}$ to the ground state (1.53 μm) by using the Judd-Ofelt (JO) theory.

The measured absorption line strength (S_{meas}) for the induced electric dipole transition of each band was determined experimentally from the area under the absorption band and can be expressed in terms of absorption coefficient α by the equation

$$S_{meas}(J \to J') = \frac{3ch(2J+1)}{8\pi^3 \lambda e^2 N_0}\left[\frac{9n}{(n^2+2)^2}\right]\int \alpha(\lambda)d\lambda \qquad (2.1)$$

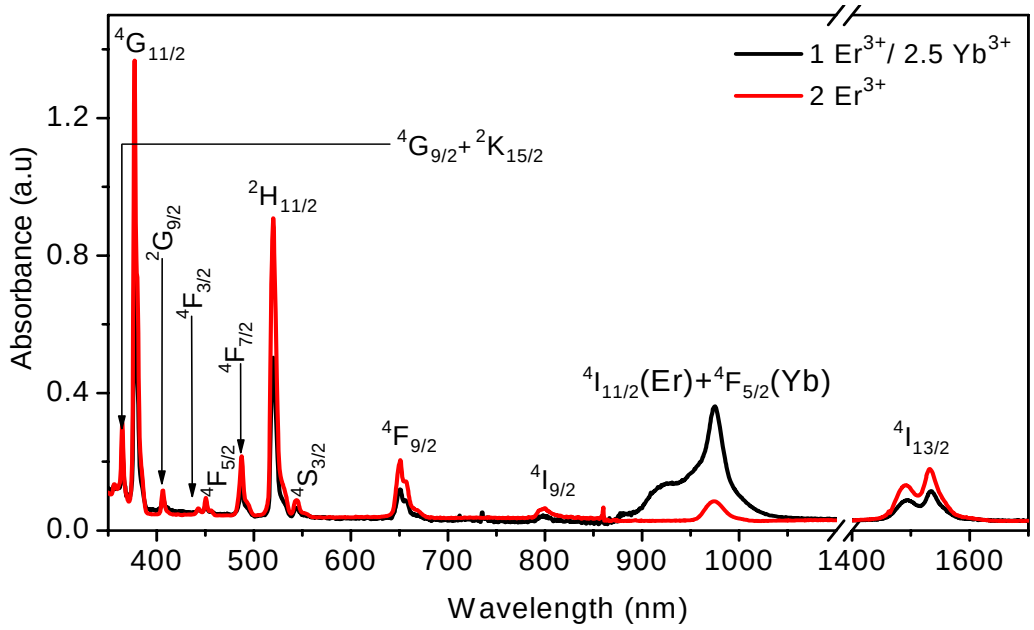

Figure 2.1 Absorption spectra of Er^{3+} doped and Er^{3+}/Yb^{3+} co-doped phosphate glasses for 2 mol% and 1/2.5 mol%, respectively.

Here, J and J' denote the total angular momentum quantum number of the initial and final states, respectively, $e=4.8032x10^{-10}$ *esu* is the charge of the electron, $c=2.9979x10^{10}$ *cm/s* the velocity of the light in the vacuum, $h=6.625x10^{-27}$ *erg s* the Planck constant, λ is the mean wavelength of the absorption band (nm) and N_o is the Er^{3+} ion concentration per unit volume (ions/cm^3). $\alpha(\lambda)= 2.303D_0(\lambda)/d$ is the measured absorption coefficient at a given wavelength λ (nm/cm), $D_0(\lambda)$ the optical density [log I/I_0], d the thickness of the sample (cm) and n is the measured refractive index. The factor $\frac{9n}{(n^2+2)^2}$ represents the local field correction for Er^{3+} ion in the initial J manifold. The values of S_{meas} obtained by the numerical integration of the absorption

line shapes were used to obtain the phenomenological Judd-Ofelt parameters Ω_t by fitting the experimental value with the theoretical expression derived by Judd [2] and Ofelt [3]

$$S_{calc}(J \to J') = \sum_{t=2,4,6} \Omega_t \left| \langle (S,L) J \| U^{(t)} \| S', L') J' \rangle \right|^2 = \Omega_2 [U^{(2)}]^2 + \Omega_4 [U^{(4)}]^2 + \Omega_6 [U^{(6)}]^2$$

(2.2)

where Ω_2, Ω_4 and Ω_6 are J-O intensity parameters and $[U^2]^2$, $[U^4]^2$, and $[U^6]^2$ are the squared reduced matrix elements of the unit tensor operator, which are calculated from the intermediate coupling approximation. The reduced matrix elements are virtually independent of the ligand species surrounding the rare earth (RE^{3+}) ions and thus approximately unchanged from host to host. This is because the $4f^3$ electrons are well shielded by other layers in trivalent RE^{3+} ions. The values of the squared reduced matrix elements for the transitions bands considered in our calculations and for others possible transitions are listed in Table 2.2, the complete values of these elements can be found in [4]. The three phenomenological J-O parameters Ω_2, Ω_4 and Ω_6 exhibit the influence of the host on the radiative transition probabilities, since they contain implicitly the effect of the odd-symmetry crystal field terms. Thus, the small changes presented by these parameters are consequence of the changes in the host composition through the Ba content. The best set of Ω_t parameters of each glass was determined by a standard least square fitting of the theoretical line strength (S_{cal}) values to the experimental ones (S_{meas}) and are listed in Table 2.3 along with the spectroscopic quality factor $\chi=\Omega_4/\Omega_6$. The quality of the fit was determined from the RMS deviation obtained from $\Delta S_{rms}=[(q-3)^-$

$^{1}\Sigma(S_{exp} - S_{cal})]^{1/2}$, where q stand for the number of absorption band considered for calculation and the values obtained are also listed in Table 2.3.

Table 2.2 Squared reduced matrix elements for some transition of Er^{3+} ion [4].

Transition	$[U^2]^2$	$[U^4]^2$	$[U^6]^2$
$^4I_{13/2} \rightarrow {}^4I_{15/2}$	0.0195	0.1173	1.4316
$^4I_{11/2} \rightarrow {}^4I_{15/2}$	0.0282	0.0003	0.3953
$^4I_{13/2}$	0.0331	0.1708	1.0864
$^4I_{9/2} \rightarrow {}^4I_{15/2}$	0	0.1732	0.0099
$^4I_{13/2}$	0.0004	0.0106	0.7162
$^4I_{11/2}$	0.003	0.0674	0.1271
$^4F_{9/2} \rightarrow {}^4I_{15/2}$	0	0.5354	0.4619
$^4I_{13/2}$	0.0101	0.1533	0.0714
$^4I_{11/2}$	0.0704	0.0112	1.2839
$^4I_{9/2}$	0.1279	0.0059	0.0281
$^4S_{3/2} \rightarrow {}^4I_{15/2}$	0	0	0.2211
$^4I_{13/2}$	0	0	0.3462
$^4I_{11/2}$	0	0.0042	0.0739
$^4I_{9/2}$	0	0.0788	0.2542
$^4F_{9/2}$	0	0.0003	0.0264
$^2H_{11/2} \rightarrow {}^4I_{15/2}$	0.7125	0.4123	0.0925
$^4I_{13/2}$	0.023	0.0611	0.0529
$^4I_{11/2}$	0.0357	0.1382	0.0371
$^4I_{9/2}$	0.2077	0.0662	0.2858
$^4F_{9/2}$	0.3629	0.0224	0.0022
$^4S_{3/2}$	0	0.1988	0.0101
$^4F_{7/2} \rightarrow {}^4I_{15/2}$	0	0.1468	0.6266
$^4I_{13/2}$	0	0.3371	0.0001
$^4I_{11/2}$	0.0035	0.2648	0.1515
$^4I_{9/2}$	0.0163	0.0954	0.4277
$^4F_{9/2}$	0.0121	0.0342	0.0151
$^4S_{3/2}$	0.0001	0.0058	0
$^2H_{11/2}$	0.1229	0.0153	0.4017
$^4F_{5/2} \rightarrow {}^4I_{15/2}$	0	0	0.2233
$^4I_{13/2}$	0	0.1783	0.3429
$^4I_{11/2}$	0	0.0979	0.0028
$^4I_{9/2}$	0.0107	0.0576	0.1020
$^4F_{9/2}$	0.0004	0.2415	0.3575
$^4S_{3/2}$	0.0082	0.0040	0
$^2H_{11/2}$	0	0.0586	0.1825
$^4F_{7/2}$	0.0765	0.0503	0.1015
$^4F_{3/2} \rightarrow {}^4I_{15/2}$	0	0	0.1272
$^4I_{13/2}$	0	0	0.0345
$^4I_{11/2}$	0	0.0927	0.4861
$^4I_{9/2}$	0	0.2299	0.0558

$^4F_{9/2}$	0	0.0040	0.0595
$^4S_{3/2}$	0.0260	0	0
$^2H_{11/2}$	0	0.0005	0.0030
$^4F_{7/2}$	0.0028	0.0584	0
$^4F_{5/2}$	0.06180	0.0350	0
$^2G_{9/2}\rightarrow{}^4I_{15/2}$	0	0.0190	0.2255
$^4I_{13/2}$	0.0780	0.1194	0.3535
$^4I_{11/2}$	0.0428	0.0824	0.1128
$^4I_{9/2}$	0.0147	0.0062	0.0043
$^4F_{9/2}$	0.0055	0.0314	0.0369
$^4S_{3/2}$	0	0.0019	0.0025
$^2H_{11/2}$	0.0308	0.1828	0.0671
$^4F_{7/2}$	0.1058	0.0488	0.0240
$^4F_{5/2}$	0.0124	0.0259	0.0063
$^2F_{3/2}$	0	0.0208	0.0087
$^4G_{11/2}\rightarrow{}^4I_{15/2}$	0.9181	0.5261	0.1171
$^4I_{13/2}$	0.1013	0.2651	0.2594
$^4I_{11/2}$	0.0003	0.0496	0.0134
$^4I_{9/2}$	0.0716	0.0131	0.0235
$^4F_{9/2}$	0.4252	0.0368	0.0122
$^4S_{3/2}$	0	0.1302	0.0044
$^2H_{11/2}$	0.0004	0.1539	0.0494
$^4F_{7/2}$	0.0877	0.1287	0.0159
$^4F_{5/2}$	0	0.0378	0.0815
$^4F_{3/2}$	0	0.0234	0.0923
$^2G_{9/2}$	0.2906	0.01170	0.1328
$^4G_{9/2}+{}^2K_{15/2}\rightarrow{}^4I_{15/2}$	0.0219	0.2456	0.1991
$^4I_{13/2}$	1.0909	0.3536	0.0421
$^4I_{11/2}$	0.1362	0.1542	0.2632
$^4I_{9/2}$	0.0051	0.2263	0.103
$^4F_{9/2}$	0.2201	0.3897	0.389
$^4S_{3/2}$	0	0.1651	0.0132
$^2H_{11/2}$	0.1157	0.3275	1.2953
$^4F_{7/2}$	0.6062	0.0089	0.1245
$^4F_{5/2}$	0.163	0.0824	0.0489
$^4F_{3/2}$	0	0.171	0.109
$^2G_{9/2}$	0.0269	0.7106	0.121
$^4G_{11/2}$	0.097	0.2616	0.8345
	0	0.0114	0.0598

The calculated values of Ω_t parameters are in good agreement with those reported in many phosphate glass matrices [5-8]. The dependence of the Ω_t parameter as a function of Er^{3+} and Yb^{3+} concentration is plotted in Figure 2.2. For Er^{3+} doped samples, Ω_4 exhibit a monotonic variation indicating less sensitivity to the environment

of the active ion than Ω_2 and Ω_6. Both Ω_2 and Ω_6 decreases as the erbium ion concentration increases and Ba reduce, being a minimum at 2 mol% suggesting a strong dependence with the environment around the active ion. The Ω_2 parameter is closely related to the hypersensitive transitions, i.e., the larger the line strength of the hypersensitive transition, the larger will be the value of Ω_2.

Table 2.3 J-O parameters, spectroscopic quality factor and a measure of accuracy of the fit for different Er^{3+} concentration in Er^{3+} doped and Yb^{3+}-Er^{3+} co-doped phosphate glasses.

Er^{3+}/Yb^{3+} (mol %)	Ω_2	Ω_4	Ω_6	$\chi = \Omega_4/\Omega_6$	ΔS_{rms} (10^{-20} cm^2)
	$10^{-20}\ cm^2$				
0.5/0	5.20	0.81	1.35	0.61	0.184
1/0	4.72	0.92	1.20	0.76	0.144
2/0	4.77	1.15	1.12	1.02	0.170
3/0	4.37	1.10	1.10	1.00	0.193
0.25/2.5	5.81	0.44	1.44	0.30	0.324
0.5/2.5	5.68	0.48	1.42	0.33	0.190
0.75/2.5	4.99	0.64	1.31	0.497	0.158
1.0/2.5	4.55	0.79	1.22	0.648	0.174
0.5/1.5	4.73	1.16	1.32	0.87	0.169
0.5/2	5.17	0.91	1.36	0.67	0.166
0.5/3	5.78	0.58	1.32	0.43	0.240

It is well known that the hypersensitivity is related to the covalency parameter through nephelauxetic effect and it is attributed to the increasing polarizability of the ligands around the rare earth ions. Higher ligand polarizability results in a larger overlap between rare earth and ligands orbital, i.e., higher degree of covalency between rare earth ion and the ligands. Thus, the increment of the rare earth ions concentration and reduction of barium content decreases the Ω_2 and the degree of covalency. This result is contrary to reported ones where an increment of the Ω_2 value was observed with the ionic concentration [9]. This difference suggests that the environment effect is

dominated by Ba ion and is understood considering that having larger field strength is responsible for a higher polarizability of oxygen at the rare earth site.

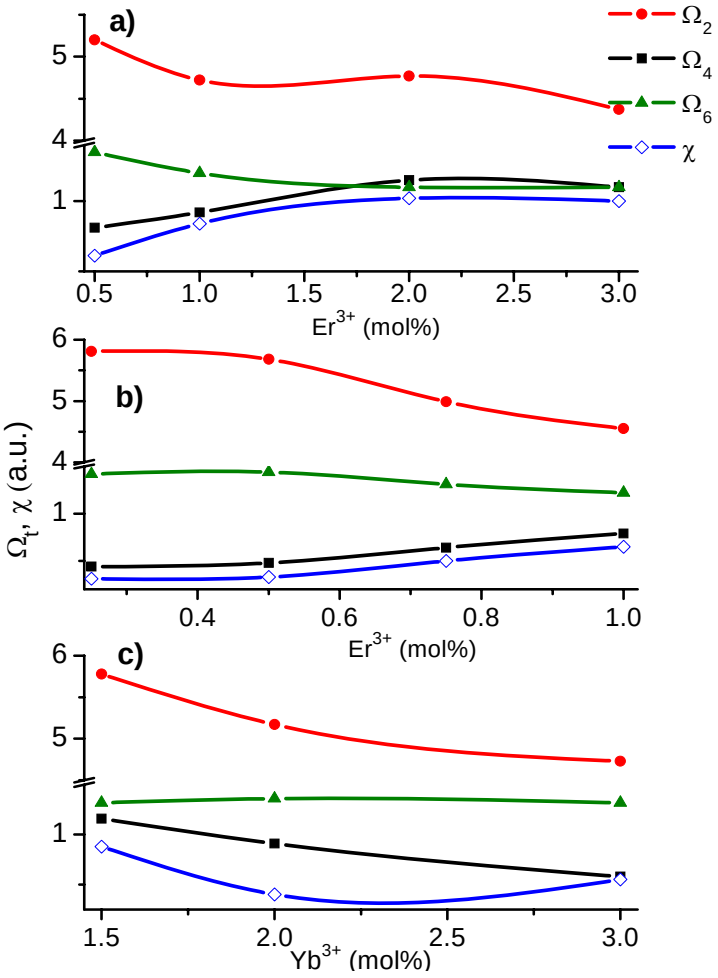

Figure 2.2 Ω_2, Ω_4, Ω_6 and χ for: a) Er^{3+} doped phosphate glasses, b) Er^{3+}/Yb^{3+} (x/2.5) and c) Er^{3+}/Yb^{3+} (0.5/y) co-doped phosphate glasses (all samples in mol%).

The value of Ω_2 is also affected by the asymmetry of the rare earth sites that is reflected in the crystal field parameter. The lower values of Ω_2 result from lower rigidity of the host matrix and may be due to the low asymmetry and rigidity of the rare earth sites. Typically, Ω_6 depend less on the environment than Ω_2 but is more dependent on electron charge density of the 4f shell and the excited orbital. The similar behavior of Ω_2 and Ω_6 suggest that the environment effect is dominant. The increment of Ω_2 after

the minimum suggests an increment on the covalency parameter for concentration higher than 2 mol% of Er^{3+}. In the Yb^{3+}-Er^{3+} co-doped samples, all Ω_t parameters shows a monotonic variation suggesting low sensitivity to the environmental change of Er^{3+} ion, although the presence of Yb^{3+} ion and the net reduction of the Ba content induce an important change in the values of Ω_t parameters. These changes indicate that the presence of Yb^{3+} disturbs the environment of Er^{3+} ion. The spectroscopic quality factor χ is important in predicting the behavior of various lasing transitions in a given matrix. In these samples χ shows an increasing tendency with the increment of Er^{3+} content while a decreasing with the increment of Yb^{3+} content, and reduction of Ba content. For Er^{3+} doped phosphate glasses (series PE) the values range from 0.61 to 1.00, and for Yb^{3+}-Er^{3+} co-doped phosphate glasses (series PEY) it ranges from 0.31 to 0.87; the complete values are displayed in Table 2.3 and the behavior as a function of concentration is shown in Figure 2.2. These values are higher than the most standard laser material (0.3 for Nd^{3+}:YAG) [4] and are in excellent agreement with the values reported for other phosphate glassy host of (0.74 for Er^{3+}/Yb^{3+}:P_2O_5) [5]. It should be noted that the presence of Yb^{3+} ion as sensitizer reduces the quality factor indicating the important role in the dynamics of the Yb^{3+}-Er^{3+} co-doped systems.

Using the Ω_t parameters the radiative transition probability (A_{rad}) from different upper states to the corresponding lower manifold states can be evaluated from the relation

$$A_{rad}(J \to J') = \frac{64\pi^4 e^3}{3h(2J+1)\lambda^3} \times \left[\frac{n(n^2+2)^2}{9} S_{ed} + n^3 S_{md} \right] \tag{2.3}$$

where S_{ed} and S_{md} represent the predicted fluorescence line strength for the induced electric and magnetic dipole transition respectively. S_{ed}, is calculated using Eq. 2.2 and presents a host dependence trough the Ω_t parameters. S_{md}, is ignored here, but will be presented later and can be calculated using the expression

$$S_{md} = \left(\frac{e^2 h^2}{16\pi^2 m^2 c^2} \right) \left| \langle (S,L)J \| L + 2S \| (S',L')J' \rangle \right|^2 \tag{2.4}$$

The values of the radiative transition probabilities as well as the branching ratios for the most common emission bands and for the different concentrations under study are shown in Table 2.4. It can be observed that in general, there is a decreasing tendency in every transition as the Er^{3+} concentration increases except at 3 mol%. In this case a small increment was observed indicating that at certain ionic concentration the dynamics of the ion emission could change. A clear tendency was not observed for the Yb^{3+}/Er^{3+} co-doped samples but certainly the Yb^{3+} content reduces the radiative transition probability. In general, the obtained values are in good agreement with other reported values [5, 10-11].

Table 2.4 Calculated radiative decay rate and branching ratios of Er^{3+} ion for, a) 0.5, 1, 2 and 3 of Er^{3+} doped samples, b) 0.25/2.5, 0.5/2.5, 0.75/2.5 and 1/2.5 of Er^{3+}/ Yb^{3+} and c) 0.5/1, 0.5/2 and 0.5/3 of Er^{3+}/ Yb^{3+} co-doped samples (all glasses in mol%).

a)

Transition	0.5 Er^{3+}(mol%)		1 Er^{3+}(mol%)		2 Er^{3+}(mol%)		3 Er^{3+}(mol%)	
	$A_{JJ'}(s^{-1})$	$\beta_{JJ'}$	$A_{JJ'}(s^{-1})$	$\beta_{JJ'}$	$A_{JJ'}(s^{-1})$	$\beta_{JJ'}$	$A_{JJ'}(s^{-1})$	$\beta_{JJ'}$
$^4I_{13/2} \rightarrow {}^4I_{15/2}$	101.93	1.00	88.59	1.00	85.23	1.00	83.754	1.00
$^4I_{11/2} \rightarrow {}^4I_{15/2}$	142.78	0.89	123.09	0.89	120.99	0.89	114.543	0.89
$^4I_{13/2}$	16.87	0.11	14.88	0.11	14.55	0.11	14.235	0.11
$^4I_{9/2} \rightarrow {}^4I_{15/2}$	71.19	0.60	75.20	0.65	97.18	0.72	89.794	0.71
$^4I_{13/2}$	46.58	0.39	39.99	0.35	37.83	0.28	37.227	0.29

$^4I_{11/2}$	0.19	0.00	0.17	0.00	0.17	0.00	0.168	0.00
$^4F_{9/2}\rightarrow{}^4I_{15/2}$	890.45	0.89	845.16	0.90	994.87	0.91	900.371	0.90
$^4I_{13/2}$	42.49	0.04	40.77	0.04	46.50	0.04	44.062	0.04
$^4I_{11/2}$	63.46	0.06	54.37	0.06	52.04	0.05	50.979	0.05
$^4I_{9/2}$	3.72	0.00	3.24	0.00	3.30	0.00	3.078	0.00
$^4S_{3/2}\rightarrow{}^4I_{15/2}$	1076.52	0.53	920.14	0.53	975.05	0.54	856.999	0.52
$^4I_{13/2}$	443.34	0.22	377.90	0.22	370.78	0.21	352.494	0.21
$^4I_{11/2}$	32.11	0.02	27.43	0.02	26.56	0.01	25.975	0.02
$^4I_{9/2}$	463.39	0.23	413.56	0.24	432.72	0.24	406.651	0.25
$^4F_{9/2}$	0.60	0.00	0.50	0.00	0.47	0.00	0.471	0.00
$^2H_{11/2}\rightarrow{}^4I_{15/2}$	5806.01	0.96	5129.70	0.96	6091.98	0.96	4952.22	0.96
$^4I_{13/2}$	94.47	0.02	86.01	0.02	95.18	0.02	86.426	0.02
$^4I_{11/2}$	49.04	0.01	45.86	0.01	51.12	0.01	47.806	0.01
$^4I_{9/2}$	89.98	0.01	79.13	0.01	80.18	0.01	75.248	0.01
$^4F_{9/2}$	22.20	0.00	19.49	0.00	19.60	0.00	18.293	0.00
$^4S_{3/2}$	0.02	0.00	0.02	0.00	0.03	0.00	0.029	0.00

b)

Transition	$0.25Er^{3+}$(mol%)		$0.5Er^{3+}$(mol%)		$0.75Er^{3+}$(mol%)		$1Er^{3+}$(mol%)	
	$A_{JJ'}(s^{-1})$	$\beta_{JJ'}$	$A_{JJ'}(s^{-1})$	$\beta_{JJ'}$	$A_{JJ'}(s^{-1})$	$\beta_{JJ'}$	$A_{JJ'}(s^{-1})$	$\beta_{JJ'}$
$^4I_{13/2}\rightarrow{}^4I_{15/2}$	102.46	1.00	103.98	1.00	96.06	1.00	90.50	1.00
$^4I_{11/2}\rightarrow{}^4I_{15/2}$	147.91	0.90	148.86	0.90	135.07	0.90	125.40	0.89
$^4I_{13/2}$	16.71	0.10	16.94	0.10	15.77	0.10	14.97	0.11
$^4I_{9/2}\rightarrow{}^4I_{15/2}$	40.18	0.46	43.39	0.47	56.05	0.56	66.47	0.62
$^4I_{13/2}$	47.58	0.54	48.30	0.53	44.26	0.44	41.36	0.38
$^4I_{11/2}$	0.17	0.00	0.17	0.00	0.17	0.00	0.17	0.00
$^4F_{9/2}\rightarrow{}^4I_{15/2}$	726.82	0.88	752.50	0.88	781.01	0.89	808.99	0.89
$^4I_{13/2}$	34.14	0.04	35.10	0.04	36.72	0.04	38.35	0.04
$^4I_{11/2}$	65.49	0.08	66.03	0.08	60.06	0.07	55.87	0.06
$^4I_{9/2}$	3.97	0.00	3.89	0.00	3.44	0.00	3.15	0.00
$^4S_{3/2}\rightarrow{}^4I_{15/2}$	1104.40	0.54	1120.87	0.54	1024.69	0.54	955.57	0.53
$^4I_{13/2}$	454.83	0.22	461.61	0.22	422.00	0.22	393.53	0.22
$^4I_{11/2}$	32.40	0.02	32.92	0.02	30.37	0.02	28.56	0.02
$^4I_{9/2}$	438.04	0.22	447.54	0.22	427.76	0.22	415.04	0.23
$^4F_{9/2}$	0.61	0.00	0.62	0.00	0.57	0.00	0.53	0.00
$^2H_{11/2}\rightarrow{}^4I_{15/2}$	5961.83	0.96	5860.11	0.96	5304.77	0.96	4954.08	0.96
$^4I_{13/2}$	89.22	0.01	89.43	0.01	85.14	0.02	82.81	0.02
$^4I_{11/2}$	43.51	0.01	43.74	0.01	43.12	0.01	43.19	0.01
$^4I_{9/2}$	93.70	0.02	92.62	0.02	83.36	0.02	77.26	0.01
$^4F_{9/2}$	23.69	0.00	23.16	0.00	20.51	0.00	18.77	0.00
$^4S_{3/2}$	0.01	0.00	0.01	0.00	0.02	0.00	0.02	0.00

c)

Transition	$1Yb^{3+}$ (mol%)		$2Yb^{3+}$(mol%)		$3\ Yb^{3+}$(mol%)	
	$A_{JJ'}(s^{-1})$	$\beta_{JJ'}$	$A_{JJ'}(s^{-1})$	$\beta_{JJ'}$	$A_{JJ'}(s^{-1})$	$\beta_{JJ'}$
$^4I_{13/2}\rightarrow{}^4I_{15/2}$	98.41	1.00	100.19	1.00	96.80	1.00
$^4I_{11/2}\rightarrow{}^4I_{15/2}$	133.26	0.89	139.07	0.89	140.06	0.90

$^4I_{13/2}$	16.45	0.11	16.61	0.11	15.96	0.10
$^4I_{9/2}\rightarrow{}^4I_{15/2}$	94.37	0.68	75.96	0.62	50.35	0.53
$^4I_{13/2}$	44.44	0.32	45.68	0.37	44.46	0.47
$^4I_{11/2}$	0.19	0.00	0.19	0.00	0.17	0.00
$^4F_{9/2}\rightarrow{}^4I_{15/2}$	998.17	0.90	907.77	0.89	750.99	0.88
$^4I_{13/2}$	47.73	0.04	43.27	0.04	36.25	0.04
$^4I_{11/2}$	59.55	0.05	61.91	0.06	61.88	0.07
$^4I_{9/2}$	3.27	0.00	3.55	0.00	3.94	0.00
$^4S_{3/2}\rightarrow{}^4I_{15/2}$	1023.42	0.53	1054.91	0.53	1029.90	0.54
$^4I_{13/2}$	421.47	0.22	434.45	0.22	424.14	0.22
$^4I_{11/2}$	30.97	0.02	31.57	0.02	30.42	0.02
$^4I_{9/2}$	470.87	0.24	461.13	0.23	423.13	0.22
$^4F_{9/2}$	0.57	0.00	0.59	0.00	0.57	0.00
$^2H_{11/2}\rightarrow{}^4I_{15/2}$	5296.86	0.96	5592.41	0.96	6002.85	0.96
$^4I_{13/2}$	94.07	0.02	93.15	0.02	90.28	0.01
$^4I_{11/2}$	51.03	0.01	48.84	0.01	45.50	0.01
$^4I_{9/2}$	81.70	0.01	86.72	0.01	92.36	0.01
$^4F_{9/2}$	19.43	0.00	21.17	0.00	23.63	0.00
$^4S_{3/2}$	0.03	0.00	0.02	0.00	0.01	0.00

The total radiative transition probabilities permit to calculate the radiative lifetime τ_{rad} for an excited state J by using the expression

$$\tau_{rad} = \left\{ \sum_{'} A(J \rightarrow J') \right\}^{-1} \tag{2.5}$$

From equations 2.3 and 2.5 it may be observed that the radiative lifetime is inversely proportional to the refractive index of the glass host. The numerical values of the radiative lifetimes for all concentrations are shown in Table 2.5. In general, the values range of radiative decay time of $^4I_{13/2}\rightarrow{}^4I_{15/2}$ transition of Er^{3+} is around 10 ms, changing a little with the Er^{3+} concentration and is less sensitive to the Yb^{3+} ion concentration. Adding the radiative transition probability of every transition (running over all final state J') results in the total radiative transition probability that is related with the fluorescence branching ratio β_R by the expression

$$\beta_R(J \to J') = \frac{A(J \to J')}{\sum A(J \to J')} \tag{2.6}$$

The fluorescence branching ratio characterize the possibility to attain stimulated emission from any specific transition and shows a host dependence trough the Ω_t parameters and the numerical values are also shown in Table 2.4.

Table 2.5 Stimulated emission-cross section (σ_{emi}), radiative (τ_{rad}) and fluorescence decay time (τ_{exp}), and quantum efficiency (η) of $^4I_{13/2} \rightarrow {}^4I_{15/2}$ transition of Er^{3+} doped and Yb^{3+}/Er^{3+} co-doped phosphate glasses.

Er^{3+}/ Yb^{3+} (mol %)	σ_{emi} (10^{-21} cm^2)	τ_{rad} (ms)	τ_{exp}(ms)	η(%)
0.5/0	5.6	10.1	6.0	60
1/0	5.0	11.3	4.8	42
2/0	4.33	11.6	3.16	27
3/0	4.13	11.9	2.98	25
0.25/2.5	5.76	9.71	8.2	84
0.5/2.5	5.78	9.62	6.95	72
0.75/2.5	4.88	10.4	6.20	50
1.0/2.5	4.52	11.0	6.14	55
0.5/1.5	5.47	10.2	6.58	64
0.5/2	5.65	9.98	6.86	68
0.5/3	5.24	10.3	7.0	67

2.4 Fluorescence analysis

2.4.1 Infrared and up-conversion luminescence spectra

The normalized emission spectra of 0.5 and 3 mol% of Er^{3+} doped phosphate glasses are shown in Figure 2.3. The peak wavelength of this emission was observed at 1.532 μm and the entire band ranges from 1400 to 1700 nm corresponding to $^4I_{13/2} \rightarrow {}^4I_{15/2}$ transition. From this figure it can be observed that the bandwidth increased significantly from 33 to 40 nm when the Er^{3+} concentration increased from 0.5 to 3 mol%. This phenomenon has been observed on other glass hosts [12-13] and it is

explained on the basis of number of structural units present in glasses [14]. Particularly this increment is beneficial for optical amplifiers because the transmission capacity of WDM systems increase (i.e. the number of combination of communication of channels to be amplified increases).

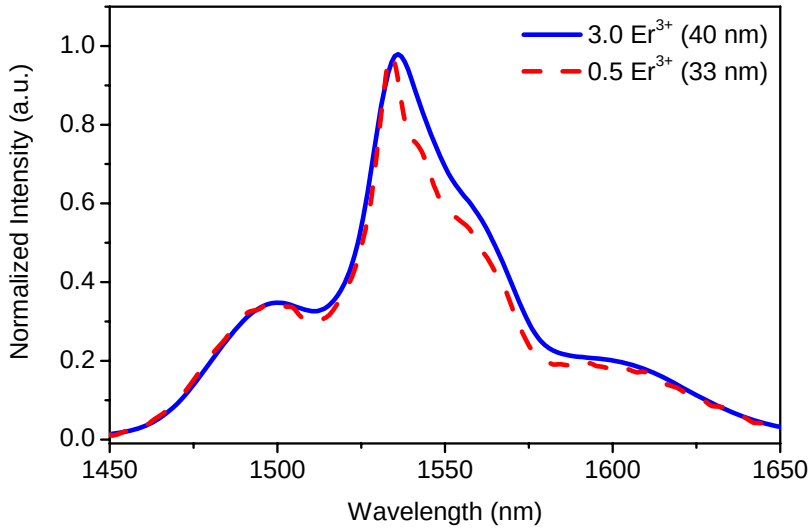

Figure 2.3 Emission spectra bandwidth of $^4I_{13/2} \rightarrow {}^4I_{15/2}$ Er^{3+} transition for 0.5 and 3 mol% of Er^{3+} doped phosphate glasses.

For Er^{3+} doped samples no visible up-conversion signal was observed in our system due to the high phonon energy of the host. However, in Er^{3+}/Yb^{3+} co-doped phosphate glasses three weak emission bands in 526 nm ($^2H_{11/2} \rightarrow {}^4I_{15/2}$), 548 nm ($^4S_{3/2} \rightarrow {}^4I_{15/2}$) and 660 nm ($^4F_{9/2} \rightarrow {}^4I_{15/2}$) were observed, see figure 2.4. That means that the Yb^{3+} concentration plays an important role in the dynamic of the Er^{3+} emission. Notice that the intensity of red band is larger than green bands. This characteristic is promoted partly by the addition of Yb^{3+} ions and partly by the high phonon energy of phosphate glass. The complete analysis of the effect of Yb^{3+} concentration and other possible mechanism will be studied later.

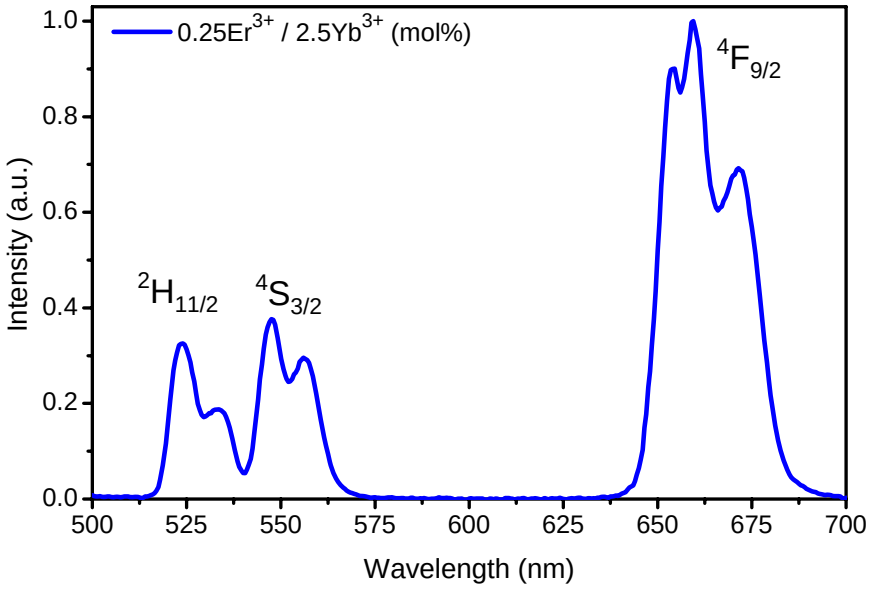

Figure 2.4 Up-conversion emission of Er^{3+}/Yb^{3+} co-doped phosphate glass

2.4.2 Emission cross section (ECS) of $^4I_{13/2} \rightarrow {}^4I_{15/2}$ transition of Er^{3+}

The stimulated emission cross section (ECS) for $^4I_{13/2} \rightarrow {}^4I_{15/2}$ transition was evaluated from the measured emission line shape using the expression [15]

$$\sigma_{emi}(\lambda_p) = \frac{\lambda_p^4 A_{rad}}{8\pi c n^2 \Delta\lambda_{eff}}, \tag{2.7}$$

where λ_p is the peak fluorescence wavelength and A_{rad} is the radiative transition probability, which can be expressed in terms of Ω_t by

$$A_{rad}(^4I_{13/2} \rightarrow {}^4I_{15/2}) = \frac{64\pi^4 e^3}{3h(2J+1)\lambda^3} \times \left[\frac{n(n^2+2)^2}{9}(0.0188\Omega_2 + 0.1176\Omega_4 + 1.4617\Omega_6)\right]$$

(2.8)

Since the emission band is found to be slightly asymmetric an effective line width ($\Delta\lambda_{eff}$) was determined using the expression

$$\Delta \lambda_{eff} = \int \frac{I(\lambda)}{I_p} d\lambda \tag{2.9}$$

where I_p is the peak fluorescence intensity corresponding to λ_p. The calculated values of the emission cross-section as a function of the ionic concentration are listed in Table 8 and their behavior is shown in Figure 2.5. The emission cross section decreases with the increment of the Er^{3+} concentration, both in Er^{3+} doped and Er^{3+}/Yb^{3+} co-doped samples, being the maximum for lower concentration, as is shown in Figure 2.6a

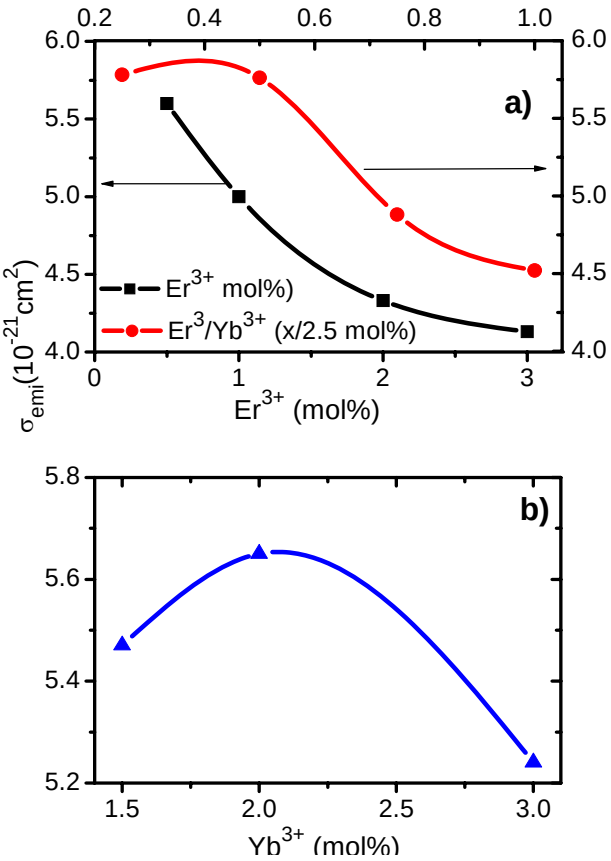

Figure 2.5 Emission cross-section as a function of the Er^{3+} concentration for doped and Yb^{3+}/Er^{3+} co-doped system a)Er^{3+}/Yb^{3+} (x/2.5 mol %) b) Er^{3+}/Yb^{3+} (0.5/y mol %).

The changes in Yb^{3+} concentration suggest an optimum concentration of 2.5 mol% where the maximum emission cross section for 0.5 mol% of Er^{3+} was obtained, see Figure 2.5b. Notice that these behaviors are similar to the Ω_6 behavior suggesting that the influence of the matrix changes the spectroscopic properties. From equation 5.8 it can be seen that the parameter Ω_6 is more dominant in the value of A_{rad}. This is because, among the three squared reduced matrix element, $[U^6]^2$ has the highest value. Thus an increas in the value of Ω_6 means necessarily an increas in the value of ECS, as shown in Figure 2.6.

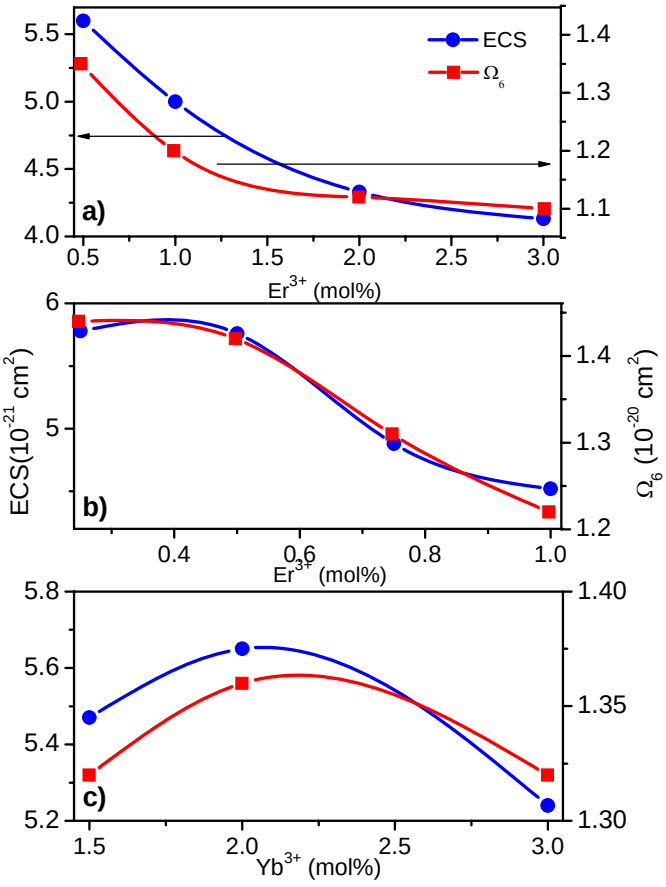

Figure 2.6 Behavior of emission cross section and Ω_6 as a function of Er^{3+} and Yb^{3+} for a) Er^{3+} doped samples, b) Er^{3+}/Yb^{3+} (x/2.5) co-doped samples and c) Er^{3+}/Yb^{3+} (0.5/y) co-doped samples (mol%)

2.4.3 Fluorescence lifetime and quantum efficiency

The fluorescence decay time of $^4I_{13/2} \rightarrow {}^4I_{15/2}$ transition was measured to evaluate the quantum efficiency of the samples as a function of the rare earth concentration. It was found that the lifetime decrease with the increase of Er^{3+} concentration and slightly increases with the increment of sensitizer Yb^{3+} ion, see Figure 2.7. The decrease of lifetime is associated to the fluorescence quenching phenomenon, up-conversion and cross-relaxation [16,17]. In addition to the concentration quenching process, OH content and multiphonon relaxation could also contribute to the non-radiative processes [17]. On the other hand the lifetime of such transition increase from 6.59 to 7.0 ms when Yb_2O_3 increase from 1.5 to 3.0 mol%, see Figure 2.7. This is the result of a better dispersion of Er^{3+} avoiding cluster formation that in turn avoids fluorescence quenching.

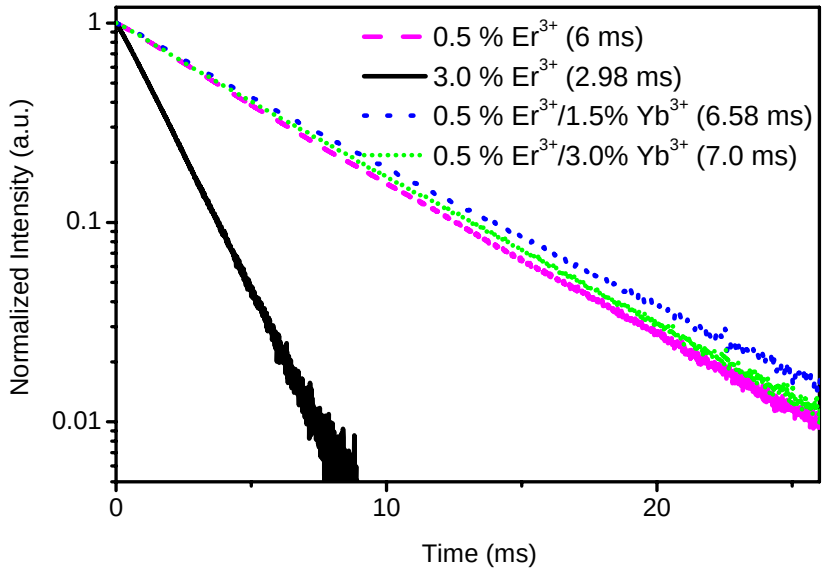

Figure 2.7 Fluorescence lifetime of $^4I_{13/2} \rightarrow {}^4I_{15/2}$ transition for 0.5 and 3 mol% of Er^{3+} doped samples and 0.25/2.5 mol% of Er^{3+}/Yb^{3+} co-doped sample.

With these measured values quantum efficiency (η) was calculated as the ratio of the effective radiative decay time to the radiative decay time expressed by

$$\eta = \frac{\tau_{rad}}{\tau_{\exp}} \tag{2.10}$$

The obtained values are summarized in Table 2.5 and the behavior of η is shown on Figure 2.8. The experimental results show a decrease of the quantum efficiency with the increase of the Er^{3+} concentration. The highest and lowest efficiency obtained is 84% for $0.25Er^{3+}/2.5Yb^{3+}$ (mol %) and 25% for $3Er^{3+}$ (mol %) respectively.

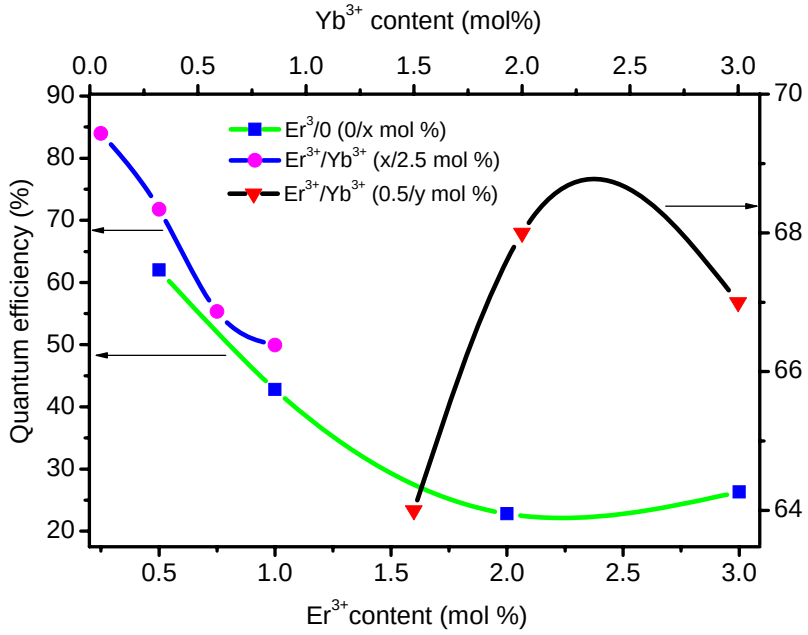

Figure 2.8 Quantum efficiency of Er^{3+} doped and Er^{3+}/Yb^{3+} co-doped samples as a function of the Er^{3+} and Yb^{3+} concentration.

The obtained quantum efficiency is comparable to other results reported recently, is good enough such that this glassy system could be considered as a good

candidate for the eye safe laser emission at 1.53 μm. The low quantum efficiency is consequence of the presence of non-radiative processes due to the cluster formation of Er^{3+} ion and probably due to the presence of OH content.

Bibliography

[1]. E. Desurvire, Erbium doped fiber amplifiers: principles and applications, 1994 Wiley Interscience.

[2]. B.R. Judd; Phys. Rev. 127(1962) 750.

[3]. G.S. Ofelt; J. Chem. Phys. 37(1962) 511.

[4]. A.A. Kaminskii, Laser Crystals: Their Physics and Properties, Springer Verlag, New York, 1990

[5]. D. K. Sardar, J.B. Gruber, B. Zandi, J.A. Hutchinson and C.W. Trussell; J. Appl. Phys. 93, (2003) 2041.

[6]. A. Speghini, R. Francini, A. Martinez, M. Tavernese and M. Bettinelli ; Spect. Acta Part A, 57 (2001) 2001.

[7]. G.C. Reghini, S. Pelli, M. Fossi, M. Brenci, A.A. Lipovski, E.V. Kolobkova, A. Speghini and M. Bettinelli; SPIE 4282, (2001) 210.

[8]. L. Zhang, H. Hu, C. Qi and F. Lin; Opt. Mat. 17, (2001) 371.

[9]. S. Tanabe, T. Ohyagi, N. Soga and T. Hanada; Phys. Rev. B 46, (1992) 3305.

[10]. A. Speghini, R. Francini, A. Martinez, M. Tavernese and M. Bettinelli ; Spect. Acta Part A, 57(2001) 2001.

[11]. G. C. Reghini, S. Pelli, M. Fossi, M. Brenci, A.A. Lipovski, E.V. Kolobkova, A. Speghini and M. Bettinelli; SPIE 4282, (2001) 210

[12]. H. Desirena, E. De la Rosa, A. Schülzgen, S. Sabet, N. Peyghambarian, J. Phys D: Appl. Phys. 41 (2008) 095102.

[13]. W.J. Chung, A. Jha, S. Shen, P. Joshi, Philos. Mag. 84 (2004) 1197.

[14]. A. Jha, S. Shen, and M. Naftaly, Phys. Rev. B 62 (2000) 6215.

[15]. J.F. Philipps, T. Topfer, H. Ebendorff-Heidepriem, D. Ehrt and R. Sauerbrey; Appl. Phys. B 72 (2001) 399.

[16]. M.P. Hehlen, N.J. Cockroft, T.R. Gosnell and A.J. Bruce; Phys. Rev. B 15, (1997) 9302.

[17]. B.C. Hwang, S. Jiang, T. Luo, J. Watson, G. Sorbello and N. Peyghambarian; J.Opt. Soc. Am. B, 17 (2000) 835.

CHAPTER 3
EFFECT OF Ce^{3+} AND B_2O_3 CO-DOPING ON FLUORESCENCE PROPERTIES IN Er^{3+}/Yb^{3+} CODOPED PHOSPHATE GLASSES

In this chapter, it is reported a comparative study of Ce^{3+} and B_2O_3 concentration effect on the fluorescence properties of Er^{3+}/Yb^{3+} co-doped phosphate glasses. Ce^{3+} and B_2O_3 co-doping improved the accumulation of population of $^4I_{13/2}$ level, resulting on an enhancement of the fluorescence quantum yield at 1.53 μm. The obtained results show that by choosing the right Ce^{3+} and B_2O_3 concentration is possible to increase the $^4I_{13/2}$ fluorescence lifetime as long as 9 ms. The best combination of $Yb^{3+}/Er^{3+}/Ce^{3+}$ and Yb^{3+}/Er^{3+}/B ions concentration in order to maximize the efficiency of the eye-safe laser emission were found.

3.1 Name of phosphate glasses

The samples glasses were prepared from the starting chemical constituents, sodium phosphate ($NaH_2PO_4H_2O$), boron oxide (B_2O_3), aluminium oxide (Al_2O_3), barium oxide (BaO), potassium carbonate (K_2CO_3), erbium oxide (Er_2O_3), ytterbium oxide (Yb_2O_3) and cerium oxide (Ce_2O_3) (all from Aldrich 99.99% pure) according to the glass composition, P_2O_5-Al_2O_3-BaO-K_2O-Er_2O_3-Yb_2O_3-X_2O_3 where X = Ce and B. The samples were prepared reducing the potassium content with the Ce^{3+} or B^{3+} addition and keeping the rare earth constant; the change of the potassium content ranges from 0.5 to 6 mol%. Four samples were prepared for 0.5, 1.0, 2.0 and 4.0 mol% of Ce_2O_3 denoted by PEYC05, PEYC1, PEYC2 and PEYC4 respectively. And four samples doped with 1, 1.5, 2.0, 4, and 6 mol% of B_2O_3 were prepared and denoted by PEYB1, PEYB15, PEYB2, PEYB4, and PEYB6, respectively. The tag of samples and

corresponding concentration are listed in table 3.1. The complete procedure to prepare phosphate glass was described in chapter 1.

Table 3.1 Name of phosphate glasses under study.

Tag	$0.15Er^{3+}/2.5Yb^{3+}/xCe^{3+}$	Tag	$0.15Er^{3+}/2.5Yb^{3+}/xB^{3+}$
PEYC01525	0	PEYB01525	0
PEYC0152505	0.5	PEYB015251	1
PEYC015251	1	PEYB0152515	1.5
PEYC015252	2	PEYB015252	2
PEYC015254	4	PEYB015254	4
		PEYB015256	6

3.2 Infrared and up-conversion emission spectra

Er^{3+} doped glasses with low phonon energy have been studied for visible upconversion laser due to strong emission of $^4S_{3/2} \rightarrow {}^4I_{15/2}$ transition [1-4]. When considering the applications of active materials such as amplifiers and laser, this visible emission is associated to an efficiency decrease because population from is $^4I_{11/2}$ re-exited and populates $^4S_{3/2}$ that produces radiation at 548 nm by relaxation to the ground state ($^4I_{15/2}$). All this process produce a deleterious to pathway associated to 1.53 μm emission. As is expected this visible emission decrease gradually as the phonon energy increase. Then, a host glass with high phonon energy is necessary. However if the phonon energy is too high a deleterious effect is also observed in the 1.53 μm emission. No visible up-conversion has been observed on Er^{3+} doped phosphate glasses, which have phonon energy of 1100 cm^{-1}. However in Er^{3+}/Yb^{3+} codoped glasses, due to high cross section of Yb more ions are exited to $^4I_{11/2}$ and $^4F_{7/2}$ level by ET from Yb to Er. The overall process produces green and red up-conversion emission [5], reducing the efficiency of $^4I_{13/2} \rightarrow {}^4I_{15/2}$ transition. Thus in order to avoid the promotion $^4I_{11/2} \rightarrow {}^4F_{7/2}$

and increase the non-radiative relaxation to $^4I_{13/2}$ level Ce^{3+} and B_2O_3 were incorporated. However, the shortening of $^4I_{11/2}$ lifetime with the Ce^{3+} and B_2O_3 concentration is accompanied by a rather pronounced simultaneous quenching of $^4I_{13/2}$ level. This effect has been reported by different authors [6-12]. Interestingly, in our samples follow different behavior and this effect will be discussed below.

3.2.1 NIR emission

The infrared emission spectrum ($^4I_{13/2} \rightarrow {}^4I_{15/2}$) of Er^{3+} in $Yb^{3+}/Er^{3+}/Ce^{3+}$ and $Yb^{3+}/Er^{3+}/ B_2O_3$ co-doped phosphate glasses are illustrated in Figure 3.1.

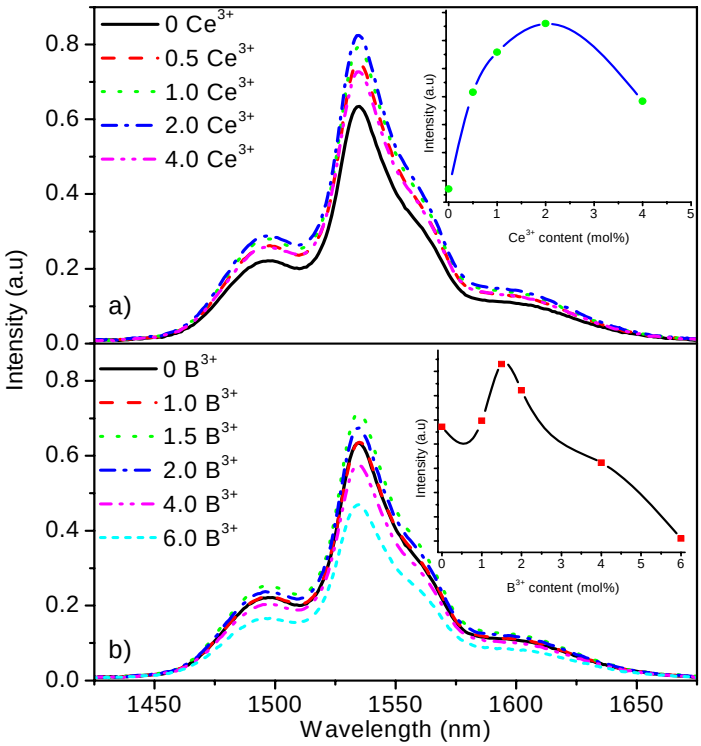

Figure 3.1 Er^{3+} emission spectra in a)$Er^{3+}/Yb^{3+}/Ce^{3+}$ and b)$Er^{3+}/Yb^{3+}/B_2O_3$ co-doped samples

The eye safe emission peak is centered at 1.53 μm with an spectral bandwidth of 38 nm for both, $Yb^{3+}/Er^{3+}/Ce^{3+}$ and $Yb^{3+}/Er^{3+}/B^{3+}$ co-doped systems. The Ce^{3+} and B_2O_3

concentration modifies the intensity of the signal increasing monotonically with the increment of both ions and showing a maximum at 2.0 mol% and 1.5 mol% respectively, see Figure 3.1a and 3.1b. It is also observed that at higher concentrations the intensity decrease, as is show in inset curve of Figure 3.1.

.

3.2.2 Up-conversion emission

Three weak visible transition $^2H_{11/2}$, $^4S_{3/2}$, $^4F_{9/2} \rightarrow {}^4I_{15/2}$ centered at 526, 548 and 660 nm, respectively, were observed and are shown in Figure 3.2. This visible emission is the result of well-know up-conversion process and, in this case, it depends on the concentration of both Ce^{3+} and B_2O_3 ions. The overall intensity of the upconverted signal decreases monotonically with the increment of Ce^{3+} and B^{3+} concentration, see Figure 3.2.

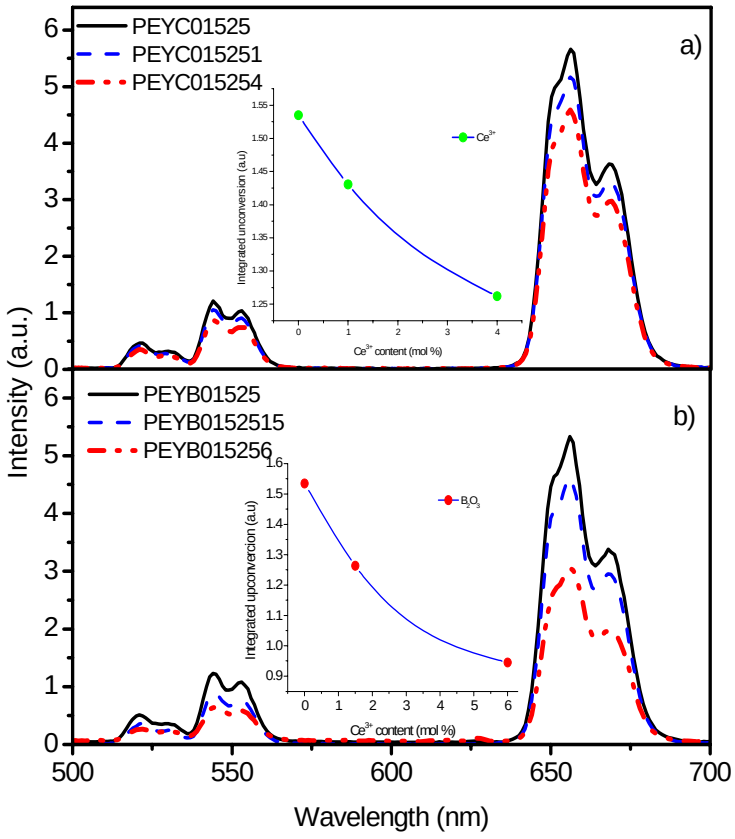

Figure 3.2 Up-conversion emissions as a function of a) Ce^{3+} and b) B_2O_3 concentration.

It is observed that the red emission is larger than the green one, partly because of the high phonon energy of phosphate glass that depopulate the $^4I_{11/2}$ level and partly by the presence of Yb^{3+} that promote population to $^4F_{9/2}$.

3.3 Physical mechanism

The physical mechanism that describes both weak visible and strong NIR emissions may be described as follow. Er^{3+} ion, are excited by direct excitation from the ground state ($^4I_{15/2} + h\nu \rightarrow {}^4I_{11/2}$) and by energy transfer from the Yb^{3+} that is also are excited directly ($^2F_{5/2} + h\nu \rightarrow {}^2F_{7/2}$) by the pumping signal. However, the most probably mechanism is the energy transfer (ET) expressed as $^4I_{15/2}(Er^{3+}) + {}^2F_{5/2}(Yb^{3+}) \rightarrow {}^4I_{11/2}(Er^{3+}) + {}^2F_{7/2}(Yb^{3+})$ and is due to the larger absorption cross section of Yb^{3+} and the resonance between $^2F_{5/2} \rightarrow {}^2F_{7/2}$ and $^4I_{15/2} \rightarrow {}^4I_{11/2}$ transitions of Yb^{3+} and Er^{3+}, respectively, as is shown in the energy diagram in Figure 3.3. Mostly of the $^4I_{11/2}$ excited ions relaxes non-radiatively to $^4I_{13/2}$ level due to high phonon energy of phosphate glass and from here relaxes to ground state producing the strong 1.53 μm emission band. A little part of the population was promoted to $^4F_{7/2}$ level by the ET from the relaxation of another excited Yb^{3+} ($^2F_{5/2} \rightarrow {}^2F_{7/2}$) or Er^{3+} ($^4I_{11/2} \rightarrow {}^4I_{15/2}$) ion. The ions in $^4F_{7/2}$ level decay non-radiatively to $^2H_{11/2}$ and $^4S_{3/2}$ due to phonon energy. From here only little part of the population decay to ground state producing the weak green emissions centered at 526 and 548 nm. Most of population decay non-radiatively to $^4F_{9/2}$ level and subsequently partly decay radiatively to $^4I_{15/2}$ producing the red emission centered at 670 nm and partly decay non-radiatively to $^4I_{9/2}$. The enhancement of the 1.53 μm signal emitted with increment of Ce^{3+} concentration is explained in terms of the increment of population on $^4I_{13/2}$ band due to non-radiative transition $^4I_{11/2} \rightarrow {}^4I_{13/2}$ promoted by the presence of Ce^{3+} according to the equation $^4I_{11/2}$ (Er^{3+})+

$^2F_{5/2}(Ce^{3+})\rightarrow{}^4I_{13/2}(Er^{3+})+{}^2F_{7/2}(Ce^{3+})$. That means the resonance between transitions $^4I_{11/2}\rightarrow{}^4I_{13/2}$ of Er^{3+} and $^2F_{5/2}\rightarrow{}^2F_{7/2}$ of Ce^{3+} promotes the non-radiative decay of $^4I_{11/2}$ increasing the population of $^4I_{13/2}$ level. The faster relaxation of $^4I_{11/2}$ reduces the promotion of population to $^4S_{3/2}$, $^4F_{9/2}$ level of Er^{3+} that are also resonant with the $^2F_{5/2}$ level of Ce^{3+}, see figure 3.3. The enhancement with B_2O_3 is explained in terms of increment of population of $^4I_{13/2}$ level as result of non-radiative relaxation produced by increment of phonon energy. The overall result is a quenching of the up-converted signal and an enhancement of the 1.53 μm emitted. The mechanism proposed to explain the signal emitted of co-doped glasses is well described in Figure 3.3.

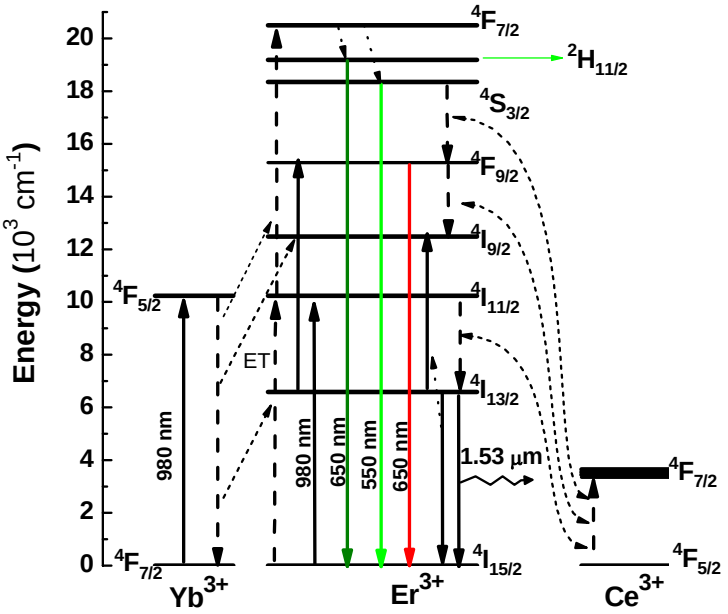

Figure 3.3 Energy level diagram of the $Er^{3+}/Yb^{3+}/Ce^{3+}$ system and the mechanism proposed to explain both visible and infrared emissions.

3.4 $^4I_{13/2}$ Fluorescence lifetime in $Er^{3+}/Yb^{3+}/Ce^{3+}$ and $Er^{3+}/Yb^{3+}/B^{3+}$ co-doped phosphate glasses.

The addition of $Ce^{3+}$to Er^{3+} doped samples increment the non-radiative transition rate from $^4I_{11/2}$ to $^4I_{13/2}$ level and reduce the green and red signal intensity, resulting on

enhancement of 1.53 μm emission intensity associated to $^4I_{13/2} \rightarrow {}^4I_{15/2}$ transition. However, it have been reported that the enhancement of such transition has an effect adverse on fluorescence lifetime, this phenomenon has been observed in different Er^{3+}/Ce^{3+} co-doped samples [6-9]. Interestingly in our samples ($Er^{3+}/Yb^{3+}/Ce^{3+}$ and $Er^{3+}/Yb^{3+}/B^{3+}$ co-doped phosphate glasses) an opposite trend of fluorescence lifetime was observed. Figure 3.4 shows the typical plot of decay time for different Ce^{3+} and B^{3+} concentrations. The fluorescence decay time of all samples at 1.53 μm emissions are resumed in Table 3.2 and the behavior is shown in Figure 3.5. In our samples increase from 8.2 to 8.9 ms when Ce_2O_3 increase from 0 to 1 mol % and then decrease to 8.5 ms for 4 mol %. The increment on the decay time is the result of the increment of population on $^4I_{13/2}$ level. The decrement on the decay time is the result of the fluorescence quenching of Er^{3+} according to the equation $^4I_{13/2}(Er^{3+})+ {}^4I_{13/2}(Er^{3+}) \rightarrow {}^4I_{15/2}(Er^{3+}) + {}^4I_{9/2}(Er^{3+})$.

Table 3.2 $^4I_{13/2}$ Fluorescence lifetimes as a function of Ce^{3+} and B_2O_3 concentrations.

Ce^{3+} content (mol%)	$^4I_{13/2}$ (ms)	B^{3+} content (mol%)	$^4I_{13/2}$ (ms)
0	8.2	0	8.2
0.5	8.7	1	8.44
1	8.9	1.5	8.64
2	8.75	2	8.44
4	8.5	4	7.99
		6	7.8

For $Er^{3+}/Yb^{3+}/B^{3+}$ system, the fluorescence lifetime of such transition increase monotonically from 8.2 to 8.64 ms when B_2O_3 increase from 0 to 1.5 mol% and decrease to 7.8 ms for 6 mol%. The increment is partly the result of optimization population of $^4I_{13/2}$ level and partly because B_2O_3 is glass networks former, thus their addition into phosphate glasses increase the solubility of Er^{3+} avoiding the cluster

formation that in turn avoids fluorescence quenching. The decrement is attributed to the increment of high phonon that promotes non-radiative relaxation. Such radiation could promote the cross relaxation according to the equation $^4I_{13/2}(Er^{3+})+ {}^4I_{13/2}(Er^{3+}) \rightarrow {}^4I_{15/2}(Er^{3+}) + {}^4I_{9/2}(Er^{3+})$.

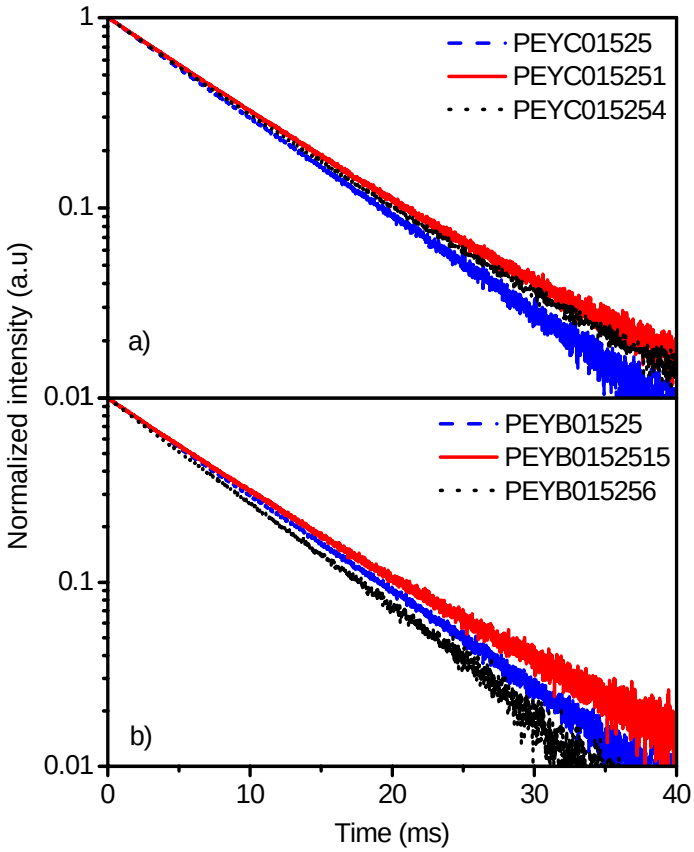

Figure 3.4 Fluorescence decay time of $^4I_{13/2} \rightarrow {}^4I_{15/2}$ transition for a) Ce^{3+} content and b) B_2O_3 content.

In this process, two Er^{3+} ions are exited to $^4I_{13/2}$ level interact. One Er^{3+} ion transfer (donor) its energy to other (acceptor), resulting an acceptor to be promoted to $^4I_{13/2}$ level while the donor is de-exited to ground state ($^4I_{15/2}$) non-radiatively. The overall result is a depopulation of $^4I_{13/2}$ level. This phenomenon has been reported previously by different authors [13-15]. Experimental results indicate that the addition

of Ce_2O_3 ions has a better performance than B_2O_3 on the fluorescence lifetime and emission intensity characteristic of Er^{3+}/Yb^{3+} co-doped phosphate glasses.

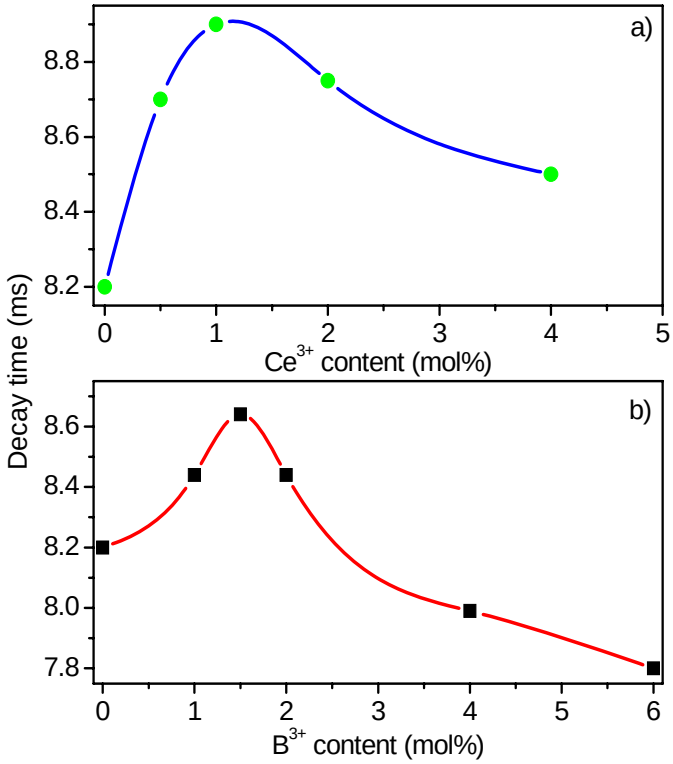

Figure 3.5 Fluorescence decay lifetime of Er^{3+} (1.53 μm) as a function of, a) Ce^{3+} and b) B_2O_3 concentration.

3.5 Quantum efficiency (QE)

Comparing the measured decay time with the calculated with JO theory, it is possible to calculate the quantum efficiency for $^4I_{13/2} \rightarrow {}^4I_{15/2}$ transition. It was calculated by using the equation 2.10. The values of quantum efficiency for all $Er^{3+}/Yb^{3+}/Ce^{3+}$ and $Er^{3+}/Yb^{3+}/ B_2O_3$ co-doped phosphate glasses are shown in Figure 3.6. The QE for $^4I_{13/2} \rightarrow {}^4I_{15/2}$ transition has a similar trend that the observed for the fluorescence lifetime of $^4I_{13/2}$ state. It can be seen that QE first increase from 82% to 90% when Ce_2O_3 increase from 0 to 1 mol % and then decrease to 86% ms for 4 mol %. And for B_2O_3, increase slightly from 82% to 87% with the increase of B_2O_3

concentration from 0 to 1.5 mol% and decrease significantly to 78% for 6 mol%, see Figure 3.6. Notice that the more significant change occur for $Er^{3+}/Yb^{3+}/B_2O_3$ codoped samples while for $Er^{3+}/Yb^{3+}/Ce^{3+}$ system keeps almost constant. The QE decrement with the increment of both ions and is consequence of the population on due to the increment of phonon energy. The obtained values of quantum efficiency are higher than the result reported recently for different phosphate glasses [16-17] and is excellent candidate for the eye safe laser emission at 1.53 μm.

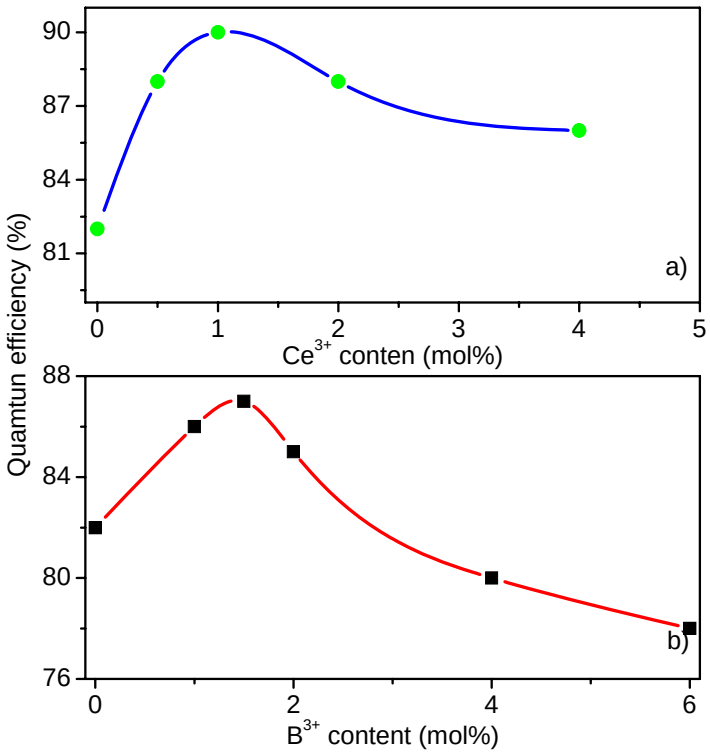

Figure 3.6 Quantum efficiency of $^4I_{13/2}$ level of Er^{3+} for, a)$Er^{3+}/Yb^{3+}/ Ce^{3+}$ and $Er^{3+}/Yb^{3+}/ B_2O_3$ co-doped samples.

Experimental results indicate that this new material is an excellent candidate for laser application.

Bibliography

[1]. M. D. Shinn, W. A. Sibley, M. G. Drexhage, and R. N. Brown, Phys. Rev. B: Condens. Matter., 27 (1983) 6635.

[2]. M. Shojiya, M. Takahashi, R. Kanno, Y. Kawamoto, and K, Kadono, Appl. Phys. Lett., 67 (1995) 2453.

[3] H. Lin, E.Y.B. Pun, X.R. Liu, J. Non-Cryst. Solids 283 (2001) 27.

[4] M. Tsuda, K. Soga, H. Inoue, J. Appl. Phys. 85 (1999) 29.

[5]. Y. Hu, S. Jiang, G. Sorbello, T. Luo, Y. Ding, B. C. Hwang, J. H. Kim, H. J. Seo, N. Peyghambarian, Proc SPIE 4282 (2001) 57.

[6]. Y. G. Choi, K. H. Kim, S. H. Park, J. Heo, J. Appl. Phys. 88 (2000) 3832.

[7]. E. Sani, A. Toncelli, M. Tonelli, Opt. Express 13 (2005) 8980.

[8]. J. Yang, L. Zhang, L. Wen, S. Dai, L. Hu, Z. Jiang, Chem. Phys. Lett. 384 (2004) 295.

[9]. E. Sania, A. Toncelli, and M. Tonelli, D. A. Lis and E. V. Zharikov, K. A. Subbotin and V. A. Smirnov, J. Appl. Phys. 97 (2005) 123531.

[10]. D. H. Choo, Y. G. Choi, K. H. Kim, ETRI 23 (2001) 151.

[11]. J. Yiang, L. Hu, S. Dai, N. Dai, Z. Yang, Z. Yiang, J. Mat. Scien. Lett. 22 (2003) 575.

[12]. X. Wang, Q. Nie, T. Xu, S. Dai, X. Shen, L. Liu, J. Opt. Soc. Am. B 24 (2007) 972.

[13]. E. Snoeks, G. N. van den Hoven, A. Polman, B. Hendrikseny, M. B. J. Diemeer, F. Priolo, J. Opt. Soc. Am. B 12 (1995) 1468.

[14]. P. Blixt, J. Nilsson, T. Carlnas, B. Jaskorzynska, IEEE Photonics Technol. Lett. 3 (1991) 996

[15]. G. Nykolak, P. C. Becker, J. Shmulovich, Y. H. Wong, D. J. DiGiovanni, A. J. Bruce, IEEE Photonics Technol. Lett. 5 (1993) 1014.

[16]. D.K. Sardar, J.B. Gruber, B. Zandi, J.A. Hutchinson and C.W. Trussell; J. Appl. Phys. 93 (2003) 2041.

[17]. H. Desirena, E. De la Rosa, L.A Diaz-Torres, G.A Kumar, Opt. Mat 28 (2006) 560.

CHAPTER 4

SELECTION OF TELLURITE GLASS COMPOSITION

This chapter is devoted to optical, chemical and thermo-mechanical properties of tellurite glasses as function of alkali metals as network modifiers (R_2O) and network intermediates (MO). Several properties were measured, such as thermal expansion coefficient (α), glass transition temperature (T_g), refractive index (n), transmittance, chemical durability (DR), density (ρ) and the third-order nonlinear optical susceptibility ($\chi^{(3)}$) and the obtained results indicate that both R_2O and MO affect greatly such properties. Experimental results indicate that alkali metals with small ionic radii improve chemical durability (DR), and mechanical (α, ρ, T_g) properties, while refractive index (n), third order nolinearlirity ($\chi^{(3)}$), and density (ρ) increment. Lower thermal expansion coefficient was obtained for Zn and Mg while the better chemical durability corresponds to Pb and Zn.

4.1 Name of glass samples

The samples glasses were prepared from the starting chemical constituents, tellurium oxide (TeO_2), lead oxide (PbO), zinc oxide (ZnO), barium oxide (BaO), magnesium oxide (MgO), lithium oxide (Li_2O), sodium carbonate (Na_2CO_3), potassium carbonate (K_2CO_3), cesium carbonate (Ce_2CO_3) and rubidium carbonate (Rb_2CO_3) (all from Aldrich 99.99% pure) according to the following composition: (70)TeO_2-(20)MO-(10)R_2O where M = Pb, Zn, Ba and Mg and R= Li, Na, K, Rb and Cs. The samples were prepared changing the compound of one of the alkali metal (R_2O) keeping the network intermediator constant (MO) for the four batches. The tag of glass samples and

concentration in mol% are presented in Table 2.1 and the procedure to make glasses was described in chapter 1.

Table 4.1 Name of tellurite glass and concentration (mol %)

Tag	Te	Pb	Zn	Ba	Mg	Cs	Rb	K	Na	Li
T11	70	20				10				
T12	70	20					10			
T13	70	20						10		
T14	70	20							10	
T15	70	20								10
T21	70		20			10				
T22	70		20				10			
T23	70		20					10		
T24	70		20						10	
T25	70		20							10
T31	70			20		10				
T32	70			20			10			
T33	70			20				10		
T34	70			20					10	
T35	70			20						10
T41	70				20	10				
T42	70				20		10			
T43	70				20			10		
T44	70				20				10	
T45	70				20					10

4.2 Experimental measurements

The density of each sample was measured by Archimedes method using water distilled as immersion liquid. The samples were cut and then polished to 1 mm thick slabs for different measurements. The chemical durability of the glasses with dimensions 5 x 5 x 5 mm was evaluated from the weight loss in boiling deionized water at 100 ºC during 1 h. The refractive indices of the samples were measured at 632.8 and 1550 nm by prism coupler (Metricon, Model 2010). The glass transition temperature (T_g) and the coefficient of thermal expansion (CTE) were carried out using a thermo-mechanical analyzer (TA Instruments, TMA 2940) at a heating rate of 10 °C/min in the

20-380 °C temperature range. The transmission spectrum of MO-R_2O-TeO_2 glasses were measured using two spectrophotometers one in the range from 300 to 2000 nm (Carry 500 UV-Vis-NIR) and other from 2000 to 8000 nm (Spectrum BX FTIR from Perkin Elmer) with a resolution of 1 nm. The third-order nonlinear optical susceptibility was studies using the THG-maker fringes technique at near infrared wavelengths. All the optical measurements were performed at room temperature.

4.3 Coefficient of thermal expansion (CTE) and glass transition temperature (T_g)

A representative measured thermal expansion and T_g curves for glasses is shown in Figure 4.1. The coefficient of thermal expansion was measured from the slope in the 30-300 ºC range, while the glass transition temperature was determined from the change of slope on dimension change versus temperature plot.

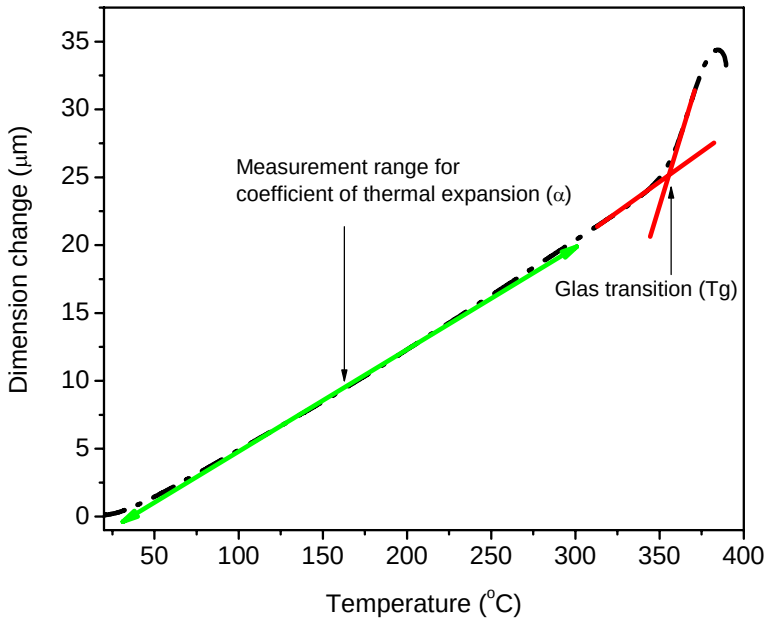

Figure 4.1 Coefficient of thermal expansion range (green line) and glass transition temperature (red line) curve.

The behavior of CTE for the twenty glasses was plotted in Figure 4.2. These glasses were analyzed as function of field strength calculated as $F = \frac{q_c q_o e^2}{(r_o + r_c)^2}$, where q_c and q_o are the valence of cation and anion respectively, e is the electron charge, r_c and r_o are the ionic radii of cation and oxygen, respectively. The values of both field strength and ionic radius of alkali metal and network intermediate are listed in Table 4.2.

4.2 Cation field strength [1] and ionic radius [2] of modifiers.

Cation	Field Strenght (10^{-16} esu/cm^2)	Ionic radius (Å)
Li	0.23	0.76
Na	0.19	1.02
K	0.13	1.51
Rb	0.12	1.61
Cs	0.11	1.74
Mg	0.45	0.72
Zn	0.44	0.74
Pb	0.30	1.19
Ba	0.24	1.42

These values are in the range from 224 x 10^{-7} $^oC^{-1}$ to 158 x 10^{-7} $^oC^{-1}$, showing a trend to decrease with the decrement of ionic radii, see Table 4.3. For alkali metal decrease from Cs to Li through Rb, K and Na while network intermediator decrease from Ba to Mg through Pb and Zn for all glasses. This behavior indicates that a decrease in the strength of cationic field (and then larger ionic radii) results in the observed increase in the coefficient of thermal expansion. CTE is controlled primarily by the interaction of cation with nonbridging oxygens [3]. Since Li and Mg from group IA an IIA of periodic table, have the highest cation field strength, it is expected that Li_2O-MgO-TeO_2 glass could provide the lowest thermal expansion, see figure 4.2. The obtained values of CTE in this work are lower than 200 x 10^{-7} $^oC^{-1}$ to 300 x 10^{-7} $^oC^{-1}$ measured from 50 to 200 ^{o}C reported in phosphate by other authors [4].

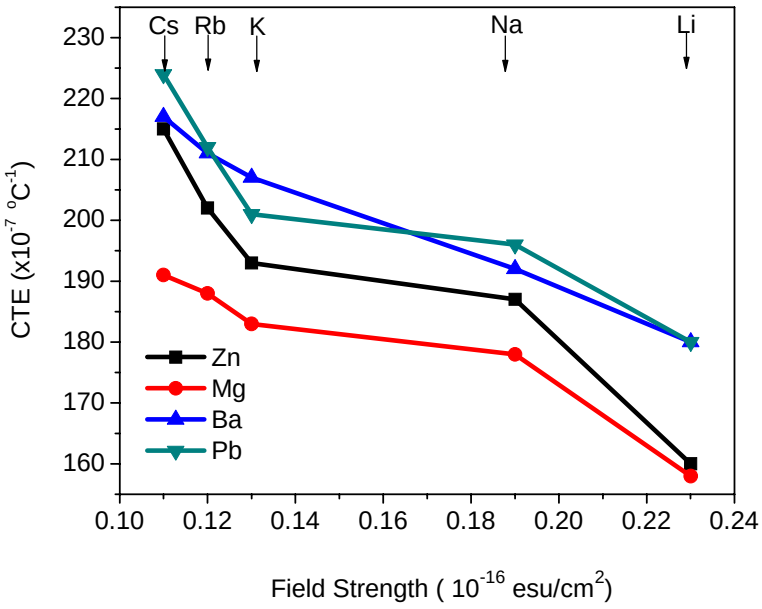

Figure 4.2 CTE as function of Field Strength.

On the other hand, the glass transition temperature (T_g) shows an opposite trend to coefficient of thermal expansion. This parameter increases monotonically with the decrease of ionic radii of alkalis for four batches, see Figure 4.3. It increases from Cs to Li in a range from 277 to 306 ºC, 295 to 335 ºC, 311 to 347 ºC and 352 to 373 ºC for series T1 (Pb), T2 (Zn), T3 (Ba) and T4 (Mg), respectively. The decrement was associated to very large ionic radii and consequently small field strength of Cs. However when Cs was replaced by Li through Rb, K and Na the ionic radius decrease and in consequence the field strength becomes greater. Thus, the Li-O bonds in the glass network are stronger and then Tg will be increased. It is not completely clear the relationship of Tg with intermediate ion. Apparently it increases with the decrement of ionic radius, however there is a different behavior of Ba suggesting the presence of an additional mechanism, see Figure 4.3.

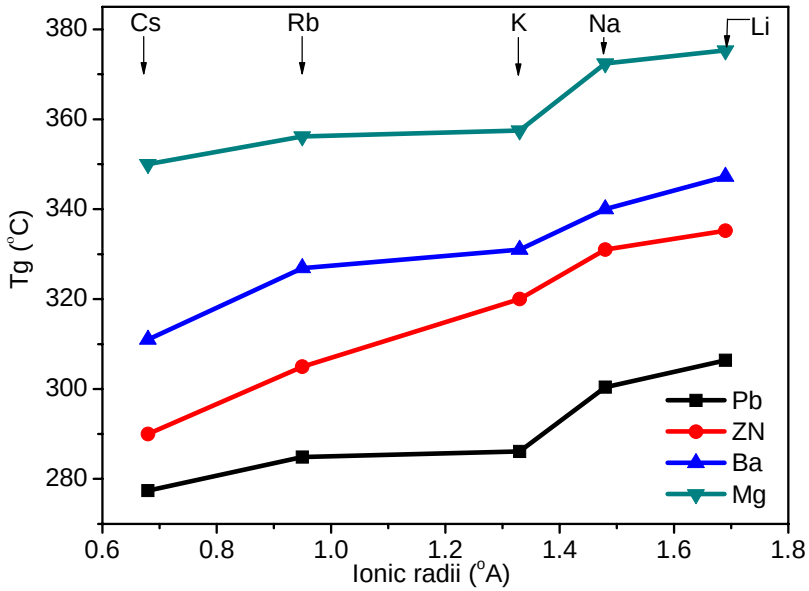

Figure 4.3 Glass transition temperatures (T_g) as a function of ionic radii.

4.4 Chemical durability

Good chemical durability is a very important parameter to make high quality optical fiber. Under normal conditions of operation glasses should not exhibit any noticeable degradation caused by environment. For this reason, good chemical durability is a critical requirement. The chemical durability of R_2O-MO-TeO_2 glasses was determined from measurements of their dissolution rate (DR) in boiling water. A small value of DR indicates a good chemical durability, while a large value indicates poor chemical durability. For the measurements of the weigh loss per surface area, samples were cut and polished with a dimension of 5 x 5 x 5 mm. Then, were carefully weighed and placed in a baker with 200 ml of deionized boiling water. After 1 h, glasses were removed and washed with acetone, subsequently were dried in a furnace at 80 ºC for 1 h and weighed again. All measurements were made in duplicate and the averages of two values are shown in Table 4.3. The dissolution rate (DR) of glasses were determined using the relation

$$DR = \Delta W/(S \cdot t) \tag{4.1}$$

where ΔW is the difference in the initial and final weight, t is the time of glasses immersed in water and S is the total surface area of the cube calculated by

$$S = 6a \tag{4.2}$$

The behavior of DR as a function of field strength of alkali metals is shown in Figure 4.4. DR for glasses decrease monotonically with the increment of field strength, from Cs to Li through Rb, K and Na. However, no specific trend as function of field strength was observed for network intermediate.

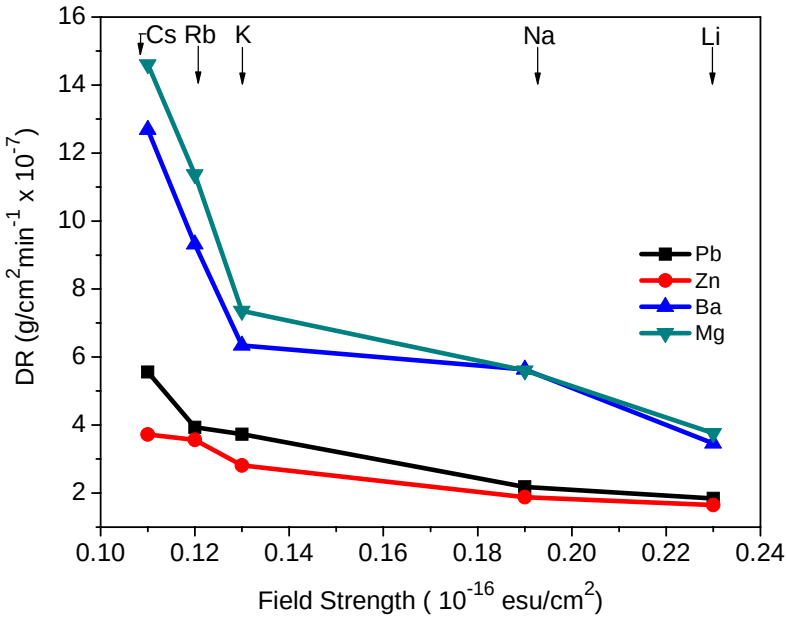

Figure 4.4 Dissolution rates of tellurite glasses as a function of alkali metals.

DR decrease from Mg to Zn through Ba and Pb, but in all cases chemical durability was improved when Cs was replaced by Li. In fact, DR is 2.5, 3, 3.5 and 4

times bigger for R_2O-ZnO-TeO_2, R_2O-PbO-TeO_2, R_2O-BaO-TeO_2 and R_2O-MgO-TeO_2 glasses, respectively, see Table 4.3. Li has high field strength and Li-O bonds are stronger, in consequence the chemical durability of R_2O-MO-TeO_2 glass is greater.

4.5 Transmission spectra of tellurite glasses

The transmission spectra of a few representative glass compositions was measured with two different experimental setup over a spectral range from 0.3 to 2.0 μm and 2 to 8 μm, as is shown in Figure 4.5. All samples present good transparency in a range from 0.35 to 6.4 μm depending on the glass composition. Figure 4.5a shows the UV transmission cutoff of R_2O-PbO-TeO_2 glasses being centred around 360 nm. No significant change was observed in the λ_{cutoff} with the replace of alkali metals. Only a slight shift (10 nm) on λ_{cutoff} was observed by the substitution of different alkali metals and 25 nm for different intermediate. This indicates that λ_{cutoff} depends mostly of the network intermediate. Notice that theses glasses have low UV transmission in comparison with phosphate and borate glasses indicating weak Te-O bond [5].

The cut-off in the IR range is shown in Figure 4.5b. The λ_{cutoff} was shifted from 6.170 to 6.410 μm when Mg was replaced by Pb through Ba and Zn. That means, λ_{cutoff} was shifted to larger wavelength by increasing the molecular weight of the intermediate. Just by introducing the right network intermediate, a 240 nm broad bandwidth in the transmission spectra is observed. On the other hand, no significant change was observed when the alkali metals were replaced one by one. This indicates that intermediate dependence of IR λ_{cutoff} is stronger than alkali metal. Figure 4.5b shows a strong absorption band at approximately 3290 nm, which is associated to OH-group stretching vibrations, as well as a weaker band at 4248 nm.

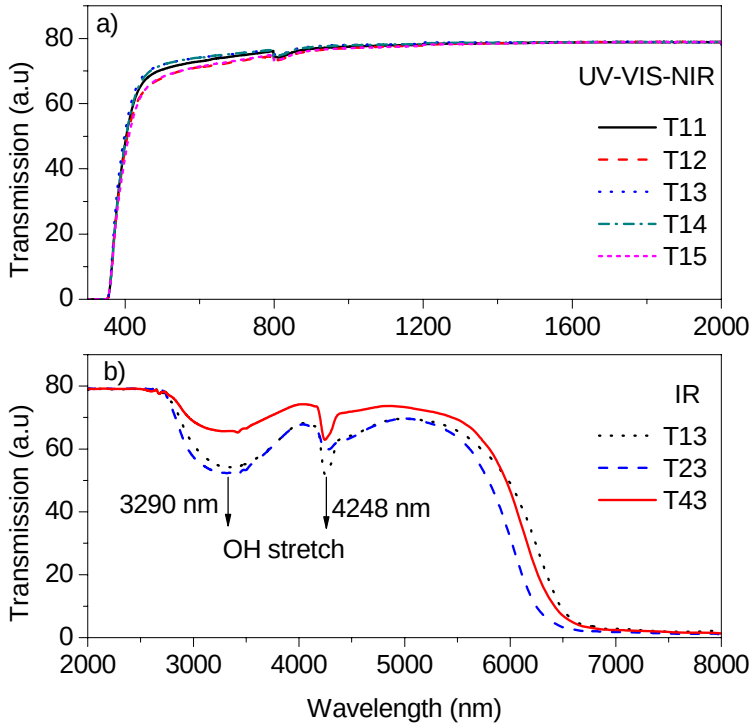

Figure 4.5 Transmission spectra for a) visible and NIR nm and b) MIR wavelength.

4.6 Refractive index and density of MO-R_2O-TeO_2

The measured values of refractive indices as function of ionic radii are shown in Figure 4.6, measured at 632.8 nm and 1550 nm. It can be seen that refractive index increase from Cs to Li for the four batches, in a range from 1.9705 to 2.0626, 1.8817 to 1.9728, 1.8603 to 1.9375 and 1.8598 to 1.9379 for R_2O-PbO-TeO_2, R_2O-ZnO-TeO_2, R_2O-BaO-TeO_2 and R_2O-MgO-TeO_2 glasses respectively, see Table 4.3. The results show that highest values of refractive index were obtained when lithium was incorporated into the tellurite glass. The observed trend is an increment of refractive index with a decrement of the ionic radii or an increment of field strength. Notice that such effect depends on the intermediate ion being more pronounced for PbO and ZnO, but diminish for BaO and MgO. It is clear that by modifying the glass composition is possible to increase or decrease the refractive index, such dependence indicates the

importance of the right glass composition of both modifiers. The difference of refractive indices is very useful as core and cladding glasses for optical fiber fabrication. However, core and cladding glasses must have similar thermal properties in order avoid crystallization when preform is drawing. In our case, T22-T14, T34-T41 and T35-T43 samples have similar thermal properties (T_g and coefficient of thermal expansion) and also keep the difference of refractive indices that make those glasses ideal for optical fiber fabrication.

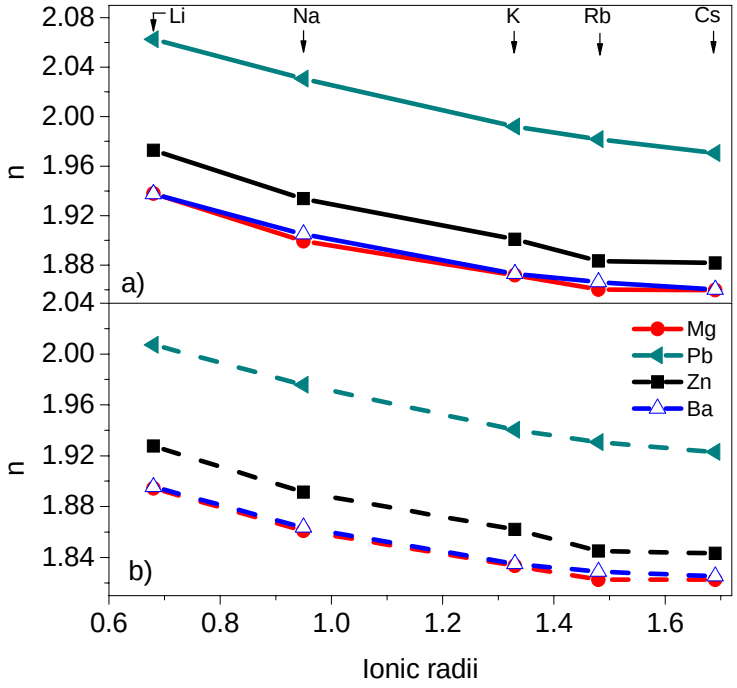

Figure 4.6 Refractive indices as a function of ionic radii at a) 632.8 nm and b) 1550 nm.

The linear refractive index (n) is related with the electronic polarizability (α_e) and molar volume (V_m) by the Lorentz-Lorenz equation [4]

$$n = \left(\frac{1 + 2\frac{4\pi N_A}{3}\frac{\alpha_e}{V_m}}{1 - \frac{4\pi N_A}{3}\frac{\alpha_e}{V_m}} \right)^{\frac{1}{2}} \qquad (4.3)$$

where N_A stand for the Avogadro's number. This equation indicates that refractive index increases as the term α_e/V_m increases. Since the polarizability increase with the ion size, it is expected that, for group IA of periodic table the refractive index should increase with increasing atomic number from Li to Cs. However, the experimental data shows an opposite trend, the index increases from Cs to Li. Such behavior suggests that the molar volume increases faster than electronic polarizability and as consequence the term α_e/V_m diminishes. This explains why the refractive index is largest when Li is incorporated into tellurite glass. Such behavior has been reported previously for phosphate glasses [1].

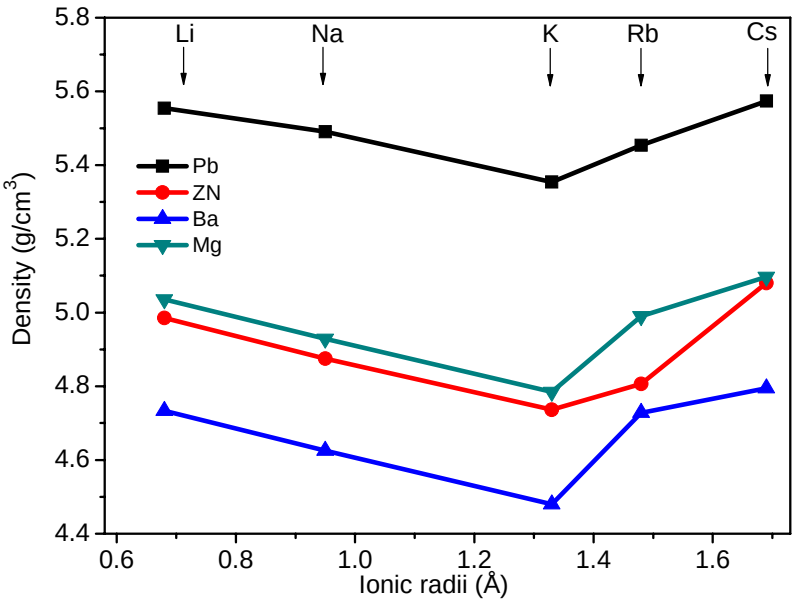

Figure 4.7 Density of tellurite glasses introducing several modifiers.

Figure 4.7 shows the density for all the samples under study. Those values are in the range from 5.35 to 5.75, 4.73 to 5.07, 4.78 to 5.09, 4.47 to 4.79 g/cm^3 for the series T1, T2, T3 and T4, respectively, see table 2. It is observed that density decrease by reducing the ionic radii of the alkali metals, Li, Na and K. Such trend has been reported

for phosphate and silicate glasses [6]. However, density increases with the introduction of Cs and Rb. The reason for this anomalous behavior is not clear at this stage. One possible explanation of this phenomenon is based on the fact that decomposition temperature of Cs and Rb is lower than that of K, Na and Li. Probably, both Cs and Rb are decomposed and evaporated due to the high melting temperature used. Consequently, when the glass is solidified Te-O and M-O bonds are larger than R-O bonds producing an increment on glass density. More experiments are in progress to elucidate this point.

4.7 Third-order nonlinear optical susceptibility ($\chi^{(3)}$)

The third-order nonlinear optical susceptibility $\chi^{(3)}$ for the MO-R_2O-TeO_2 glasses were measured by the well-known third harmonic generation (THG) method [7-12] with nanosecond excitation at 1550 nm. THG is a coherent four photon process in which three photons with angular frequency ω create one photon with tripled frequency 3ω through a material medium polarization. In this method $\chi^{(3)}$ was calculated from the THG output intensity measured as a function of angle of incident beam respect to the normal of surface sample, detail of experimental setup can be found elsewhere [13]. $\chi^{(3)}$ was calculated by the expression

$$\chi^{(3)}_{Sample}(-3\omega;\omega,\omega,\omega) = \chi^{(3)}_{SiO_2}\frac{L_{C,SiO_2}}{L_{C,Sample}}\sqrt{\frac{I_{3\omega,Sample}}{I_{3\omega,SiO_2}}}\sqrt{\frac{T^3_{\omega,SiO_2}.T_{3\omega,SiO_2}}{T^3_{\omega,Sample}.T_{3\omega,Sample}}}\sqrt{\frac{n^3_{\omega,Sample}.n_{3\omega,Sample}}{n^3_{\omega,SiO_2}.n_{3\omega,SiO_2}}} \quad (4.4)$$

Here, $L_{C,\text{ Sample}}$ and $I_{3\omega,Sample}$ represent the coherence length and the intensity of the third harmonic generation for the sample, respectively. L_{C,SiO_2} and $I_{3\omega,SiO_2}$ are the corresponding parameters for fused silica used as a standard sample. The value of $L_{C,SiO_2} = 14.7$ μm at 1550 nm was used for all calculation performed. $\chi^{(3)}_{SiO_2} = 3.1\times10^{-14}$ esu (dispersion of nonlinearities in fused silica was ignored) was used as a reference for nonlinear susceptibility. The coherent length of the sample $L_{C,Sample}$ was determined by $L_{C,Sample} = \dfrac{\lambda_\omega}{6(n_{3\omega} - n_\omega)}$, where λ_ω is the incident beam wavelength, $n_{3\omega}$ and n_ω represent the linear refractive indices at 517 nm and 1550 nm, respectively. $T_{3\omega}$ and T_ω represent the apparent transmittance including the reflection loss at the surface. The calculated values of third-order nonlinear optical susceptibility are listed in Table 4.3 and the behavior as function of polarizability is shown in Figure 4.8.

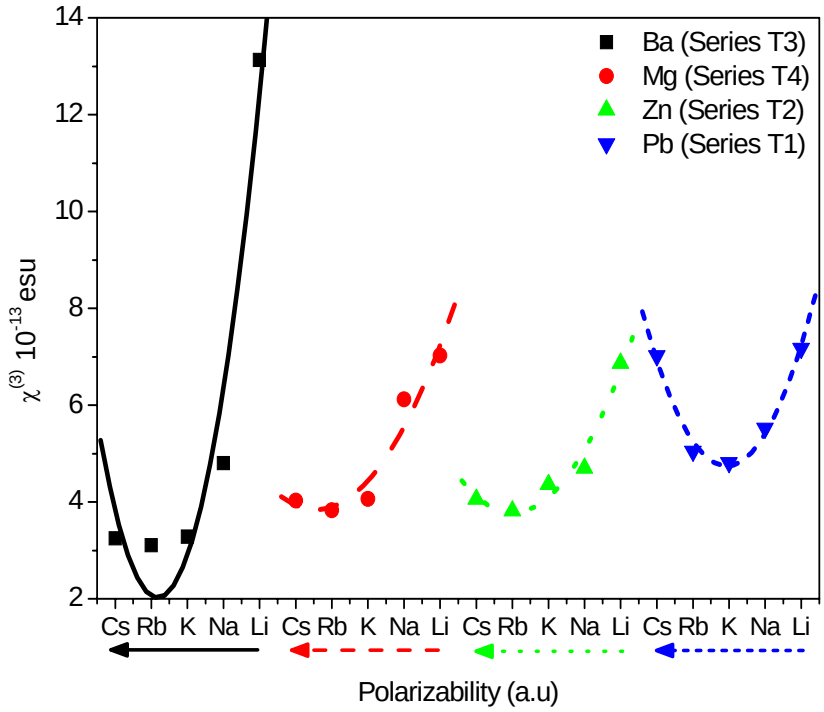

Figure 4.8 Third-order nonlinear optical susceptibility $\chi^{(3)}$ for R_2O- MO-TeO_2 glasses

All samples under study present an increment of $\chi^{(3)}$ as polarizability and ionic radii decreases, from K, Na and Li. Values range from 4.81 to 7.17 x 10^{-13} esu, 4.35 to 6.86 x 10^{-13} esu, 4.06 to 7.02 x 10^{-13} esu and 3.28 to 13.1 x 10^{-13} esu for series T1, T2, T3 and T4, respectively. These results are in good agreement with data previously reported for various tellurite glass compositions, smaller than 8.2 x 10^{-13} esu and 12.8 x 10^{-13} esu measured at 1500 and 1900 nm, respectively [14-15]. Notice the little fluctuation of $\chi^{(3)}$ for Cs and Rb. Apparently nonlinearity diminish from K to Rb but increase for Cs. Such behavior is similar than the observed for density. The value obtained for Cs in T3 series is much larger than other series. Probably, such deviation is associated with some surface irregularities of the sample that is well-known affect strongly the nonlinear calculation.

Since the refractive indices of tellurite glasses increase from Cs to Li (section 3.1), it is expected that $\chi^{(3)}$ increases with the increment of linear refractive index [16]. Unfortunately, it is not possible to establish a direct relationship between $\chi^{(3)}$ and n_2. However, preliminary results obtained by z-scan technique confirm such trend, i.e., an increment of $\chi^{(3)}$ produce an increment of n_2. Furthermore, it presents a positive behavior that promotes the self-focusing. Non-linear refractive index is an important parameter to be considered in laser application in order to prevent spatial intensity fluctuations and self-focusing. These effects degrade the beam focal spot, reduce the focusable power of the laser and increase the risk of laser-induced damage [17-18]. On the other hand, because the power in optical amplifiers is lower than in laser operation such non-linear effect should be negligible. However if the n_2 is high, then such non-

linear effects must be considered. In general, n_2 should be as low as possible to avoid undesirable effects.

Table 4.3 Coefficient of thermal expansion (CTE), dissolution rate (DR), refractive index (n), density and third order nonlinear optical susceptibility ($\chi^{(3)}$) of various R_2O-MO-TeO_2 glasses.

Code	CTE (C^{-1} 10^{-7})	DR (10^{-7} g/cm^{2}min^{-1})	Density (g/cm^3)	*n*		$\chi^{(3)}$ (10^{-13} esu)
				632.8 nm	*1550 nm*	
T11	224	5.562	5.554	2.0626	2.0071	7.18
T12	212	3.734	5.490	2.0306	1.9758	5.52
T13	201	3.733	5.354	1.9919	1.9404	4.81
T14	196	1.88	5.454	1.9817	1.9306	5.04
T15	180	1.84	5.574	1.9706	1.9229	7.02
T21	215	3.725	4.984	1.9728	1.9276	6.86
T22	202	3.566	4.874	1.9337	1.8914	4.69
T23	193	2.813	4.736	1.9007	1.862	4.35
T24	187	1.882	4.806	1.8834	1.845	3.81
T25	160	1.806	5.079	1.8817	1.8432	4.05
T31	217	12.68	4.733	1.9375	1.8954	7.02
T32	211	9.312	4.625	1.9049	1.8637	6.11
T33	207	9.343	4.479	1.8729	1.835	4.06
T34	192	5.632	4.727	1.8663	1.8289	3.83
T35	180	3.761	4.794	1.8603	1.8251	4.02
T41	191	14.61	5.035	1.9379	1.8945	13.12
T42	188	11.37	4.928	1.8994	1.8611	4.80
T43	183	7.360	4.784	1.8718	1.8335	3.28
T44	178	5.603	4.990	1.8602	1.8225	3.10
T45	158	3.761	5.097	1.8598	1.8225	3.24

Based on the experimental results obtained from the systematic characterization of R_2O-MO-TeO_2 glasses it is concluded that optical, chemical and thermo-mechanical properties of tellurite glasses are strongly influenced by the introduction of alkali metals and network intermediates. The introduction of such ions modifies the glass network and as consequence their properties. Low coefficient of thermal expansion, good chemical durability, wide transmission region and high density were obtained by choosing adequately the glass composition. Some properties were improved but others

were reduced. Then, it is necessary to make a compromise of desired properties and then defines the glass composition.

Bibliography

[1]. J. S. Hayden, Y. T. Hayden, J. H. Campbell, SPIE 1277 (1990) 121.

[2]. CRC Handbook of chemistry and physics 81a. ed. 2000-2001.

[3]. T. Minami, J. D. Makenzie, J. Am. Ceram. Soc. 60 (1977) 232.

[4]. J. Heo, D. Lam, G.H. Sigel, Jr. E. A. Mendoza, D. Hensley, J. Am. Ceram. Soc. 75 (1992) 277.

[5]. H. Burger, W. Vogel, V. Kozhukharov, Infrared Phys. 25 (1985) 395.

[6]. H. Takebe, Y. Nageno, and K. Morinaga, J. Am. Ceram Soc, 77 (1994) 2132.

[7]. S. H. Kim, T. Yoko, and S. Sakka, J. Am. Ceram. Soc. 76 (1993) 865.

[8]. M. C. Kuzyk and , C. W. Dirk, Characterization techniques and tabulation for organic nonlinear optical materials, Marcel Dekker, 1998.

[9]. H. Nasu, T. Ito, H. Hase, J. Matsuoka, K. Kamiya, J. Non-Cryst. Solids 204 (1996) 78.

[10]. N. Sugimoto, H. Kanbara, S. Fujiwara, K. Tanaka, Y. Shimizugawa, K. Hirao, J. Opt. Soc. Am. B 16 (1999) 1904.

[11]. F. Kajzar and J. Messier, Thin Solids Film 132 (1985) 11.

[12]. X. H. Wang and D. P. West, N. B. McKeown, T. A. King , J. Opt. Soc. Am. B 15 (1998) 1895.

[13]. G. Ramos-Ortiz, J.L. Maldonado, M.A. Meneses-Nava, O. Barbosa-Garcıa, M. Olmos, M. Cha, Opt. Mater. 29 (2007) 636.

[14] S. Hoom Kim, J. Mater. Research 14 (1999) 1074.

[15] J. Lin, W. Huang, Z. Sun, C.S. Ray, D.E. Day, J. Non-Cryst. Solids 336 (2004) 189.

[16] C.C. Wang, Phys. Rev. B 2 (1970) 2045.

[17] J. T. Hunt, J. A. Glaze, W. W. Simmons, P. A. Renard, Appl. Opt. 17 (1978) 2053.

[18] J. T. Hunt, K. R. Manes, P. A. Renard, Appl. Opt. 32 (1993) 5973.

CHAPTER 5
SPECTROSCOPIC PROPERTIES AND ENERGY TRANSFER OF Er^{3+}/Yb^{3+} CO-DOPED TELLURITE GLASSES

In this chapter, it is reported the spectroscopic properties of Er^{3+}/Yb^{3+} co-doped tellurite glasses. Emission characteristics and fluorescence lifetimes at visible (525, 546 and 656 nm) and infrared (1.53 μm) region as a function of Er^{3+} and Yb^{3+} concentration have been measured. The addition of Yb^{3+} to Er^{3+} doped tellurite glass enhances greatly the green emission, which can be observed with the naked eye. The Judd-Ofelt and quantum efficiency in infrared and visible up-conversion emissions was calculated. The stimulated emission cross section (ECS) for $^4I_{13/2} \rightarrow {}^4I_{15/2}$ transition was higher at low Er^{3+} concentrations, being the maximum value 1.0 x 10^{-20} cm^2 for 0.10 mol% of Er^{3+} with 0.5 mol% of Yb^{3+}. The energy transfer efficiencies (ET) from Yb^{3+} to Er^{3+} ($^4F_{5/2}$) + ($^4I_{15/2}$) → ($^4F_{7/2}$) + ($^4I_{13/2}$) changing the Er^{3+} and Yb^{3+} concentration were calculated. The maximum ET obtained were 66% for $0.75Er^{3+}/0.5Yb^{3+}$ and 69% for $0.5Er^{3+}/4.5Yb^{3+}$. Results indicate that ET depends mostly on Er^{3+} rather than Yb^{3+} concentration.

5.1 Preparation of Er^{3+}/Yb^{3+} codoped tellurite glass

The glass composition used was $70TeO_2$-$20ZnO$-$5Li_2O$-$(5-x-y)La_2O_3$-xEr_2O_3-yYb_2O_3 (x = 0.10, 0.15, 0.30, 0.5, 0.75 at y=0.5 and y = 1, 2, 3, 4.5 at x=0.5), all the concentration in mol %. The samples were prepared from the starting chemical constituent tellurite oxide (TeO_2), zinc oxide (ZnO), lithium carbonate (Li_2CO_3), erbium oxide (Er_2O_3), ytterbium oxide (Yb_2O_3), and lanthanum oxide (La_2O_3). The glass fabrication, annealing and different measurements has been described in chapter 1 and

section 2.2. The tag of samples glass with both ions concentration Er^{3+} and Yb^{3+} are show in Table 5.1.

Table 5.1 Name of Er^{3+}/Yb^{3+} co-doped tellurite glasses.

Tag	Er^{3+}/Yb^{3+} (mol %)
TEY0105	0.10/0.5
TEY02505	0.25/0.5
TEY03505	0.35/0.5
TEY0505	0.5/0.5
TEY07505	0.75/0.5
TEY051	0.5/1
TEY052	0.5/2
TEY053	0.5/3
TEY0545	0.5/4.5

5.2 Judd-Ofelt parameters (J-O) of Er^{3+}/Yb^{3+} co-doped glasses

From the absorption spectrum of Er^{3+}/Yb^{3+} co-doped tellurite glasses, ten bands were considered to predict the Judd-Ofelt parameter (J-O), see Figure 5.1. The complete procedure to obtain the J-O parameters and some spectroscopic properties in tellurite glasses have been described in chapter 2 [1-3].

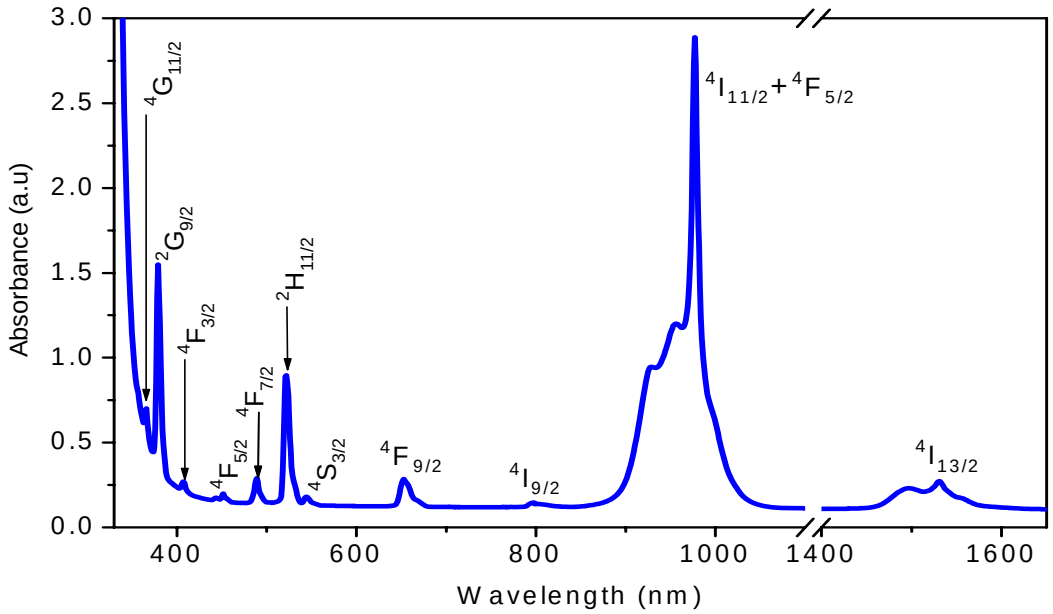

Figure 5.1 Absorption spectra of Er^{3+}/Yb^{3+} co-doped TeO_2-ZnO-Li_2O- La_2O_3 glass.

The values of such parameters and the root mean square deviation for Er^{3+}/Yb^{3+} co-doped tellurite glasses under study are, Ω_2=6.56 x 10^{-20} cm^2, Ω_4=1.60 x 10^{-20} cm^2 and Ω_6=1.44 x 10^{-20} cm^2 with RMS= 0.142 x 10^{-20} cm^2. The calculated values were performed with an accuracy of ±10 %. The obtained JO parameters follow the typical behavior $\Omega_2>\Omega_4>\Omega_6$ reported for tellurite glasses and are in agreement with results reported recently for various glass compositions as shown in Table 5.2.

Table 5.2 J-O parameters for various tellurite glass composition.

Glass composition	Ω_2 (10^{-20} cm^2)	Ω_4 (10^{-20} cm^2)	Ω_6 (10^{-20} cm^2)	Ref.
TeO_2-ZnO-Na_2O	5.98	1.32	1.47	1
TeO_2-Nb_2O_5-Na_2O	6.86	1.53	1.12	4
TeO_2-WO_3-Bi_2O_3	6.06	1.57	0.95	5
TeO_2-ZnO-K_2O	5.95	2.06	1.07	6
TeO_2-BaO-La_2O_3	6.31	1.76	1.05	7
TeO_2-WO_3-BaO	6.64	1.45	0.96	8
TeO_2-ZnO-Li_2O	6.56	1.60	1.44	This work

Once the JO parameters are known, several spectroscopic properties can be calculated, such as the radiative decay probability (A_{rad}), radiative lifetimes (τ_{rad}), branching ratios (β) and spectroscopy quality factor (χ), see Table 5.3. The parameter $\chi = \Omega_4/\Omega_6$ was found to be 1.11 and is in agreement with results reported by other authors [4, 9].

Table 5.3 Calculated radiative decay rates, branching ratios and radiative lifetimes of Er^{3+} ion in Er^{3+}/Yb^{3+} codoped tellurite glass.

Transition	$A_{JJ'}$(s^{-1})	$B_{JJ'}$	τ_{rad} (ms)
$^4I_{13/2}\rightarrow{}^4I_{15/2}$	263.4	1.00	3.80
$^4I_{11/2}\rightarrow{}^4I_{15/2}$	350.8	0.90	2.56
$^4I_{13/2}$	40.1	0.10	
$^4I_{9/2}\rightarrow{}^4I_{15/2}$	303.6	0.73	2.40

$^4I_{13/2}$	112.9	0.27	
$^4I_{11/2}$	0.6	0.00	
$^4F_{9/2}\rightarrow{}^4I_{15/2}$	2917.0	0.90	0.308
$^4I_{13/2}$	144.9	0.04	
$^4I_{11/2}$	170.3	0.05	
$^4I_{9/2}$	10.6	0.00	
$^4S_{3/2}\rightarrow{}^4I_{15/2}$	2650.9	0.67	0.252
$^4I_{13/2}$	1089.2	0.27	
$^4I_{11/2}$	85.1	0.02	
$^4I_{9/2}$	136.7	0.03	
$^4F_{9/2}$	1.5	0.00	
$^2H_{11/2}\rightarrow{}^4I_{15/2}$	17199.2	0.96	0.055
$^4I_{13/2}$	287.6	0.02	
$^4I_{11/2}$	168.0	0.01	
$^4I_{9/2}$	253.4	0.01	
$^4F_{9/2}$	63.6	0.00	
$^4S_{3/2}$	0.1	0.00	
$^4F_{7/2}\rightarrow{}^4I_{15/2}$	6575.0	0.79	0.012
$^4I_{13/2}$	972.1	0.12	
$^4I_{11/2}$	497.8	0.06	
$^4I_{9/2}$	305.0	0.04	
$^4F_{9/2}$	14.9	0.00	
$^4S_{3/2}$	0.1	0.00	
$^2H_{11/2}$	2.2	0.00	

5.3 Absorption (ACS) and emission cross-section (ECS) as function of Er^{3+} and Yb^{3+} concentration.

Cross sections quantify the ability of an ion to absorb or emit light, large emission cross section means high gain coefficient and low threshold energy of laser pump. Thus, in order to obtain the best performance of laser and optical amplifiers, it is necessary to obtain the stimulated emission cross section as high as possible. The absorption cross-section of the $^4I_{13/2}\rightarrow{}^4I_{15/2}$ (1.53 μm) transition of Er^{3+} has been determined from the absorption spectra of Er^{3+}/Yb^{3+} co-doped tellurite glass, using the equation

$$\sigma_a = \frac{2.303\log(I_0/I)}{NL}. \quad (5.1)$$

where $\log(I_0/I)$ is the optical density, L is the sample thickness and N is the concentration of Er^{3+} ion. The stimulated emission cross section is obtained according to the McCumber theory from the expression [10].

$$\sigma_e(\nu) = \sigma_a(\nu)\exp[(\varepsilon - h(c/\lambda))/kT] \quad (5.2)$$

where ν is the photon frequency, ε is the net free energy required to excite one erbium ion from the $^4I_{15/2}$ to the $^4I_{13/2}$ level at temperature *T*, *h* is the Planck's constant, *k* is the Boltzmann constant and *c* is the light velocity in the vacuum. ε = 6550 cm^{-1} was estimated by using the approximation $\varepsilon=E_o+21E_2-28E_1$ [11]. In this case, three basic assumption are considered, 1) the Stark levels for a given manifold is equally spaced, $E_{ij}=(j-1)E_i$ with a degeneracy equal to 7 and 8 for $^4I_{13/2}$ and $^4I_{15/2}$, respectively; 2) E_0 is the energy between the two levels and was calculated taking the average between the absorption and emission peaks; 3) E_1 and E_2 are calculated measuring the half width energy calculated from the wavelength peak to the point where signal decreased to 5%. Both ACS and ECS were calculated as a function of Er^{3+} and Yb^{3+} concentration. It was made by changing the concentration of one ion keeping the other one constant and analyzed the effect on the emission cross section. The values of both, absorption and emission cross section as a function of Er^{3+} and Yb^{3+} concentrations are shown in Figure 5.2. The ECS increase from 9.25 (TEY07505) to 10.2 x 10^{-21} cm^2 (TEY0105) when Er_2O_3 decreased from 0.75 to 0.10 mol %, see Figure 5.2a. For Yb^{3+} concentration, it first increase reaching the maximum 9.71 x 10^{-21} cm^2 (TEY053) at 3 mol % of Yb^{3+} and then diminish to 9.52 x 10^{-21} cm^2 for higher concentration (TEY0545), see Figure 5.2b. The calculated values of stimulated emission cross section

are in agreement with results reported recently [4] and are higher than the values reported for silica (7.9 x 10^{-21} cm^2) [12] and phosphate glass (6.8 x 10^{-21} cm^2) [13].

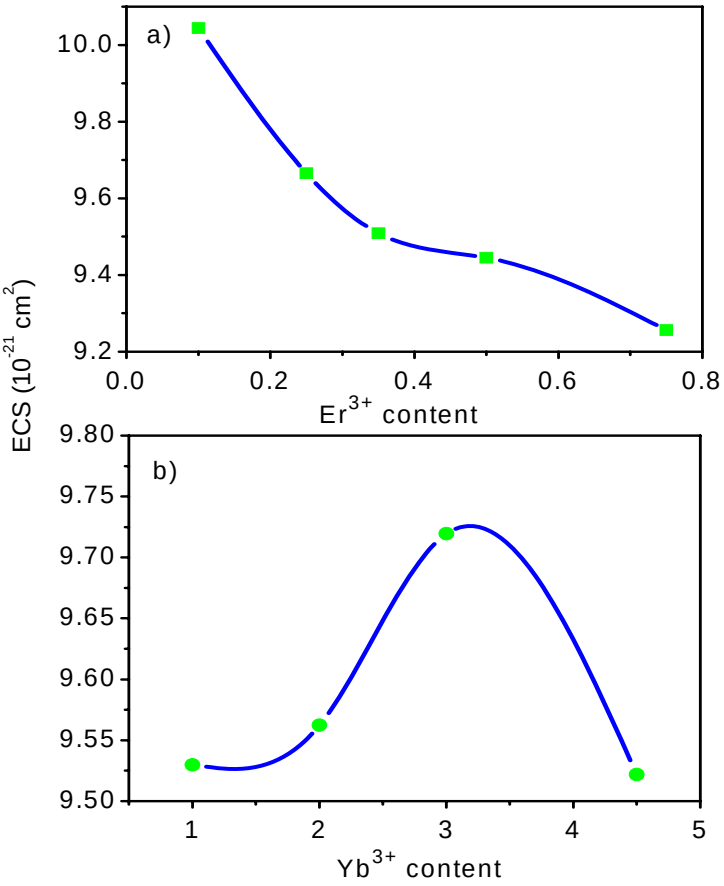

Figure 5.2 Emission cross section of Er^{3+} in Er^{3+}/Yb^{3+} co-doped tellurite glass as a function of a) Er^{3+} and b) Yb^{3+} concentration

5.4 Fluorescence characteristic of Er^{3+}/Yb^{3+} co-doped tellurite glass

5.4.1 Infrared and up-conversion emission

The well-known near infrared (NIR) emission ($^4I_{13/2} \rightarrow {}^4I_{15/2}$) of Er^{3+} in the Yb^{3+}/Er^{3+} co-doped tellurite glasses was centered at 1.532 μm with a spectral bandwidth ranging from 51 to 71 nm, depending on the concentration of both ions, as shown in Figure 5.3. That means an increment of up to 18 nm in the bandwidth by just controlling

the ion concentration. The obtained results show a continuous increment of the bandwidth from 51 to 65 nm and from 53 to 71 nm by increasing the Er^{3+} and Yb^{3+} concentration respectively. Notice that lower changes concentration of Er^{3+} produces almost similar bandwidth broadening than higher change concentration of Yb^{3+}. The increment of bandwidth is explained in terms of site distribution and radiation trapping of Er^{3+} ions [14-15].

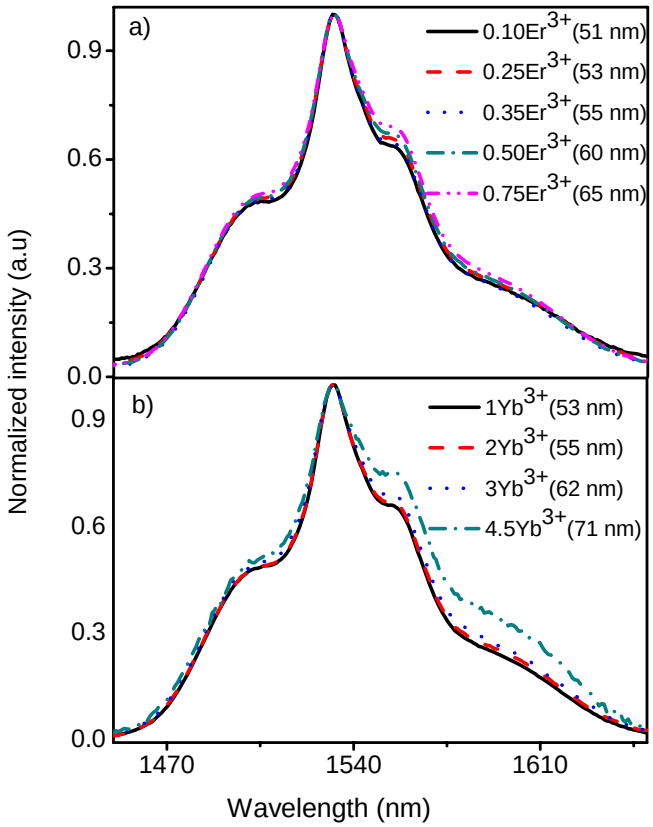

Figure 5.3 FWHM as a function of a) Er^{3}+ and b) Yb^{3+} concentration.

The ion concentration also modifies the intensity of the signal thar increase monotonically with the increment of Yb^{3+} and presents a maximum at 0.5 mol% of Er^{3+} ion as is indicated in Figure 5.4. Such dependence clearly indicates the importance of the right concentration of both ions, in particular the important role of as Yb^{3+} sensitizer. The concentration of both ions should be appropriate in order to minimize the up-

conversion emission and non-radiative processes due to cluster formation. Both phenomena reduce the fluorescence lifetime of $^4I_{13/2}$ level, which leads to a decrease of the laser efficiency. Additionally larger concentrations of sensitizer ion help to disperse Er^{3+} ions and enhance its excitation. However, it also enhances the up-conversion emission, which present stronger dependence at high pump powers and this effect is much more pronounced for larger concentration of dopant. In addition, it has been demonstrated hat higher concentrations of Yb^{3+} induce an increment of heat that induce a deleterious effect on the laser efficiency. Those results suggest the use of higher concentration of ions for amplifiers and lower concentration for laser devices [16].

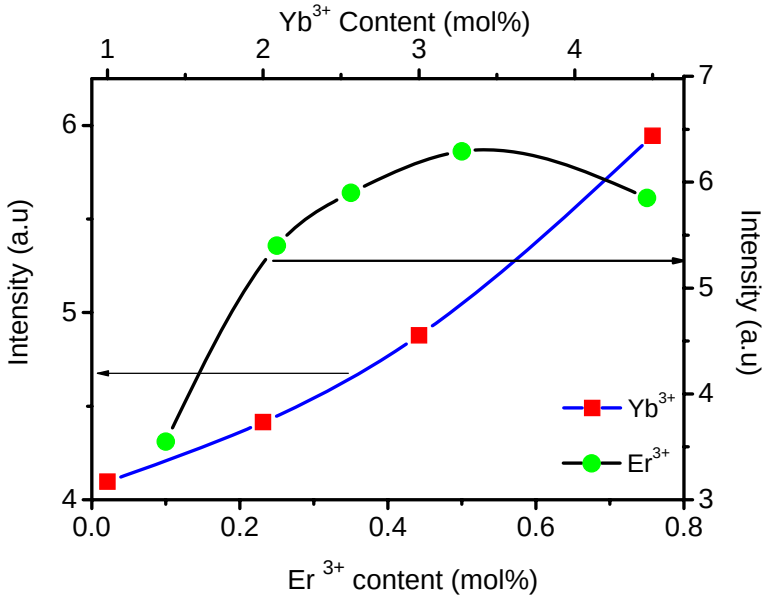

Figure 5.4 Intensity at 1.53 μm band as a function of Er^{3+} and Yb^{3+} concentration

In addition to the 1.55 μm signal emitted, three strong visible bands green ($^2H_{11/2} \rightarrow {}^4I_{15/2}$ and $^4S_{3/2} \rightarrow {}^4I_{15/2}$) and red ($^4F_{9/2} \rightarrow {}^4I_{15/2}$) centered at 526, 548 and 660 nm, respectively, were observed and are shown in Figure 5.5. The visible emission is the result of the well-known up-conversion process and it depends on the concentration of both Yb^{3+} and Er^{3+} ions. However, because Yb^{3+} exhibits a large absorption cross

section and broad absorption band between 850 and 1080 nm compared to the weak absorption of Er^{3+} ion, more ions are excited to $^4F_{7/2}$ level. The overall result is the increment of population in the level $^2H_{11/2}$ and $^4S_{3/2}$ of Er^{3+}, as a consequence the luminescence intensity is stronger after relaxation to ground state such as observed in Figure 5.6

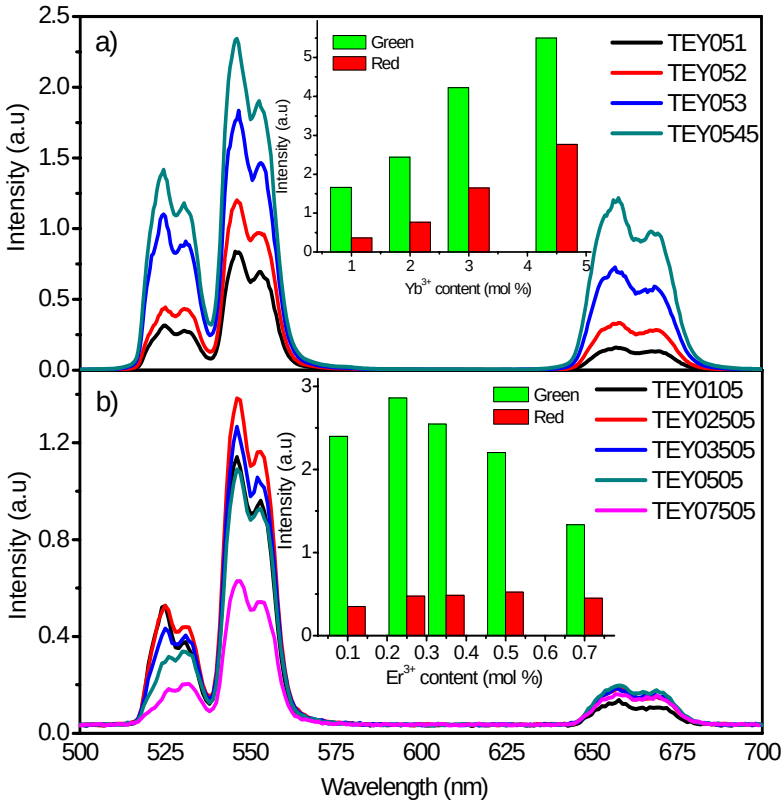

Figure 5.5 Up-conversion emission for, a) Er^{3+}/Yb^{3+} (x/0.5 mol%) and b) Er^{3+}/Yb^{3+} (0.5/y mol%).

The results show that the overall intensity of the upconverted signal increases as Yb^{3+} concentration increase from 0.5 to 4.5 mol% and with the Er^{3+} concentration first increase from 0.10 to 0.25 mol% and then decreases as Er^{3+} increase such as is shown in the inset of Figure 5.5a and 5.5b respectively. The increment is explained in terms of the energy transfer efficiency due to the increment of donors while the decrement of signal is presumable due to quenching effect of acceptors. Both visible bands increase

but the red one increase faster as is shown in the inset of Figure 5.5a. This behavior is in agreement with other reports where the red band increases with the increase of Yb^{3+} concentration [17-18]. The visible emissions are relaxation pathways contrary to pathway associated to 1.53 μm emission, and then the enhancement of the former is deleterious to the very important emission associated to the optical fiber communication window.

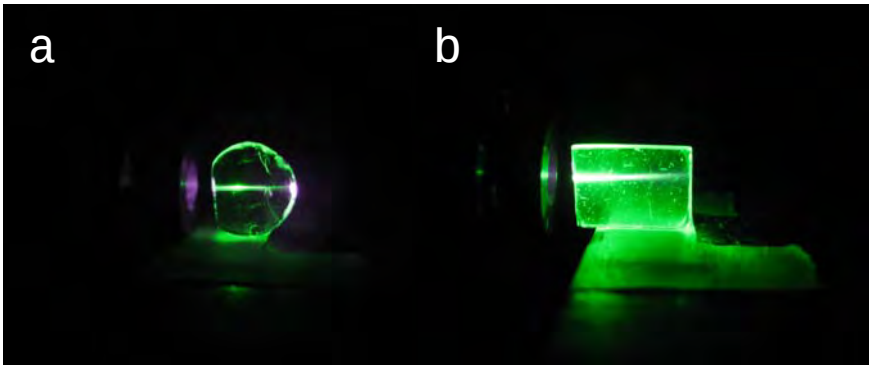

Figure 5.6 Photograph of the green up-conversion fluorescence for a) Er^{3+} doped and b) Er^{3+}/Yb^{3+} co-doped tellurite glass.

The integrated upconverted (I_{upc}) signal was plotted as function of the pumping power (I_{pp}). Experimental data were fitted by the expression $I_{upc} = kI_{pp}^{n}$ where *n* denote the number of photons involved in the process and *k* is a proportionality constant. Figure 5.7 shows such behavior for 0.5 of Er^{3+} with lowest (0.5 mol%) and highest (4.5 mol%) concentration of Yb^{3+} ions, in both cases *n~2* for green and red bands. This value is the indicative of the involvement of two photons in the excitation process of $^2H_{11/2}$, $^4S_{3/2}$ and $^4F_{9/2}$ levels. In order to justify the decrement of n_r from 1.8 to 1.6 in Figure 5.7b, we suggest it is an enhancement of the red band, that is produced by the cross relaxation process, $Er^{3+}(^2H_{11/2}) + Er^{3+}(^4I_{13/2}) \rightarrow Er^{3+}(^4I_{9/2}) + Er^{3+}(^4I_{13/2})$.

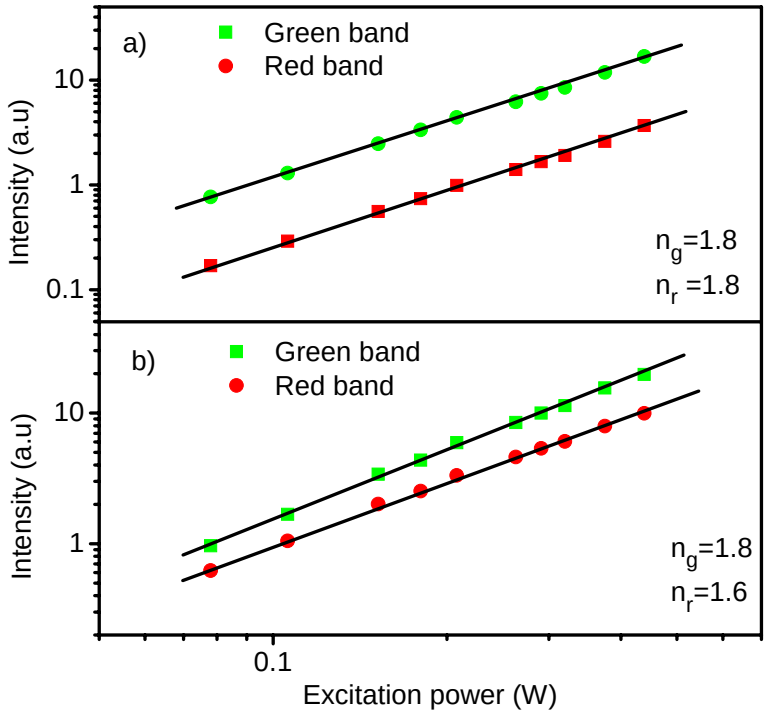

Figure 5.7 Pump power dependence of green and red emission for a) $0.5Er^{3+}/0.5Yb^{3+}$ and b) $0.5Er^{3+}/4.5Yb^{3+}$ (mol %).

5.4.2 Mechanism analysis of Er^{3+}/Yb^{3+} codoped tellurite glass

The physical mechanism describing both visible and NIR emission is as follows. Er^{3+} ion (acceptors) are excited by the energy transfer from the Yb^{3+} (donor) that are excited directly ($^2F_{5/2} + h\nu \rightarrow {}^2F_{7/2}$) by the pumping signal. In all cases direct excitation of Er^{3+} from ground state ($^4I_{15/2} + h\nu \rightarrow {}^4I_{11/2}$) is also possible, however energy transfer is most probable due to the larger absorption cross section of Yb^{3+} [19] and the resonance between the transitions of Yb^{3+} ($^2F_{5/2} \rightarrow {}^2F_{7/2}$) and Er^{3+} ($^4I_{15/2} \rightarrow {}^4I_{11/2}$) ions, as is shown in the energy diagram of Figure 5.8. Partly of the $^4I_{11/2}$ excited ions relaxes non- radiatively to $^4I_{13/2}$ level and from here relaxes to ground state producing the 1.532 μm emission band. Another part is promoted to $^4F_{7/2}$ level by the energy transfer according to the equations $Yb^{3+}(^2F_{5/2})+Er^{3+}(^4I_{11/2})\rightarrow Yb^{3+}(^2F_{7/2})+Er^{3+}(^4F_{7/2})$ and

$Er^{3+}(^4I_{11/2})+Er^{3+}(^4I_{11/2})\rightarrow Er^{3+}(^4I_{15/2})+Er^{3+}(^4F_{7/2})$. The ions in $^4F_{7/2}$ level decays non-radiatively to $^2H_{11/2}$ + $^4S_{3/2}$ due to phonon energy. From here, most of the population decay to ground state producing the green emissions centered at 526 and 548 nm. And partly decay non-radiatively to $^4F_{9/2}$ from where they decay to ground state ($^4F_{9/2} \rightarrow {}^4I_{15/2}$) producing the red emission centered at 670 nm.

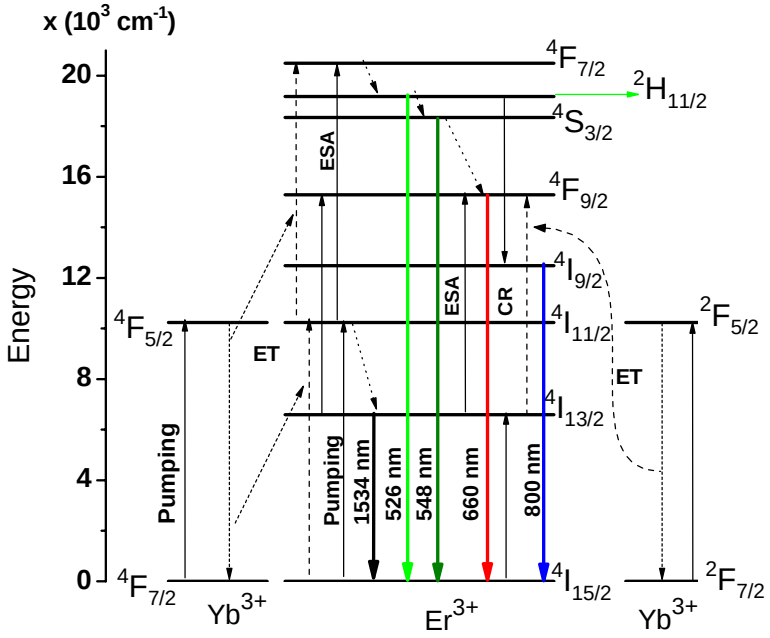

Figure 5.8 Energy diagram of the Er^{3+}/Yb^{3+} system and the mechanism proposed to explain both visible and infrared emission.

This visible band is also enhanced by increasing the concentration of both donor and acceptors. In this case, part of the population in the $^4I_{13/2}$ level is promoted to $^4F_{9/2}$ by the energy transfer from another donor $Yb^{3+}(^2F_{5/2}) + Er^{3+}(^4I_{13/2}) \rightarrow Yb^{3+}(^2F_{7/2})+ Er^{3+}(^4F_{9/2})$. The enhancement of the red band with Er^{3+} concentration is explained in terms of the increment of population of $^4I_{13/2}$ due to cross-relaxation process $Er^{3+}(^2H_{11/2}) + Er^{3+}(^4I_{13/2}) \rightarrow Er^{3+}(^4I_{9/2}) + Er^{3+}(^4I_{13/2})$. And the enhancement with Yb^{3+} is explained in terms of the energy transfer from donor to acceptors due to the high concentration of

donors, see Figure 5.8. The mechanism proposed to explain the signal emitted of co-doped glasses is well described in Figure 5.8.

5.4.3 Fluorescence lifetime of $^4S_{3/2}$, $^4F_{9/2}$ and $^41_{13/2}$levels

Fluorescence lifetime 1.53 μm is an important parameter for optical amplifiers and laser applications. Long lifetime of the $^41_{13/2}$ level permits high stored energy while a low value degrades the laser performance. Thus, in order to obtain the maximum value and choose the best concentration, lifetime were measured as a function of both ions Er^{3+} and Yb^{3+} concentration. Figure 5.9 shows typical plot of decay time for different concentrations for each signal emitted. The fluorescence decay time of all samples under study for green (560 nm), red (670 nm) and NIR (1.532 μm) emissions are resumed in Table 5.4. The fluorescence decay time of $^4I_{13/2} \rightarrow {}^4I_{15/2}$ transition increase from 4.00 to 4.23 ms when Er^{3+} increase from 0.10 (TEY0105) to 0.35 mol % (TEY03505) and then decrease to 3.69 ms for 0.75 mol% (TEY07505), see Figure 5.9a. The increment in the fluorescence lifetime of $^4I_{13/2}$ level is the result of the concentration optimization of the acceptor and the decrease is the result of the fluorescence quenching of Er^{3+} due to cluster formation provided by the higher concentration. The stand is explained by differential site occupancy [20]. Additional explication for the increase in lifetime is radiation trapping effect. In this phenomenon, photons that are spontaneously relaxed from the $^4I_{13/2}$ level are re-absorbed by the neighboring ions in the ground state ($^4I_{15/2}$ level). This process of re-absorption and re-emission is repeated several times and the overall result is an increasing in the lifetime in comparison with a single ion. This effect is more pronounced with the sample size, refractive index and spectral overlap between fluorescence and absorption [21]. On the other hand, the fluorescence lifetime of such transition increase monotonically from

4.60 to 6.90 ms when Yb^{3+} increases from 1.0 (TEY051) to 4.5 mol% (TEY0545), see Figure 5.9a. This is partly the result of the higher concentration of sensitizer and the better excitation process of Er^{3+} via the energy transfer from Yb^{3+}, as has been reported previously [22]. And partly is the result of a better dispersion of Er^{3+} avoiding cluster formation that in turn avoids fluorescence quenching.

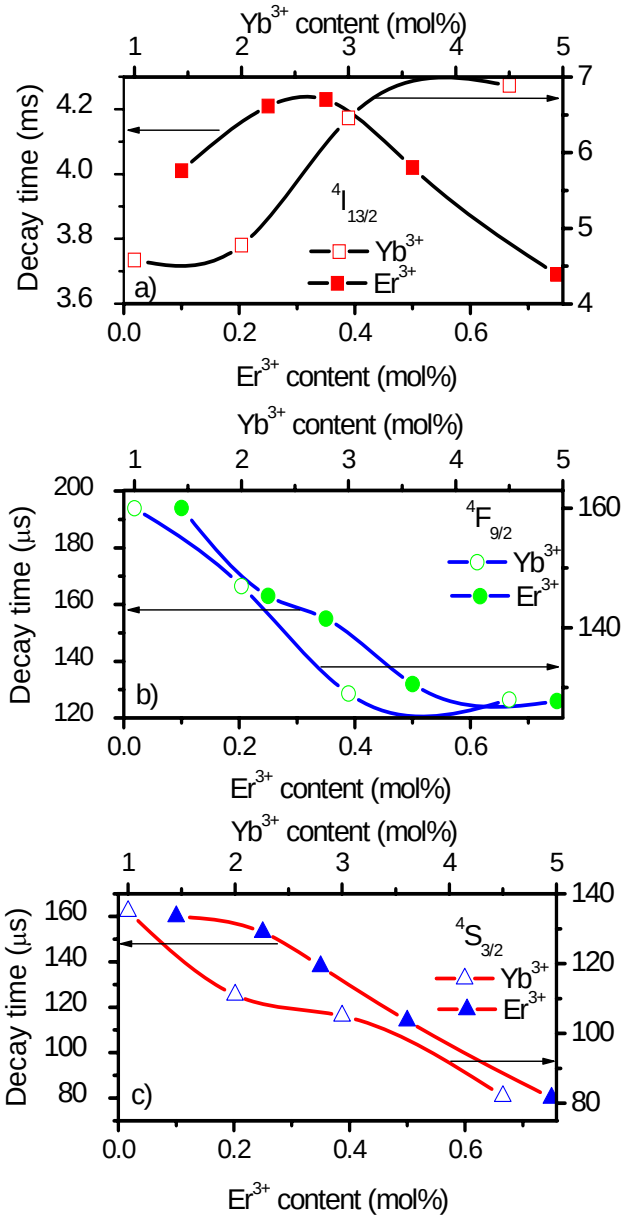

Figure 5.9 Fluorecence decay time as a function of Er^{3+} and Yb^{3+} concentration of a) $^4I_{13/2}$, b) $^4F_{9/2}$ and c) $^4S_{3/2}$ levels.

The ionic radius of Yb^{3+} ions is similar to that of Er^{3+} ions, as consequence Yb^{3+} ions can act as a disperser, occupying the position close to Er^{3+} ions. And it may lead to an increase of the average distance of Er^{3+}-Er^{3+} ions, that in turn reduce the cluster formation. The measured lifetime confirm that the effect of concentration quenching of $^4I_{13/2}$ level decrease with an increase of Yb^{3+} in this glass host.

Table 5.4 Fluorescence lifetime and quantum efficiency as function of Er^{3+} and Yb^{3+} concentration.

Er/Yb	Fluorescence lifetime			Quantum efficiency (%)		
(mol %)	$^4S_{3/2}$ (μs)	$^4F_{9/2}$ (μs)	$^4I_{13/2}$ (ms)	$^4S_{3/2}$	$^4F_{9/2}$	$^4I_{13/2}$
TEY0105	160	194	4.01	63	67	100
TEY02505	153	163	4.21	61	55	100
TEY03505	138	155	4.23	55	51	100
TEY0505	114	132	4.02	45	42	100
TEY07505	80	126	3.69	31	40	96
TEY051	135	160	4.58	91	56	100
TEY052	111	147	4.78	76	52	100
TEY053	105	129	6.46	71	46	100
TEY0545	82	128	6.89	55	45	100

The fluorescence decay time of $^4F_{9/2}$ and $^4S_{3/2}$ levels decreases as both Er^{3+} and Yb^{3+} concentration increase. For $^4F_{9/2}$ level, decreases from 194 to 126 μs and 160 to 128 μs for Er^{3+} and Yb^{3+} respectively. And for $^4S_{3/2}$ level decrease from 160 to 80 μs when Er^{3+} increase from 0.10 (TEY0105) to 0.75 mol% (TEY07505) and 135 to 82 μs when Yb^{3+} increase from 1.0 (TEY051) to 4.5 mol% (TEY0545), such as is shown in Figures 5.9b and 5.9c. Comparing the measured decay time with the calculated with JO theory, it is possible to calculate the quantum efficiency for the three observed transition. It was calculated by using the equation

$$\eta = \tau_{mea} / \tau_{rad} \tag{5.3}$$

The values of quantum efficiency for all Yb^{3+}/Er^{3+} co-doped tellurite glass are listed in Table 5.4. The QE for $^4S_{3/2} \rightarrow {}^4I_{15/2}$ and $^4F_{9/2} \rightarrow {}^4I_{15/2}$ transitions decrease with the increase of Er^{3+} and Yb^{3+} concentrations, while the $^4I_{13/2} \rightarrow {}^4I_{15/2}$ transition is 100 % for almost all samples with an exception of TEY07505.

5.5 Energy transfer efficiency of Yb^{3+}/Er^{3+} doped tellurite glasses

The fluorescence lifetime (τ_f) is related with the radiative decay rate (A_R) and non-radiative decay rate (A_{NR}) by the equation [23]

$$\frac{1}{\tau_f} = A_R + A_{NR} = A_R + W_{MP} + W_{CR} + W_{ET} \tag{5.4}$$

where W_{MP} is the multiphonon decay rate, W_{CR} is cross relaxation rate and W_{ET} is energy transfer rate. In the absence of Er^{3+} ions (acceptors), W_{ET} is zero and τ_f becomes τ_o, which is the fluorescence lifetime of Yb^{3+} ions (donor). Thus equation 5.4 is given as

$$\frac{1}{\tau_o} = A_R + W_{MP} + W_{CR} \tag{5.5}$$

From equation 5.5 and 5.4

$$\frac{1}{\tau_f} = \frac{1}{\tau_o} - W_{MP} - W_{CR} + W_{MP} + W_{CR} + W_{ET} \tag{5.6}$$

Thus W_{ET} is obtained by the equation

$$W_{ET} = \frac{1}{\tau_f} - \frac{1}{\tau_o} = \frac{\tau_o - \tau_f}{\tau_f \tau_o} \tag{5.7}$$

where τ_f and τ_o is t is the measured lifetime of $^2F_{5/2}$ level of Yb^{3+} in the presence and absence of Er^{3+}. Finally the energy transfer (ET) efficiency from Yb^{3+} to Er^{3+}, $Yb^{3+}(^2F_{5/2})+Er^{3+}(^4I_{15/2}) \rightarrow Yb^{3+}(^2F_{7/2})+Er^{3+}(^4I_{11/2})$ can be evaluated by using the expression.

$$\tau_f W_{ET} = \eta = 1 - \frac{\tau_f}{\tau_o} \tag{5.8}$$

The ET efficiency increase from 36% to 66% by increasing the Er^{3+} concentration and from 56% to 69% by increasing Yb^{3+} ions, see Figure 5.10. This last value is in agreement with other reports published recently [24]. The obtained results show that the major changes in ET efficiency occur by increasing the Er^{3+} concentration (acceptors). One possible explanation of this phenomenon is as follow. Because the absorption cross section of Yb^{3+} ($^4F_{7/2} \rightarrow {}^4F_{5/2}$) is much larger than that of Er^{3+} ($^4I_{15/2} \rightarrow {}^4I_{11/2}$), mostly all the absorption energy is taken for donors (Yb^{3+}). Thus, there are much more free donors than acceptors (Er^{3+}) to make the ET. However with the increment of Er^{3+} concentration, the probability of Er^{3+} to absorb the energy from Yb^{3+} become higher and consequently the ET efficiency will be increased. The increment of Yb^{3+} concentration increase the probability to form pairs Yb^{3+}-Er^{3+} enhancing the ET, but at the same time the number of acceptor will be reduced explaining the slow increment of ET, see Figure 5.10.

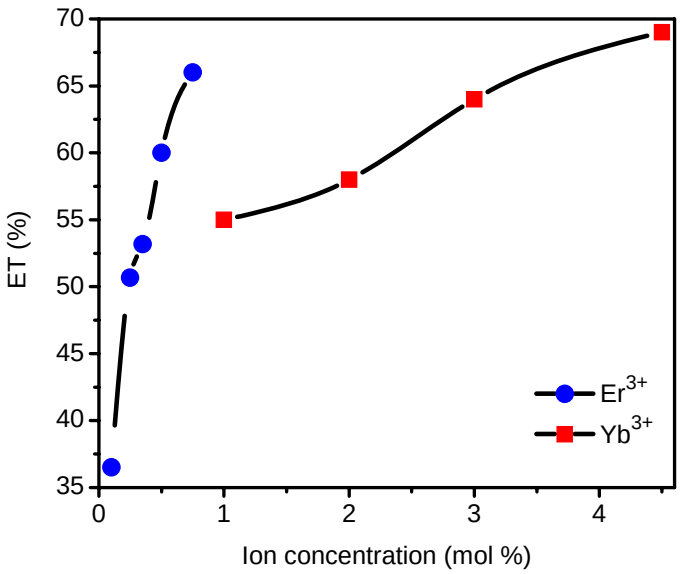

Figure 5.10 Energy transfer efficiency as a function of Yb^{3+}/Er^{3+} concentration.

It was demonstrated that emission cross section, FWHM and quantum efficiency of the characteristic 1.53 μm signal can be improved by choosing properly the concentration of both Yb^{3+}/Er^{3+} ions. Large concentration of Yb^{3+} ion improves the signal emitted, partly because help to reduce quenching of Er^{3+} and partly because energy transfer was enhanced. The large quantum efficiency and stimulated emission cross section of this signal suggest that this glass composition present strong possibilities to be used in lasers and amplifiers design at the eye safe emission.

Bibliography

[1]. H. Desirena, E. De la Rosa, L. A. Diaz-Torres, G.A. Kumar, Opt. Mat. 28 (2006) 560.

[2]. G. A. Kumar, E. De la Rosa, H. Desirena, Opt. Comm. 260 (2006) 601.

[3]. H. Desirena, E. De la Rosa, A. Schülgen, S. Sabet, N. Peyghambarian, J. Phys D: Appl. Phys. 41 (2008) 095102.

[4]. H. Lin, S. Jiang, J. Wu, F. Song, N. Peyghambarian, E. Y. B. Pun, J. Phys. D: Appl. Phys. 36 (2003) 812.

[5]. X. Shen, Q. Nei, T. Xu, Y. Gao, Spectrochim. Acta Part A 61 (2005) 2827.

[6]. D. H. Cho, Y. G. Choi, K. H. Kim, ETRI Journal 23 (2001) 151.

[7]. H. Chen, Y. H. Liu, Y. F. Zhou, Q. Y. Zhang, Z. H. Jiang, J. Non-Crystall. Solids 351 (2005) 3060.

[8]. Tie-Feng Xu, X. Shen, Q. H. Nie, Y. Gao, Opt. Mater. 28 (2006) 241.

[9]. R. Rolli, M. Mongtagna, S. Chaussedent, A. Monteil, V. K. Tikhomirov , M. Ferrari, Opt. Mat. 21 (2003) 743.

[10]. D. E. McCumber. Phys. Rev. A, 134 (1964) A299-A306.

[11]. W.J Miniscalco, R.S. Quimby, Opt. Lett 16 (1991) 258

[12]. W. L. Barnes, R. I. Laming, E. J. Tarbox and P. R. Morkel IEEE J. of Quantum Electron. 27 (1991) 1004.

[13]. H. Bor-Chyuan, S. Jiang, T. Luo, J. Watson, G. Sorbello and N. Peyghambarian, J. Opt. Soc. Am. B 17 (2000) 833.

[14]. A. Jha, S. Shen, M. Naftaly, Phys. Rev. B 62 (2000) 6215.

[15]. W. J. Chung, A. Jhay, S. Shen, P. Joshi, Philosophi. Magaz. 84 (2004) 1197.

[16]. L. Li, M. Morell, T. Qiu, V. L. Temyanko, A. Schülzgen, A. Mafi, D. Kouznetsov, J. V. Moloney, T. Luo, S. Jiang, N. Peyghambarian, Appl. Phys. Lett. 85 (2004) 2721.

[17]. J. Yang, S. Dai, N. Dai, L. Hu, Z. Jiang, SPIE 5061 (2003) 203

[18]. Tie-Feng Xu, Guang-Po Li, Q. H. Nie, X. Shen, Spectrochim. Acta Part A 64 (2006) 560.

[19]. Y. Hu, S. Jiang, G. Sorbello, T. Luo, Y. Ding, B. C. Hwang, J.H. Kim, H.J. Seo, N. Peyghambarian, 2001 Proc SPIE 4282, 57.

[20]. S. Shen, M. Naftaly, A. Jha, Opt. Comm. 205 (2002) 101.

[21]. D. S. Sumida, T. Y. Fan, Opt. Lett. 19 (1994) 1343.

[22]. H. Bor-Chyuan, S. Jiang, T. Luo, J. Watson, G. Sorbello, N. Peyghambarian, J. Opt. Soc. Am. B 17 (2000) 833.

[23]. M.J. Weber, Phys. Rev. 157 (1957) 262

[24]. Q. Y. Zhang, Z. M. Feng, Z. M. Yang, Z. H. Jiang, J. Quantum. Spectr. & Rad. Trans. 98 (2006) 167.

CHAPTER 6

R_2O EFFECT ON THE SPECTROSCOPIC PROPERTIES OF Yb^{3+}/Er^{3+} CO-DOPED TELLURITE GLASSES

In this chapter the effect of network modifier R_2O (R= Li, Na and K) on the spectroscopic properties of Yb^{3+}/Er^{3+} co-doped tellurite glasses have been investigated. The Judd-Ofelt parameters (Ω_t), quantum efficiency and quality factor spectroscopy (χ) were calculated. Fluorescence lifetime of $^4I_{13/2}$ (Er^{3+}), $^4F_{9/2}$ (Er^{3+}), $^4S_{3/2}$ (Er^{3+}) and $^4F_{5/2}$ (Yb^{3+}) levels was observed to increase when potassium (K) replaced lithium (Li) through Na. The maximum stimulated emission cross section (ECS) for $^4I_{13/2} \rightarrow {}^4I_{15/2}$ transition of Er^{3+} is 1.02 x 10^{-20} cm^2 for La_2O_3-Li_2O-ZnO-TeO_2 glass and decrease slightly for La_2O_3-Na_2O-ZnO-TeO_2 and La_2O_3-K_2O-ZnO-TeO_2 glasses. The energy transfer efficiency (ET) from Yb^{3+} toward Er^{3+} described by the equation ($^4F_{5/2}$) + ($^4I_{15/2}$) → ($^4F_{7/2}$) + ($^4I_{13/2}$) was calculated using the measured lifetimes of Yb^{3+}, and the maximum ET was 58% for 0.25 mol% of Er^{3+} with 3 mol% of Yb^{3+} for glass containing potassium. The experimental results suggest that potassium may be best spectroscopic modifier for laser and amplification application.

6.1 Preparation of tellurite glasses

The glass composition were 75TeO_2-(15-x) ZnO-10Na_2O-xEr_2O_3 (x= 0.5, 1, 2, 3) denoted by series TE and 74TeO_2-12.75ZnO-10R_2O-0.25Er_2O_3-3Yb_2O_3 (mol %), where R=Li, Na and K (y = 1, 2, 3) denoted by TLEY, TNEY and TNEY respectively. All samples were prepared from the starting chemical constituent tellurite oxide (TeO_2), zinc oxide (ZnO), lithium oxide (Li_2O), sodium carbonate (Na_2CO_3), potassium carbonate (K_2CO_3), erbium oxide (Er_2O_3), ytterbium oxide (Yb_2O_3), and lanthanum

oxide (La_2O_3). All reactants were analytical grade and used as received. The glass fabrication, annealing and different measurements were similar as described in chapter 1 and section 2.2. All samples were prepared reducing the lanthanum content with the addition of Yb^{3+} and keeping constant the network intermediate (R=Li, Na and K); the change of the lanthanum content ranges from 0.5 to 3 mol%. Series TLEY, TNEY and TKEY correspond to glasses containing lithium, sodium and potassium respectively. All samples tag glass with both ions concentration Er^{3+} and Yb^{3+} are show in Table 6.1. The complete procedure to make tellurite glasses has been described in section 4.1.

Table 6.1 Tag of Er^{3+}/Yb^{3+} co-doped La_2O_3-R_2O-ZnO-TeO_2 glasses

Tag	Er^{3+}/Yb^{3+} (mol %)
TE05	0.5/0
TE1	1/0
TE2	2/0
TE3	3/0
TLEY0253	0.25/3
TNEY0253	0.25/3
TKEY0253	0.25/3

6.2 Influence of alkalis on Judd-Ofelt parameters

From the absorption spectrum of Er^{3+} doped and Er^{3+}/Yb^{3+} co-doped tellurite glasses, ten bands were considered to predict the Judd-Ofelt parameter, see Figure 6.1. The calculated line strength for the dipole transition between J and J' is obtained by the equation 2.2 derived by Judd [1] and Ofelt [2]. The Ω_2, Ω_4 and Ω_6 are the phenomenological J-O parameters and were described in section 2.3. Such parameters do not change with the rare earth concentration and depends strongly on its local environment that can be adjusted by network modifiers. In Er^{3+} doped glasses, compositions were controlled reducing the zinc (Zn) content with the Er^{3+} addition.

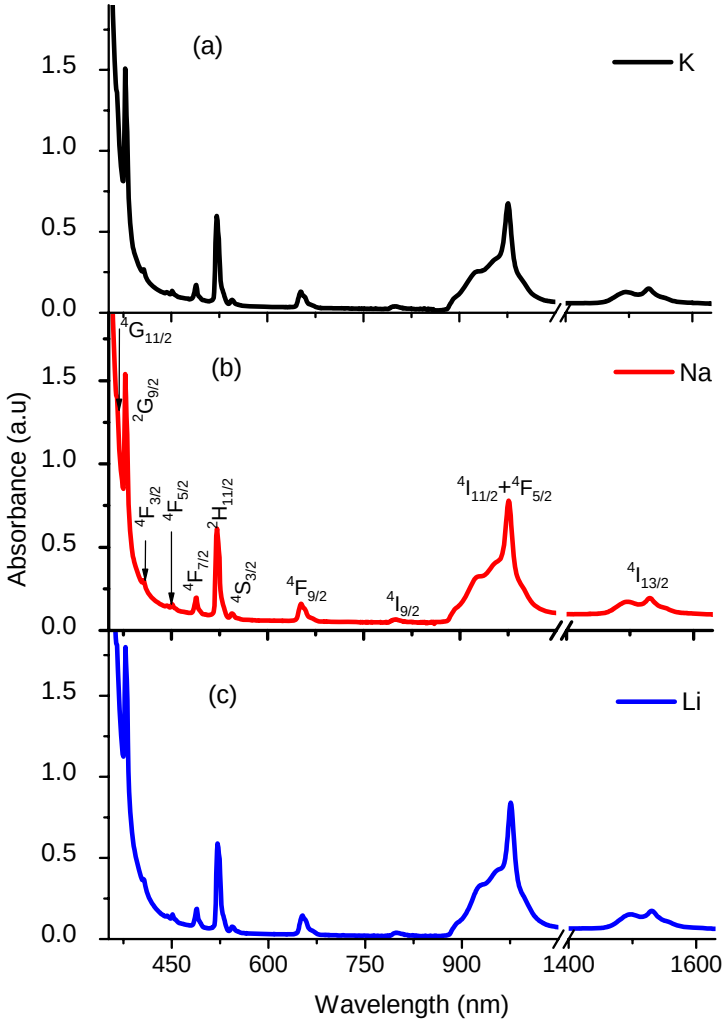

Figure 6.1 Absorption spectrum of Er^{3+}/Yb^{3+} co-doped tellurite glasses containing a) Li, b) Na and c) K.

The Er^{3+}/Yb^{3+} co-doped samples the modifier (Li, Na and K) was changed. The complete values of J-O parameters for these compositions are shown in Table 6.2. The value of Ω_2 is affected by the symmetry of the rare earth sites that is reflected in the crystal field parameter [3-4]. Larger Ω_2 means lower symmetry. The Ω_6 parameter is inversely proportional to the covalence of the Er-O bond. On the basis of the electronegativity theory [5], the smaller the difference of electronegativity between cations and anions ions, the stronger the covalency of the bond. Since the values of

electronegativity for K, Na, Li and O, are 0.8, 0.9, 1.0 and 3.5 respectively, it is expect that the covalency of Li-O is stronger than that of Na-O and K-O bonds. Therefore the influence on the local ligand environments around Er-O bond will be stronger. As a result the covalency of Er-O bond decrease whiles the parameter Ω_6 increase, such as is shown Figure 6.2.

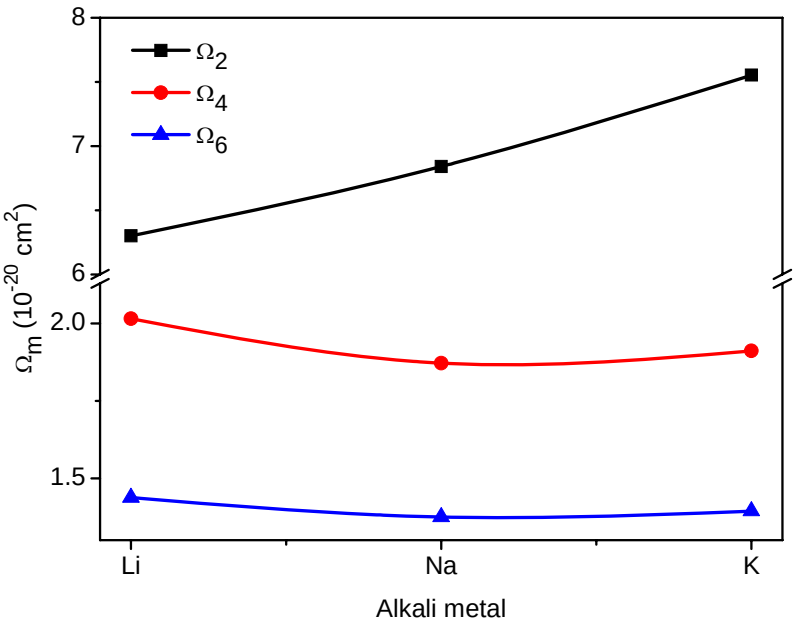

Figure 6.2 J-O parameters as a function of network modifiers.

The complete procedure to obtain the J-O parameters and some spectroscopic properties in Er^{3+} doped tellurite glass and other host has been described elsewhere [6-7]. The obtained J-O parameters follow the typical behavior $\Omega_2>\Omega_4>\Omega_6$ and are in agreement with results reported recently for various glass compositions, as is shown in Table 6.2. Once JO parameters are known, several spectroscopic properties can be calculated, e.g., the radiative transition probabilities, radiative lifetimes, branching ratios, and spectroscopy quality factor (χ). In particularly χ is important in predicting the behavior of various lasing transitions in a given matrix. For our samples, χ shows a value around 1.4, the complete values are displayed in Table 6.2. In these cases the

values are higher than the range of 0.22 to 1.5 reported for Nd^{3+} ion in different hosts and are higher than the most standard value of 0.3 [8].

Table 6.2 J-O parameters and χ for various tellurite glass composition.

Glass composition	Ω_2 (10^{-20} cm^2)	Ω_4 (10^{-20} cm^2)	Ω_6 (10^{-20} cm^2)	χ
TeO_2-WO_3-Bi_2O_3 [a]	6.06	1.57	0.95	1.652632
TeO_2-Nb_2O_5-Na_2O [b]	6.86	1.53	1.12	1.366071
TE [c]	5.98	1.32	1.47	0.897959
TKEY [c]	7.55	1.91	1.39	1.374101
TNEY [c]	6.84	1.87	1.37	1.364964
TLEY [c]	6.30	2.01	1.43	1.405594

[a] Ref [9]
[b] Ref [10]
[c] Reported in this work

6.3 Cross-section as a function of network modifier (Li, Na and K)

The absorption cross-section of the $^4I_{13/2} \rightarrow {}^4I_{15/2}$ (1.53 μm) transition of Er^{3+} has been determined from the absorption spectrum of Er^{3+}/Yb^{3+} co-doped tellurite glasses as function of network modifier (Li, Na and K) using the equation 5.1. The stimulated emission cross section is obtained according to the McCumber theory from the equation 5.2. The values of both, absorption and emission cross section of La_2O_3-K_2O-ZnO-Te_2O glass are shown in Figure 6.3a. The La_2O_3-Li_2O-ZnO-Te_2O glass has the largest emission cross section peak 1.02 x 10^{-20} cm^2 and then decrease to 0.97 x 10^{-20} cm^2 and 0.92 x 10^{-20} cm^2 for the La_2O_3-Na_2O-ZnO-Te_2O and La_2O_3-K_2O-ZnO-Te_2O glasses respectively, see Figure 6.3b. The reason why the ECS is larger when Li is used as a modifier than the Na and K is as follow. Since that stimulated emission cross section is proportional to the refractive index of the host glass [11], $\sigma_e \sim (n^2+2)^2/n$ and the refractive index increase in the way K→Na→Li (section 4.6), it is expected that the La_2O_3-Li_2O-ZnO-Te_2O glass has the larger emission cross section among the alkali. The calculated value of stimulated emission cross section are in agreement with results

reported recently [10] and are higher than values reported for silica (7.9 x 10^{-21} cm^2) [12] and phosphate glass (6.8 x 10^{-21} cm^2) [13].

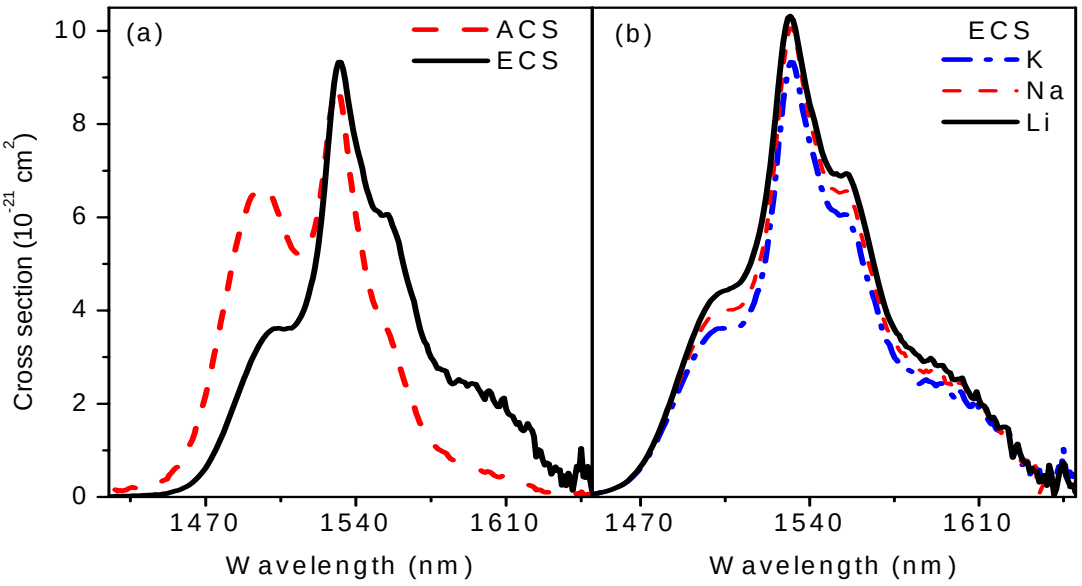

Figure 6.3 Cross section of Er^{3+} for $^4I_{13/2} \rightarrow {}^4I_{15/2}$ transition a) ACS and ECS of La_2O_3-K_2O-ZnO-Te_2O glass, b) ECS for different network modifier (Li, Na and K)

6.4 Fluorescence properties of Er^{3+} doped and Er^{3+}/Yb^{3+} codoped tellurite glass.

6.4.1 Infrared emission ($^4I_{13/2} \rightarrow {}^4I_{15/2}$)

The infrared emission of Er^{3+} ($^4I_{13/2} \rightarrow {}^4I_{15/2}$) in Er^{3+} doped and Er^{3+}/Yb^{3+} co-doped tellurite glasses was observed at 1.532 μm, with an spectral bandwidth ranging from 70 to 79 nm and 46 to 66 nm respectively as is shown in Figure 6.4. The obtained results show a continuous increment of the bandwidth with the Er^{3+} and Yb^{3+} content, being more pronounced with Er^{3+} concentration, see Figure 6.4a. The additions of a particular network modifier to tellurite glass helps to increase the bandwidth, increasing in the following way $K_2O \rightarrow Na_2O \rightarrow Li_2O$ glasses, see Figure 6.4b.

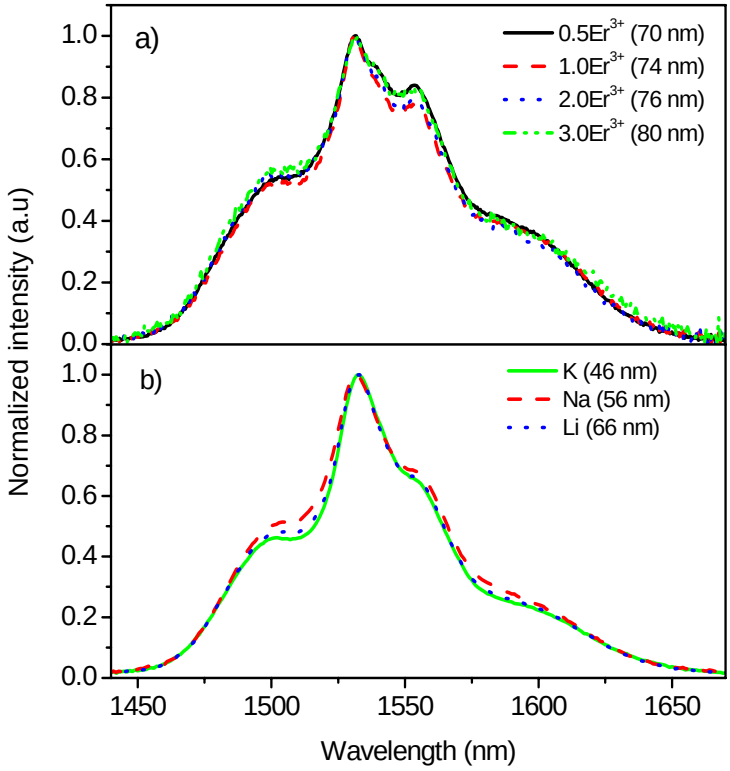

Figure 6.4 Bandwidth of $^4I_{13/2} \rightarrow {}^4I_{15/2}$ transition as a function of a) Er^{3+} concentration and b) network modifier.

In the particular case of $^4I_{13/2} \rightarrow {}^4I_{15/2}$ transition, because of its difference in the angular momentum by $\Delta J = 1$, there exists the contribution of the magnetic-dipole transition (S_{md}). In order to get broadband and flat emission spectrum, which is very useful in optical amplifiers, it is necessary to increase the relative contribution of electric-dipole transition (S_{ed}) [14]. S_{md} is independent of ligand fields and is characteristic of the transition determined by the quantum numbers, while S_{ed} is a function of ligand field. It is possible to increase S_{ed} by modifying the structure and composition of the glass host. In this particular case different network modifiers like K, Na and Li have been introduced to change the structure of glasses. According to the

Judd-Ofelt theory, the line strength of S_{ed} components of $^4I_{13/2} \rightarrow {}^4I_{15/2}$ transition is given by [15]

$$S_{ed}[^4I_{13/2} \rightarrow {}^4I_{15/2}] = 0.019\Omega_2 + 0.118\Omega_4 + 1.462\Omega_6 \quad (5.3)$$

where the coefficient of Ω_ts parameter are the reduced matrix elements of the unit tensor operator, $U^{(t)}$, which can be found in the literature [8]. It can be seen that the term containing Ω_6 is more significant in the value of S_{ed} because of the large coefficient. Therefore an increment on the value of Ω_6 means necessarily an increase of 1.53 signal bandwidth. Experimental results confirm that the bandwidth increase as the term Ω_6 increases in the following way K→Na→LI, see Figure 6.5.

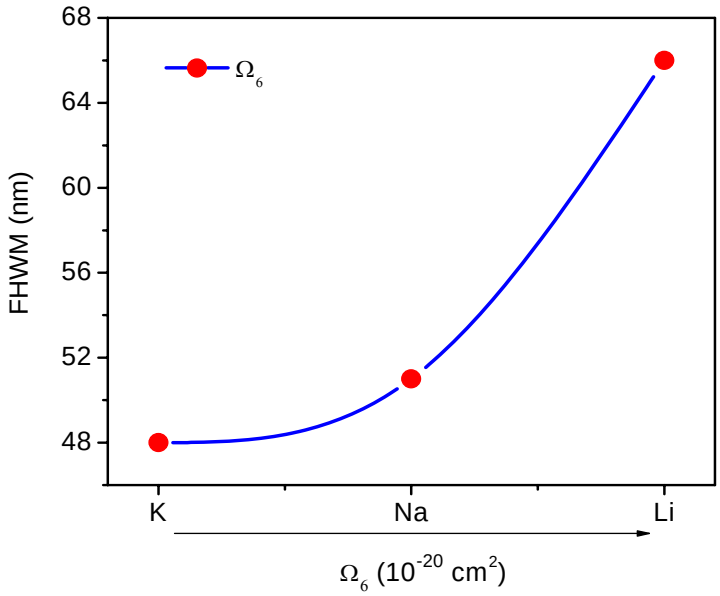

Figure 6.5 FWHM as a function of Ω_6 parameter.

In addition, the signal intensity depends on the network modifiers such as is indicated in Figure 5.6. Such dependence clearly indicates the importance of the right glass composition.

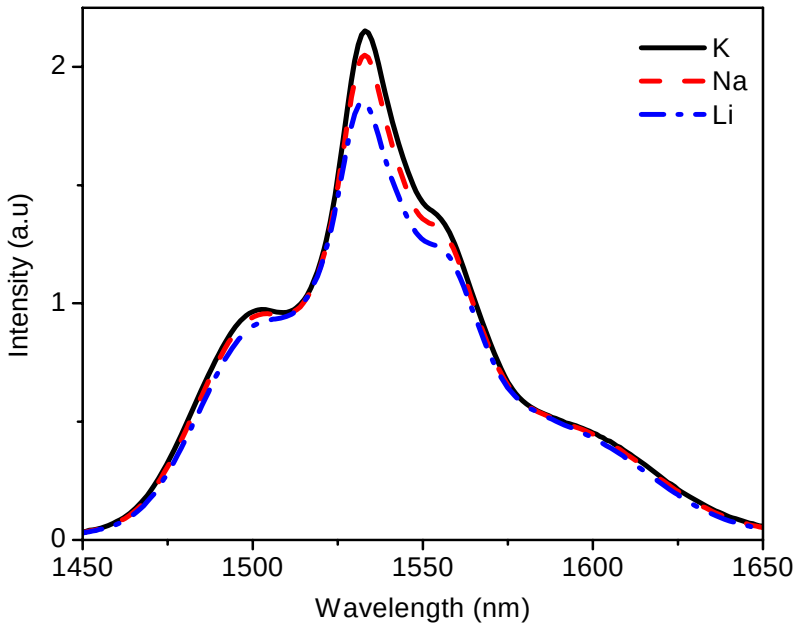

Figure 6.6 Infrared emission intensity of $^4I_{13/2} \rightarrow {}^4I_{15/2}$ transition as a function of network modifier.

6.4.2 Up-conversion emission

In addition to the 1.53 μm signal emitted, two strong visible bands green ($^2H_{11/2}$ + $^4S_{3/2} \rightarrow {}^4I_{15/2}$) and red ($^4F_{9/2} \rightarrow {}^4I_{15/2}$) centered at 526, 548 and 660 nm respectivelly, were observed. For Er^{3+} doped samples overall intensity of the up-converted signal decrease monotonically with the Er^{3+} concentration. Both bands decrease but the red one shows a trend to increase with the Er^{3+} concentration, see Figure 6.7a. In the case of Er^{3+}/Yb^{3+} co-doped samples the intensity increase in the following way Li→Na→K. That means that the replace of K by Li through Na makes to tellurite glass more radiative, consequently the intensity of green and red it will be increase, see Figure 6.7b.

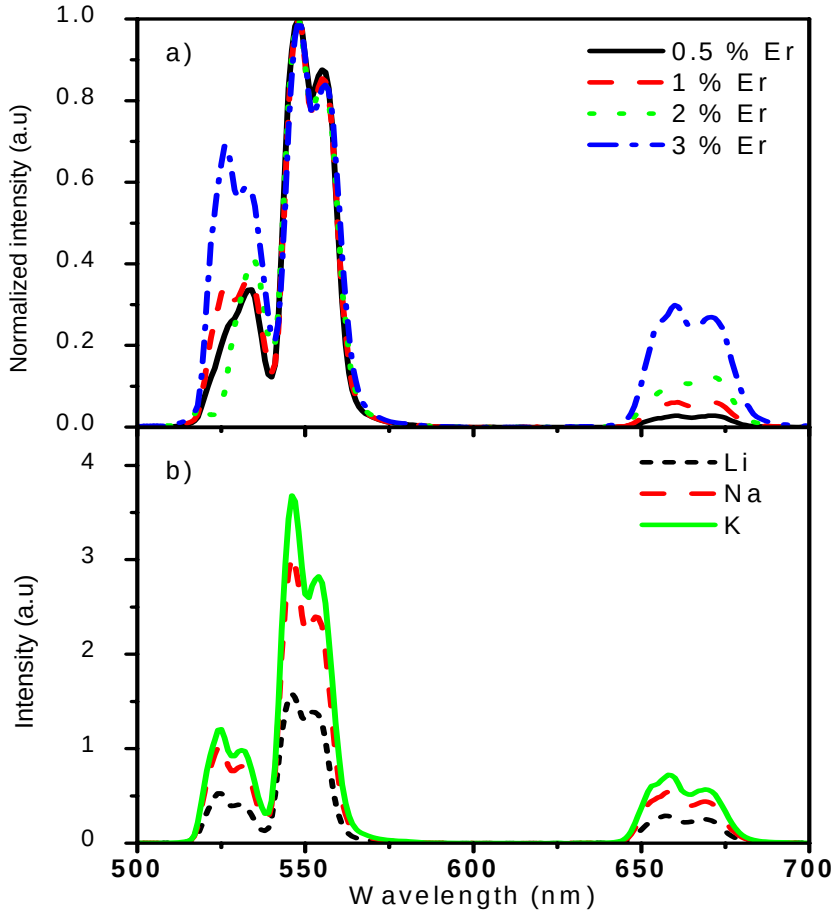

Figure 6.7 Up-conversion emission intensity of $^4S_{3/2} + {}^2H_{11/2} \rightarrow {}^4I_{15/2}$ and $^4F_{9/2} \rightarrow {}^4I_{15/2}$ transitions as a function of a) Er^{3+} concentration and b) network modifier.

6.4.3 Mechanism analysis of Er^{3+} doped tellurite glass

The mechanism of the IR and visible emission bands are explained with the help of the energy level diagram shown in figure 6.8. When the $^4I_{11/2}$ level is excited by the 968 nm photons ($^4I_{15/2} + h\nu \rightarrow {}^4I_{11/2}$), part of the excitation energy at the $^4I_{11/2}$ level relaxes non- radiatively to the $^4I_{13/2}$. The radiative transition via $^4I_{13/2} \rightarrow {}^4I_{15/2}$ leads to the characteristic 1534 nm emission. Along with this, the excited state absorption (ESA) from $^4I_{11/2}$ can populate the $^4F_{7/2}$ level ($^4I_{11/2} + h\nu \rightarrow {}^4F_{7/2}$). The lifetime of $^4I_{11/2}$ level of Er^{3+} in tellurite is 140μs [16] and is beneficial for efficient ESA process. The $^4F_{7/2}$ level decays non- radiatively to $^2H_{11/2} + {}^4S_{3/2}$ and the transition to $^4I_{15/2}$ give the green

emission. In addition to this, the possible energy transfer (ET) through $Er^{3+}(^4I_{11/2}) + Er^{3+}(^4I_{11/2}) \rightarrow Er^{3+}(^4F_{7/2}) + Er^{3+}(^4I_{15/2})$ can also increase the population of the $^4F_{7/2}$ level. The fluorescence quenching of green emission with Er^{3+} concentration may be related with the cross relaxation (CR) process Er^{3+} $(^2H_{11/2}) + Er^{3+}$ $(^4I_{15/2}) \rightarrow Er^{3+}$ $(^4I_{9/2}) + Er^{3+}$ $(^4I_{13/2})$. The red emission is due to the combined effect of the ESA from level $^4I_{13/2}$ to $^4F_{9/2}$ and the energy transfer process described by $Er^{3+}(^4I_{13/2}) + Er^{3+}(^4I_{11/2}) \rightarrow Er^{3+}(^4F_{9/2}) + Er^{3+}(^4I_{15/2})$, as shown in Figure 6.8. The mechanism for Er^{3+}/Yb^{3+} co-doped tellurite glass was described in section 5.4.2.

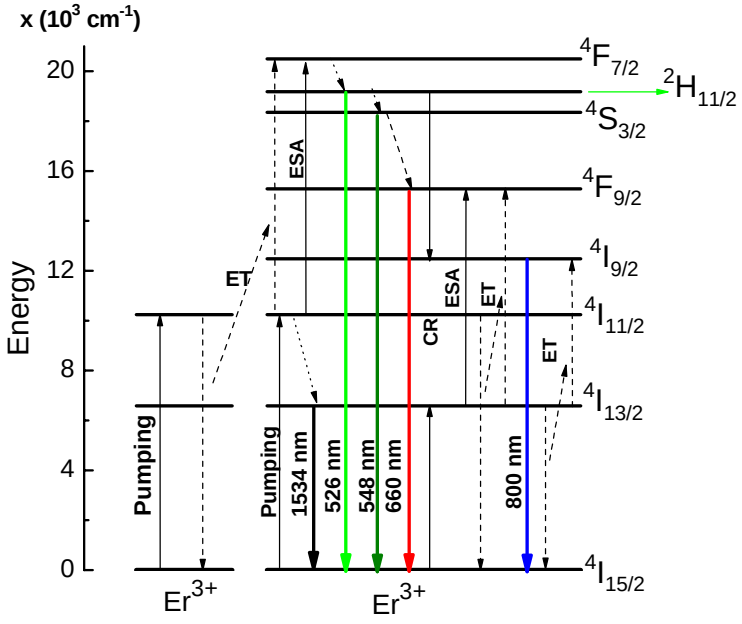

Figure 6.8 Energy level diagram of Er^{3+} doped sample and the mechanism proposed to explain both visible and infrared emission.

Since the energy transfer rate between two ions depends on their distance, the efficiency of energy transfer up-conversion depends quadratically on the Er^{3+} concentration as shown in Figure 6.9. This means that energy transfer process is the major reason for the red up-conversion.

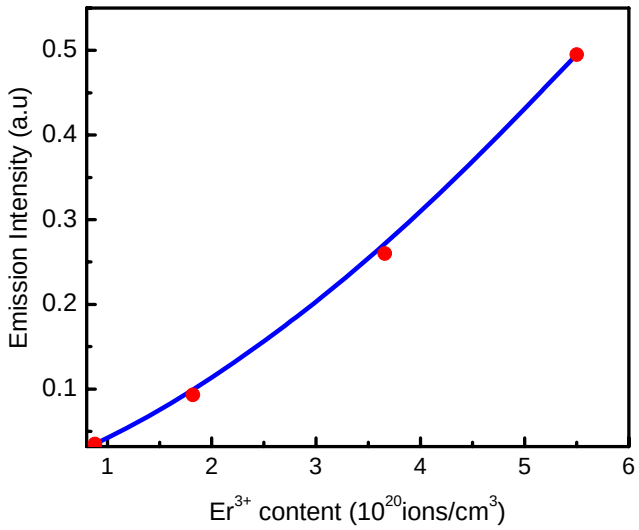

Figure 6.9 Emission intensity of red up-conversion band as function of the Er^{3+} concentration.

In order to know the origin of red band, the $^2H_{11/2}$ level was excited at 520 nm and the explanation of this phenomenon is as follow.

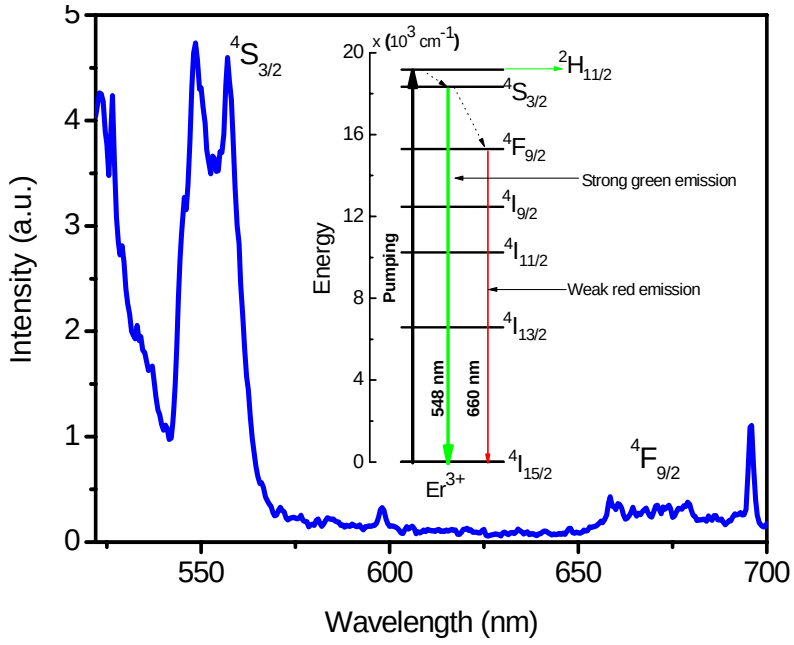

Figure 6.10 Down-conversion of Er^{3+} doped tellurite glass.

The $^4I_{11/2}$ level is exited according to the equation $^4I_{15/2} + h\nu \rightarrow {}^2H_{11/2}$. From that level the ions are relaxed non-radiatively to $^4S_{3/2}$ level and from here mostly relaxes to ground state producing the strong 548 nm emission band. Emission spectra show a weak emission band centered at 660 nm corresponding to $^4S_{3/2} \rightarrow {}^4I_{15/2}$ transition. That means that only a few ions decay non-radiatively to $^4F_{9/2}$ level and the red emission is mainly originated by energy transfer described by $Er^{3+}(^4I_{13/2}) + Er^{3+}(^4I_{11/2}) \rightarrow Er^{3+}(^4F_{9/2}) + Er^{3+}(^4I_{15/2})$.

6.5 Fluorescence lifetime

6.5.1 Fluorescence lifetime of Er^{3+} doped tellurite glass

The decay time of the $^4I_{13/2} \rightarrow {}^4I_{15/2}$ transition was measured in Er^{3+} doped $75TeO_2$-(15-x) ZnO-$10Na_2O$-xEr_2O_3 (x= 0.5, 1, 2, 3) glass.

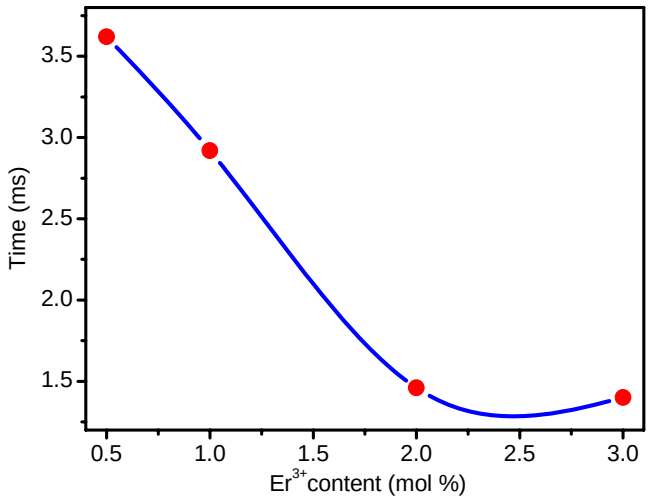

Figure 6.11 Fluorescence decay of 1.53 μm emission as a function of Er^{3+} concentration.

The Er^{3+} concentration dependence of the lifetime of $^4I_{13/2}$ level of samples is plotted in Figure 6.11. An important reduction of the $^4I_{13/2}$ level lifetime is clearly

observed with the Er^{3+} concentration. The decay time decrease from 3.62 to 1.4 ms when Er^{3+} increases from 0.5 to 3 mol %. The decrease is the result of the energy transfer and fluorescence quenching of Er^{3+} due to cluster formation provided by the higher concentration. The complete values of decay time are listed in Table 6.3.

6.5.2 Fluorescence lifetime of Er^{3+}/ Yb^{3+} co-doped tellurite glass

The fluorescence decay time of all samples under study for green (560 nm), red (670 nm) and NIR (1.532 μm) emissions of Er^{3+}/Yb^{3+} co-doped samples were plotted in Figure 5.12. Such Figure shows the individual effects of network modifiers.

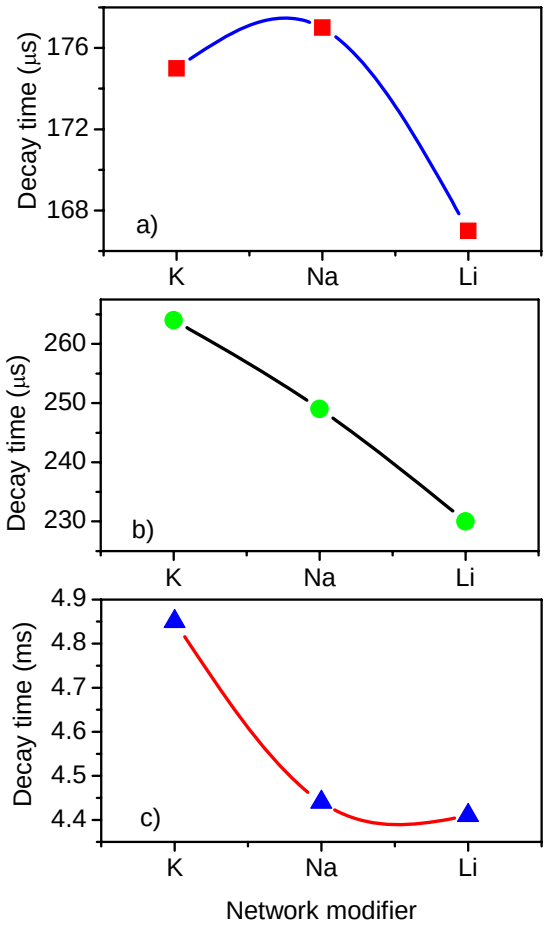

Figure 6.12 Fluorescence decay time as a function of Yb^{3+} concentration and network modifiers for a) $^4I_{13/2}$, b) $^4S_{3/2}$ and c) $^4F_{9/2}$ levels.

It has been reported that the incorporation of Na to tellurite glass improve the solubility of rare earth [10], however our studies show that the replace of K by Na, improve much more the solubility that in turn reduce the quenching concentration of Er^{3+}. The experimental results show that decay time increase from Li to K through Na, indicating that K is the best modifiers. According to Judd–Ofelt theory the radiative lifetime is inversely proportional to refractive index of the glass host [17]. The lower the refractive index of glass host, the larger the fluorescence lifetime of ion. Since the refractive index of glass host decrease from Li to K (section 4.6), it is expect that in glasses containing K is capable to providing large fluorescence lifetime.

Comparing the measured decay time with the calculated with J-O theory, it is possible to calculate the quantum efficiency (QE) for the three observed transition. It was calculated by using the equation 2.10. The values of quantum efficiency for Er^{3+} doped and Yb^{3+}/Er^{3+} co-doped tellurite glass are listed in Table 6.3.

Table 6.3 Fluorescence lifetime and quantum efficiency as a function of Er^{3+} and network modifier.

	Er/Yb	Fluorescence lifetime			Quantum efficiency (%)		
	(mol %)	$^4S_{3/2}$ (μs)	$^4F_{9/2}$ (μs)	$^4I_{13/2}$ (ms)	$^4S_{3/2}$	$^4F_{9/2}$	$^4I_{13/2}$
	0.5/0			3.62			100
	1/0			2.92			94
	2/0			1.46			45
	3/0			1.4			47
Li	0.25/3	167	237	4.41	67.3	88.8	100
Na	0.25/3	177	249	4.4	63.4	81.9	100
K	0.25/3	175	264	4.85	59.5	83.3	100

6.6 Energy transfer efficiency in Yb^{3+}/Er^{3+} doped tellurite glasses

The ET efficiency was calculated using the equation 5.8 (section 5.5). The obtained values for 0.25% of Er^{3+} with 3% of Yb^{3+} were 52, 54 and 58 % for glasses containing Li, Na and K respectively, see Figure 6.13. Experimental data show that the major ET efficiency occur when K replace Li through Na.

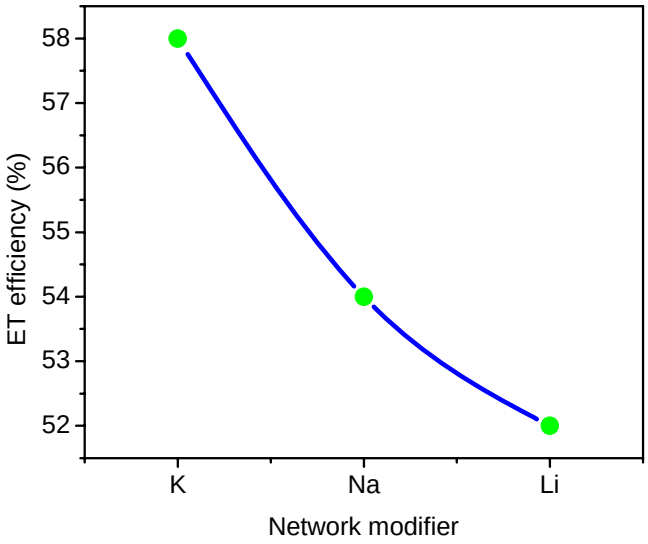

Figure 6.13 Energy transfer efficiency as a function of K, Na and Li.

According to equation 5.8 the ET increases as the term $\frac{\tau_f}{\tau_o}$ decrease. Since the lifetime of Yb^{3+} (τ_{Yb}) increase from Li to K through Na, it is expect that the maximum ET may occur in glasses containing K as network modifier. The obtained values are in agreement with other reports published recently [18] in the literature. However, the ET in tellurite glass (58%) is lower when is compared with the obtained by silicate or phosphate glasses (95%). In general the ET efficiency is influenced by the ratio W_{BT}/W_{MR}, back ET from Er^{3+} ($^4I_{11/2}\rightarrow{}^4I_{15/2}$) to Yb^{3+} ($^2F_{5/2}\rightarrow{}^4F_{7/2}$) and multi-phonon relaxation of the $^4I_{11/2}\rightarrow{}^4I_{13/2}$ transition of Er^{3+} [19]. The maximum phonon energy of

tellurite glasses is around 800 cm^{-1}, while that of silicate and phosphate glasses is around 1000 and 1100 cm^{-1} respectively [20]. Consequently, the multiphonon relaxation rate in tellurite glasses is lower and the back ET from Er^{3+} to Yb^{3+} is more significantly. This is the reason why the ET efficiency is relatively lower in tellurite than silicate o phosphate glasses.

Bibliography

[1]. B.R. Judd; Phys. Rev. 127, 750(1962).

[2]. G.S. Ofelt; J. Chem. Phys. 37, 511(1962).

[3]. S. Tanabe, J. Non-Cryst. Solids 259 (1999) 1.

[4]. S. Tanabe, J. Appli. Phys. 73 (1993) 8451.

[5]. L. Pauling, J. Am. Chem. Soc., 51 (1929) 68.

[6]. G. A. Kumar, E. De la Rosa, H. Desirena, Optcs. Comm. 260 (2006) 601.

[7]. H. Desirena, E. De la Rosa, L.A. Díaz-Torres, G.A. Kumar, Opt. Mat. 28 (200) 560.

[8]. A. Kaminskii, Laser Crystals: Their Physics and Properties, Springer-Verlag, New York, 1990.

[9]. T. Xu, X. Shen, Q. Nei, Y. Gao, Opt. Mat. 28 (2006) 241.

[10]. H. Lin, S. Jiang, J Wu, F. Song, N. Peyghambarian and E.Y.B. Pun, J. Phys. D: Appl. Phys. 36 (2003) 812.

[11]. J.S. Wang, E.M.Vogel, E. Snitzer E. Opt. Mat. 3 (1994) 187.

[12]. W. L. Barnes, R. I. Laming, E. J. Tarbox, and P. R. Morkel, IEEE J. of Quantum Electro., 27 (1991) 1004.

[13]. Bor-Chyuan Hwang, S. Jiang, T. Luo, J. Watson, G. Sorbello, and N. Peyghambarian, J. Opt. Soc. Am. B, 17 (2000) 833.

[14]. S. Tanabe, T. Hanada, J. Non-Cryst. Solids 196 (1996) 101.

[15]. M. J. Weber, Phys. Rev. 157 (1957) 262.

[16]. J. Yang, S.Dai, S.Li, L.Hu, Z.Jinag, Chin.J.Lumin. 23 (2002) 485.

[17]. M. J. Weber, J.D Myers, D. H. Blackbum, J. Appl. Phys. 52 (1981) 2944.

[18]. Q. Y. Zhang, Z.M. Feng, Z.M. Yang, Z.H. Jiang, J. Quant. Spectr. & Rad. Trans. 98 (2006) 167.

[19]. V. P. Gapontsev, S.M. Matitsin, A.A. Isineev, V.B. Kravchenko, Opt. Las. Techn. (1982) 189.

[20] C. B. Layne,W.H. Lowdermilk, M.J. Weber, Phys. Rev. B 16 (1977) 10.

CONCLUSIONS

The performance of rare earth (Er^{3+}, Er^{3+}/Yb^{3+} and $Er^{3+}/Yb^{3+}/Ce^{3+}$) doped phosphate and tellurite glasses have been evaluated to investigate the potential of laser and optical amplifiers. Based on the experimental results obtained from the systematic characterization, it is concluded that spectroscopic, optical, physical and thermo-mechanical properties of tellurite and phosphate glasses are strongly influenced by the introduction network modifiers and dopant concentration. The increment of Er^{3+} concentration induces cluster formation promoting non-radiative process that quenches the fluorescence and reduce the quantum efficiency. However, large concentration of Yb^{3+} ions improves the signal emitted and the fluorescence lifetime, partly because it helps to reduce Er^{3+} clustering and partly because energy transfer was enhanced. High quantum efficiency were obtained by properly choosing the concentration of ions being 100 % for Er^{3+}/Yb^{3+} co-doped tellurite and 90 % for $Er^{3+}/Yb^{3+}/Ce^{3+}$ co-doped phosphate glasses. The introduction of Ce^{3+} and B^{3+} ions strongly help the population inversion efficiency for the 1.532 μm emission, without greatly affecting the $^4I_{11/2} \rightarrow {}^4I_{13/2}$ transition lifetime of Er^{3+}. The results show that Ce^{3+} is more effective than B^{3+} ions in the increment of fluorescence lifetime and quantum efficiency.

Different compositions of tellurite glass as a function of network modifiers and ions concentration has been studied. Experimental results indicate that the introduction of alkali metals (Li, Na, K, Rb and Cs) with small ionic radii improve chemical (DR) and mechanical (α, Tg) properties. It also increases n and $\chi^{(3)}$ (and then n_2). The former is good for the spectroscopic properties in laser and amplifier application but non-linear response induces a deleterious effect. For network intermediate (Pb, Zn, Ba and Mg), the lower thermal expansion coefficient was obtained for Zn and Mg while the better

chemical durability corresponds to Pb and Zn. The higher refractive index was obtained for Pb and Zn intermediates. The control on the refractive index with the addition of R_2O and MO into tellurite glass, and the wide transmission range from 0.35 to 6.4 μm suggest potential application for optical devices.

A large bandwidth of signal centered a 1.53 μm was observed in Er^{3+} doped and Er^{3+}/Yb^{3+} co-doped tellurite glasses, 80 nm compared to 40 nm on phosphate glasses. Furthermore, it increases with of both Er^{3+} and Yb^{3+} ions. Ions concentration, specially Yb^{3+}, play an important role on the up-converted signal and open new possibilities of being used in design of laser on the visible, display and lighting to mention a few. Bandwidth and spectroscopic properties of Er^{3+} can be improved by properly choosing the network modifier. Then, it is necessary to make a compromise of desired properties and then defines the glass composition.

DIRECTION FOR FUTURE WORK

This work is expected to be a resource for the development of devices specially laser and optical amplifiers with high performance using the obtained properties of phosphate and tellurite glasses. The complete analysis of glasses in the spectroscopic, physical, optical, thermal and mechanical properties should aid in the design of rare earth doped materials with high performance for specific applications.

Preparation of phosphate and tellurite glasses using a quartz crucible and bubbling with oxygen the glass liquid is an important task that should be considered as part of the future work. A complete characterization of thermal-mechanical and physical properties of phosphate glass to complement previous results on spectroscopic

properties should also be considered. This work needs to be extended to the fabrication of optical fiber doped with the system $Er^{3+}/Yb^{3+}/Ce^{3+}$, a complete study about the effect of Ce^{3+} on laser threshold should be performed. In addition the effect of Ce^{3+} and B_2O_3 on tellurite glasses should be studied in detail in order to decrement the visible up-conversion and enhance the 1.53 μm signal. Special attention deserves the possibility to improve visible emission, blue, green and red on tellurite glasses for lighting and display application.

PRODUCTION OBTAINED OF THIS RESEARCH PROJECT

Accepted

- **H. Desirena**, A. Schülzgen, S. Sabet, G. Ramos-Ortiz, E. De la Rosa, N. Peyghambarian, *Effect of alkali metal oxides R_2O (R=Li, Na, K, Rb and Cs) and network intermediate MO (M=Zn, Mg, Ba and Pb) in tellurite glasses*, Optical Materials (2008) In press.

- **H. Desirena**, E. De la Rosa, A. Shulzgen, S. Shabet, N. Peyghambarian, *Er^{3+} and Yb^{3+} concentration effect in the spectroscopic properties and energy transfer in Yb^{3+}/Er^{3+} codoped tellurite glasses*, Journal of Physics D: Applied Physics 41 (2008) 095102.

- **H. Desirena**, E. De la Rosa, L. A. Díaz-Torres, G. A. Kumar, *Concentration effect of Er^{3+} ion in the spectroscopic properties of doped and Yb^{3+}/Er^{3+} codoped phosphate glasses*, Optical Materials 28 (2006) 560–568.

- G. A. Kumar, E. De la Rosa, **H. Desirena**, *Radiative and Non radiative spectroscopic properties of Er^{3+} ion in tellurite glass*. Optics Communication 260 (2006) 601–606.

- E. De la Rosa, P. Salas, **H. Desirena**, C. Angeles, R. A. Rodríguez, *Strong green upconversion emission in $ZrO_2:Yb^{3+}–Ho^{3+}$ nanocrystals*, Applied Physics Letters 87, 241912 (2005).

- L.A. Diaz-Torres, E. De la Rosa, P. Salas, **H. Desirena**, *Enhanced cooperative absorption and upconversion in Yb^{3+} doped YAG nanophosphors*, Optical Materials 27 (2005) 1305–1310.

- P. Salas, C. Angeles-Chavez, J. A. Montoya, E. De la Rosa, L.A. Diaz-Torres, **H. Desirena**, A. Martinez, M.A. Romero-Romo, J. Morales, *Synthesis, characterization and luminescence propertiesof $ZrO_2:Yb^{3+}–Er^{3+}$ nanophosphor*. Optical Materials 27 (2005) 1295–1300.

- Elder De la Rosa, **Haggeo Desirena**, Ajith Kumar, *Spectroscopic analysis of Yb^{3+}-Er^{3+} co-doped phosphate glasses*, Chapter book. Some Topics of modern Optics. Rinton Press 2008, ISBN 1-58949-057-6.

To be submitted

- **H. Desirena**, E. De la Rosa, *Enhancement of 1.53 μm signal of Er^{3+}/Yb^{3+} co-doped phosphate glasses by introducing Ce^{3+} and B^{3+} ions*, Applied Physics Letters.

- **H. Desirena**, E. De la Rosa, V. H. Romero, L. A Diaz-Torres, J. R. Oliva, J.F. Castillo, *R_2O effect on the spectroscopic properties of Yb^{3+}/Er^{3+} of co-doped tellurite glass*. Journal of Physics B: Applied Physics